

Faculty of Physics and Astronomy

University of Heidelberg

Diploma thesis

in Physics

submitted by

Martina Abb

born in Friedrichshafen

2009

Fidelity for kicked atoms at nearly resonant driving

This diploma thesis has been carried out by Martina Abb

at the

Institute for Theoretical Physics

under the supervision of

Dr. Sandro Wimberger

and

Prof. Italo Guarneri

(Università degli Studi dell'Insubria, Como)

Zusammenfassung

Gegenstand dieser Diplomarbeit ist das Verhalten von instantan gekickten Atomen in der direkten Umgebung der Frequenzen für resonanten Antrieb. Um gekickte Atome zu beschreiben, bedienen wir uns des Modells des δ -gekickten Rotors, das die Evolution von Teilchen, die einer periodischen äußeren Kraft unterliegen, angemessen beschreibt. Die sich daraus ergebende Dynamik ist für große Kräfte chaotisch, weshalb wir den Überlapp zweier anfangs identischer Wellenfunktionen unter leicht unterschiedlicher Zeitentwicklung als ein Maß für die Stabilität einführen. Diese sogenannte Fidelity ist vor Kurzem im Experiment für den speziellen Fall von resonantem Antrieb (der möglich ist aufgrund der einfachen spektralen Eigenschaften des Quantenrotors) gemessen worden. Auch für kleine Abweichungen von der Resonanzbedingung gibt es erste Messungen.

In dieser Arbeit stellen wir umfangreiche numerische Untersuchungen zur Fidelity in der Nähe der Resonanzfrequenz niedrigster Ordnung vor, sowohl für einzelne Rotoren als auch für gemittelte Ensembles. Weiterhin schlagen wir eine semiklassische Behandlung vor, mit deren Hilfe wir eine analytische Beschreibung des beobachteten Verhaltens ableiten können. Wir finden sehr gute Übereinstimmung zwischen numerischen und analytischen Ergebnissen.

Abstract

This thesis investigates the behaviour of instantaneously kicked atoms in close vicinity of the resonant driving frequencies. To describe instantaneously kicked atoms, we make use of the δ -kicked rotor model, which accurately describes the evolution of particles subject to a periodically acting external force. Since the dynamical evolution which arises from this is chaotic for a larger driving force, one may introduce the overlap of two initially identical wavefunctions with slightly different time evolution as a measure of stability. This so-called fidelity has recently been measured in atom-optics experiments for the special case of resonant driving (which is made possible by the simple spectral features of the quantum rotor). There have also been attempts to measure slight deviations from the resonance conditions.

In this thesis, we present a thorough numerical assessment of the fidelity close to the resonant frequency of lowest order, both for single rotors and ensemble averages. Furthermore, we propose a semiclassical treatment in order to derive an analytic description of the observed behaviour. We find very good agreement between our numerical and analytic results.

Contents

1	Introduction	1
1.1	Motivation	1
1.2	Outline of the thesis	4
2	Preliminaries	7
2.1	The δ -kicked rotor	7
2.2	Fidelity – a measure of stability	14
2.3	Kicked atoms in quantum resonance - a review	16
2.4	Underlying ϵ -classical phase space	22
3	Numerical observations	25
3.1	Quantum calculations of fidelity	25
3.1.1	Behaviour of fidelity for the full ensemble in β	25
3.1.2	Behaviour of fidelity for ensembles of near resonant rotors	29
3.1.3	Behaviour of fidelity for resonant rotors	30
3.1.4	Behaviour of fidelity for nonresonant rotors	32
3.2	Quantum-classical correspondence	34
3.2.1	Methods	35
3.2.2	Results	36
4	Analytical theory	41
4.1	Understanding the t^{-1} -decay from ϵ -classics	42
4.1.1	Quantum calculation with path integrals for multiply connected spaces	42
4.1.2	Semiclassical approximation with the propagators for the pendulum	45
4.1.3	Semiclassical approximation with the propagators for the harmonic oscillator	48
4.2	Semicl. approximation close to quantum resonance	50
5	Conclusion	61
5.1	Summary	61
5.2	Outlook – ideas and perspectives	62
A	Formulae	65
B	Propagator for the harmonic oscillator	67

Chapter 1

Introduction

1.1 Motivation

The definition and use of the overlap of two initially identical wavefunctions with slightly different time evolution is deeply rooted in the historical development of statistical mechanics.

In the late 19th century, when Boltzmann first introduced his approach towards equilibrium, Loschmidt was quick to point out that, since the underlying dynamics is symmetric in time, there should be no objection to return to the original non-equilibrium state by simply reversing the velocities. This soon became known as the "reversibility paradox". As a response, Boltzmann introduced his probabilistic interpretation of the second law of thermodynamics and pointed out the importance of initial conditions. A reversal of velocities is not realistic for a large number of particles, whose evolution is also extremely sensitive to small errors. Ever since this dispute about the reversibility of classical microscopic dynamic systems between Boltzmann and Loschmidt, people have been looking for measures of reversibility. From the quantum-mechanical point of view, Peres introduced the overlap of two initially identical wave functions with a slightly different time evolution, the so-called *fidelity*, as such a measure in 1984 [1]. In honour of Loschmidt, this is also often given the name "Loschmidt echo", with the interpretation of the projection of a state given to an unperturbed forward evolution followed by a perturbed backward evolution onto the initial state (thus the name "echo"). Peres interpreted it as the probability for a system to be in a certain state after having been exposed to different forward and backward evolutions.

Interestingly, this measure can be used both for classical and for quantum dynamics, which has led to some interesting discoveries of relations between the two, especially for quantum systems whose behaviour is strongly related to their classical correspondent. For regular quantum systems deep in the semiclassical limit (i.e., their effective Planck's constant not being too large), it is well established to define action-angle variables [2] at least locally, which allows us to use their classical analog in the leading order of semiclassical approximations. Therefore, we can express quantum fidelity in terms of classical quantities. By assuming perturbations with a non-zero time average, we find two different general results [3]. For coherent initial states, the fidelity decay transpires to be Gaussian, whereas for random initial states (which means pure states whose coefficients are independent Gaussian random numbers), an algebraic decay is found, depending on the dimension of the system.

For chaotic quantum systems, i.e. quantum systems with a corresponding classically chaotic system, the spectrum of regimes is much richer and less dependent on the initial state. For very small perturbation strengths, perturbation theory still holds and results in Gaussian decay (see [4]), under the assumption of eigenvalues and -functions being uncorrelated and Gaussian distributed for strongly chaotic systems. This regime is called the **perturbative regime (PR)** and it is the only one where a purely quantum mechanical calculation is sufficient. Increasing the perturbation strength by a small amount, we cross over to the **Fermi golden rule regime (FGRR)**, where exponential decay is preeminent [4, 5]. Here, the use of perturbative treatment is no longer valid, requiring a semiclassical ansatz for the derivation. The next regime is the **Ljapunov regime**, which is perhaps the most astonishing and therefore the one which attracted a lot of attention, due to its independence of the perturbation strength. Here, the fidelity decays exponentially, with the classical Ljapunov coefficient as decay rate [6, 7]. This is remarkable, since it indicates a direct connection between classical and quantum systems. Perturbing the system even stronger leads to the final breakdown of perturbation theory, even the classical one. Since the semiclassical treatment ceases to be useful, there is no theoretical understanding yet for this regime, but an even faster decay is expected. This regime is commonly known as the **strong semi-classical regime (SSCR)** [8]. All four regimes have been experimentally verified (e.g. in microwave billiards [9, 10]).

In Fig. 1.1, a graphic survey of the 4 different chaotic regimes can be found, depending on time and perturbation strength. It is plausible that small perturbations need a longer time to become evident than strong perturbations.

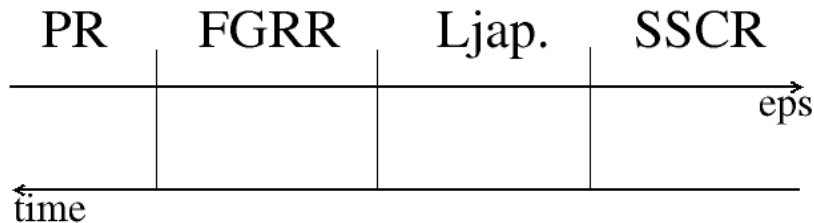


Figure 1.1: Schematic illustration of the qualitative dependence of the regimes on time t and perturbation strength ϵ . This is of course but a qualitative overview, for details please refer to the cited papers (especially [11] and [12] give a good overview).

A new access to the experimental realisation of the different regimes has been created by a revival of experiments with cold and ultracold atoms [13]. Here, the δ -kicked rotor plays an important role in the theoretical description of the experiments.

For this thesis, we investigate the kicked rotor system [14, 15, 16] in a special regime of enhanced energy transport, the so-called *quantum resonances*. The rotor model consists of a periodically driven pendulum with angle-dependent driving (see Fig. 1.2). Continued energy absorption (more specific, a ballistic growth in energy) takes place for certain driving frequencies, which can be proven to be rational multiples of π [17, 18].

This frequency-matched driving leads to an unbound ballistic growth in energy. Experimental realisations of the δ -kicked rotor build on modern atom optics: An ensemble of cooled atoms is exposed to a pulsed laser beam of a specific frequency, which is reflected by a mirror and thus constructs a stroboscopic one-dimensional standing wave, also referred to as pulsed "optical lattice" [19]. When the final position distribution of the atoms is measured after some time, this, combined with the time information, renders it possible to extract information about their momentum distribution and consequently their energies.

The only difficulty arising from this realisation is the difference in trajectories: While the particle in the rotor model moves, as the name indicates, on a circle, the particle in the experiment follows a straight line determined by the kicking potential. This conflict can be resolved by use of the Bloch theorem for spatial periodicity, leading to the conservation of a new quantum number, the "quasimomentum" [20]. This leads to a uniform description for both and results in mapping the kicked particle to the kicked rotor problem.

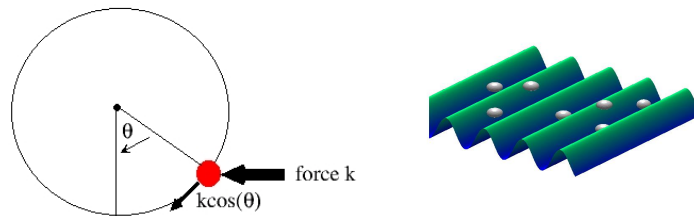


Figure 1.2: Driven pendulum with an excursion-dependent external driving force $k \cos(\theta)$, experimentally realised by a pulsed laser wave.

The experiment has been realised with great success several times already (e.g. by M. Raizen [13, 21, 22], G. Summy [23, 24] and R. Leonhardt [25, 26]). Since both the preparation of cold and ultracold atoms and the tools of atomic optics such as the modulation of optical lattices have reached hitherto unknown heights of precision, theoretical results can be verified without being impaired by experimental inaccuracies such as background noise, see e.g. [25].

The aim of this thesis is to observe the behaviour of the fidelity of the δ -kicked rotor for slight deviations from resonance conditions. We perform comprehensive numerical calculations to quantitatively characterize the dynamics for rotors with different initial quasimomenta over short and long time spans. The desire to also qualitatively describe these observations makes it necessary to accurately put the quantum system of the kicked rotor in the dynamical chaotic regime into context concerning the aforementioned regimes. While chaotic dynamics prevails for higher values of the kicking strengths, it is not possible to describe fidelity decay in this regime by one of the derivations above. The reason for this is the finite resolution determined by the effective Planck's constant, which is (per definition, since we want to investigate quantum resonances) too large to resolve anything in a sensible way [26]. We therefore have to employ a trick that was already used in [27, 28] and that will be explained in detail in the next chapter: By utilising the perturbation ϵ , in our case the deviation from the resonant frequency, as effective Planck's constant, one may derive a pseudo-classical phase space, which can (by coordinate transformations) be reduced to the well-known

standard map. The dynamics displayed by this phase space are regular and adequately resolved (see [29]). From the point of view of this ϵ -classical phase space, we will be able to derive a description for resonant rotors which matches the one found from the purely quantum mechanical calculations in the asymptotic case $\epsilon \rightarrow 0$.

Working with the classical phase space equivalent derived by ϵ -classics (usable in the vicinity of quantum resonances) is what essentially distinguishes our approach. Over the last years, various attempts have been made to explain the behaviour of fidelity for the δ -kicked rotor in different parameter regimes. For example, Sankaranarayanan and Lakshminarayan found recurrences for the near-integrable regime [30] that can be approximated by the harmonic oscillator, using very small kicking strengths and a diminutive difference in kicking strengths. This, however, has no direct relation to our results. We are (at least without ϵ -classics) deep in the chaotic regime, whereas in [30], the phase space is pretty regular.

This is also the case for other publications, e.g. [31, 32]. All of them discuss the behaviour of fidelity with underlying regular phase space, which is thus well understood by now. However, almost no explanations can be found as to the behaviour of fidelity in the chaotic regime (apart from numerical investigations). This is where our ansatz offers a whole range of new possibilities: We are able to approach part of the chaotic regime using the means known and tested for regular phase space.

Another important point, which we should mention here, is the different meaning of the classical limit in the two approaches. For the δ -kicked quantum rotor, the semiclassical limit consists of $k \rightarrow \infty$ and $\tau \rightarrow 0$, while keeping their product constant. Using ϵ -classics, we find a pseudoclassical limit $\epsilon \rightarrow 0$, for which we find ourselves at exact quantum resonance.

As we shall see when exploiting the possibilities offered by ϵ -classics, the first results are very promising. The harmonic oscillator approximation works well for the resonant rotors and we are able to considerably enlarge our understanding of the fidelity close to quantum resonance.

1.2 Outline of the thesis

Chapter 2 introduces the necessary theoretical and experimental preliminaries for the study of periodically kicked atoms, including the phenomena of enhanced energy absorption (the so-called quantum resonances). It also reviews the work that has so far been done on kicked atoms in quantum resonance [33]. The analytical derivation of fidelity for single resonant rotors as well as for ensembles being averaged over quasi-momentum is purely quantum mechanical [33]. As a further major point, we present an overview of a possible experimental realisation for the measurement of fidelity for δ -kicked atoms [34, 35, 36]. The chapter concludes with the derivation of ϵ -classical phase space, an important tool which we will need in the following chapters.

In **chapter 3**, a range of interesting phenomena in the vicinity of the fundamental quantum resonance is displayed, as obtained by numerical simulations. Furthermore, a quantum-classical correspondence is drawn by calculating the corresponding classical fidelity by use of the ϵ -classical standard map.

Chapter 4 presents a new analytical access developed in this thesis. By using a semi-classical approximation, it is possible to recover the result for the resonant rotor in exact quantum resonance as obtained in chapter 2 from the viewpoint of ϵ -classical phase space. From this result, we derive a formula for the behaviour of resonant and near-resonant rotors for small detunings from quantum resonance conditions, which successfully mirrors almost all the crucial features of the plots obtained by exact quantum simulations.

Chapter 5 concludes with a brief summary of the results that have been obtained and gives an outlook on further prospects and work to be done on this topic.

The appendices contain formulae and derivations which are used in this thesis.

Chapter 2

Preliminaries

In this chapter, we introduce both experimental and theoretical methods and review known results on which the research of chapter three and four is based. We introduce the modelling of our atomic system by the driven rotor in detail. Furthermore, an overview of the relevant phenomena occurring in this system is given. Of those phenomena, we shall especially make use of the already mentioned quantum resonances.

Another important topic is the behaviour of fidelity for the δ -kicked rotor at exact quantum resonance, which will be calculated explicitly both for single rotors and for ensembles. Furthermore, we will introduce a pseudo-classical phase space of the quantum mapping close to resonance (as the Standard Map is to the quantum mapping itself).

2.1 The δ -kicked rotor

The model

The fairly simple but important model of the δ -kicked rotor will be discussed in both its classical and quantum mechanical treatment. While the classical kicked rotor is helpful in understanding the transition into classical chaos [37], the quantum kicked rotor is also a powerful theoretical tool which can be used to provide a good local approximation for complex quantum systems [38], e.g. in the case of dynamical localisation for Rydberg atoms in microwave fields [39, 40, 41].

What distinguishes the quantum kicked rotor from its classical counterpart is its discrete spectrum and its number of parameter (two for the quantum case, only one for the classical case). This is important to know in order to retrace the quantum trajectories to the well-known *Standard Map* (also called *Chirikov-Taylor Map*), as we will do later, using only one parameter instead of two (as is the case for the quantum kicked rotor, where both kicking strength and the repetition rate of the kicks play an independent role). The Standard Map is the classical analogue of the quantum evolution of the δ -kicked rotor and displays regular, chaotic, and mixed dynamics for different parameter regimes, inspiring a broad spectrum of research topics [42, 43, 44]. In the following, we will briefly derive the Standard Map and give examples for the different dynamical behaviour.

The Hamiltonian for a kicked particle consists of a free motion part, where there is

no external influence acting, and the periodic kicks, which are experimentally realised by a pulsed optical lattice with maximal depth of potential V_0 . The time between two subsequent pulses is the period $\tilde{\tau}$. The Hamiltonian for a particle with mass m , momentum p and space coordinate x reads:

$$H'(t) = \frac{p^2}{2m} + V_0 \cos(2\pi \frac{x}{a}) \sum_{j=-\infty}^{\infty} \delta(t - j\tilde{\tau}), \quad (2.1)$$

where a is the lattice constant. We will make use of experimentally meaningful units, depicting our variables in terms of the characteristic recoil momentum $k_r = \frac{\pi}{a}$ for the lattice as well as the recoil energy $E_r = \frac{k_r^2 \hbar^2}{2m}$ (the experimental units are based on quantum-mechanical variables). By performing variable transformations

$$k = \frac{V_0 T}{\hbar}, \quad \theta = 2k_r \text{ mod } 2\pi, \quad P = \frac{p}{2k_r \hbar}, \quad \tau = \frac{8E_r T}{\hbar} \tilde{\tau}, \quad (2.2)$$

the Hamiltonian can be written in the much clearer dimensionless form:

$$H(t) \equiv \frac{H'(t)}{8E_r} = \frac{P^2}{2} + k \cos(\theta) \sum_{j=-\infty}^{\infty} \delta(t - j\tau). \quad (2.3)$$

T in the renormalisation is the Talbot time (actually, any characteristic time of the system would do here). Make note that k is not the momentum here, but the force. By using the Euler-Lagrange equations of motion,

$$\dot{P} = -\frac{\partial H(P, \theta; t)}{\partial \theta} = k \sin(\theta), \quad (2.4)$$

$$\dot{\theta} = \frac{\partial H(P, \theta; t)}{\partial P} = P, \quad (2.5)$$

one can relate P and θ immediately before the n th kick (notation: P_n, θ_n) recursively to P and θ before the $(n+1)$ th kick. Since the rotation is continuous, the rotation angle is not changed by the kicks, only by moving freely in between for a period τ . P is not changed by the free motion and the change induced by the kicks can be derived by integrating the second equation of motion. Thus, the following iteration is found:

$$\begin{aligned} P_{l+1} &= P_l + k \sin \theta_l, \\ \theta_{l+1} &= \theta_l + \tau P_{l+1} \quad \text{mod } 2\pi. \end{aligned} \quad (2.6)$$

This map is the afore mentioned Standard Map, already expressed in dimensionless action-angle variables. There are two control parameters, namely τ and k . By defining a new P by substituting $\frac{P}{\tau}$, we obtain a new pair of equations which show periodicity in θ and p very nicely:

$$\begin{aligned} P_{l+1} &= P_l + k\tau \sin \theta_l, \\ \theta_{l+1} &= \theta_l + P_{l+1} \quad \text{mod } 2\pi. \end{aligned} \quad (2.7)$$

We have already defined θ as 2π -periodic, but P now also turns out to be periodic by 2π - the equations do not change by adding multiples of 2π to P . We are thus able to plot a phase space cell of this size as representative of the whole phase space. We start

out with 80 starting points with different initial momentum and $\theta = \pi$. Iterating 500 times and plotting each trajectory, we obtain phase space portraits [45] of the Standard Map (see Fig. 2.1).

The product $k\tau$, also known as “stochasticity parameter” K , can be varied to observe the transition from regular behaviour to chaotic dynamics in phase space. For $K \simeq 1$ (see [2]), a critical value is reached and the invariant curves are starting to dissolve. For large K , all regular areas are destroyed, and only chaos remains.

If we now want to describe the quantum dynamics of a particle with the same (but quantized) Hamiltonian, we have to rescale the system. Since we want to keep the Standard Map as the classic analogue to our quantum mapping, we have to rescale τ and k and, as it turns out, P as well. Our unitary Floquet operator (being the ordinary time-evolution operator over one period) reads

$$\widehat{U} = e^{-\frac{i}{\hbar}[k \cos(\hat{\theta}) + \int_0^\tau dt \hat{P}^2/2]} = e^{-\frac{i}{\hbar}[k \cos(\hat{\theta}) + \tau \hat{P}^2/2]}. \quad (2.8)$$

In order to keep the classical stochasticity parameter constant, we have to work Planck’s constant into k and τ , in a way that the semiclassical limit is reached while keeping the classical equivalent constant. We therefore define

$$P' = \frac{P}{\hbar}, k' = \frac{k}{\hbar}, \tau' = \tau \hbar, \quad (2.9)$$

and have the quantum mapping

$$\widehat{U}' = \widehat{U} = e^{-ik' \cos(\hat{\theta}) - i\tau' \hat{P}'^2/2}. \quad (2.10)$$

The semiclassical limit then corresponds to $k \rightarrow \infty$ and $\tau \rightarrow 0$ [26].

The evolution operator yields the dynamics for one period, including free motion (\hat{P}'^2 -term) and the kick (k' -term). In order to look at the evolution of the wave function over time, \widehat{U} has to be applied a discrete number of times (time here is discretized simply by taking the number of periods, i.e. kicks).

$$|\psi(t)\rangle = \widehat{U}^t |\psi_0\rangle \quad (2.11)$$

Numerically, this is implemented by first defining the initial state in momentum representation and applying the free motion part of the Floquet operator. Then we make use of the Fourier transformation to change into coordinate space, where we can directly multiply the second part of the operator. This constitutes the most elegant and by far the fastest way of calculating the time-evolved wave function for the δ -kicked rotor for localized initial conditions and not too large times [46]. For the investigations in this thesis, Fortran90 was used to implement the algorithms, and more than one function was implemented following examples from [47].

As already mentioned in the introduction, the main difference between the δ -kicked rotor (DKR) and kicked atoms in experiments lies in their trajectories: Originating from the pendulum [14], the kicked rotor moves on a circle, whereas kicked atoms in an optical lattice do not know such a boundary (see Fig. 2.2).

However, it is possible to retrace the description of kicked atoms to the space periodic motion of the kicked rotor, thanks to the periodic potential of the standing wave (a trick often used, e.g. in solid state physics). In order to perform this transformation,

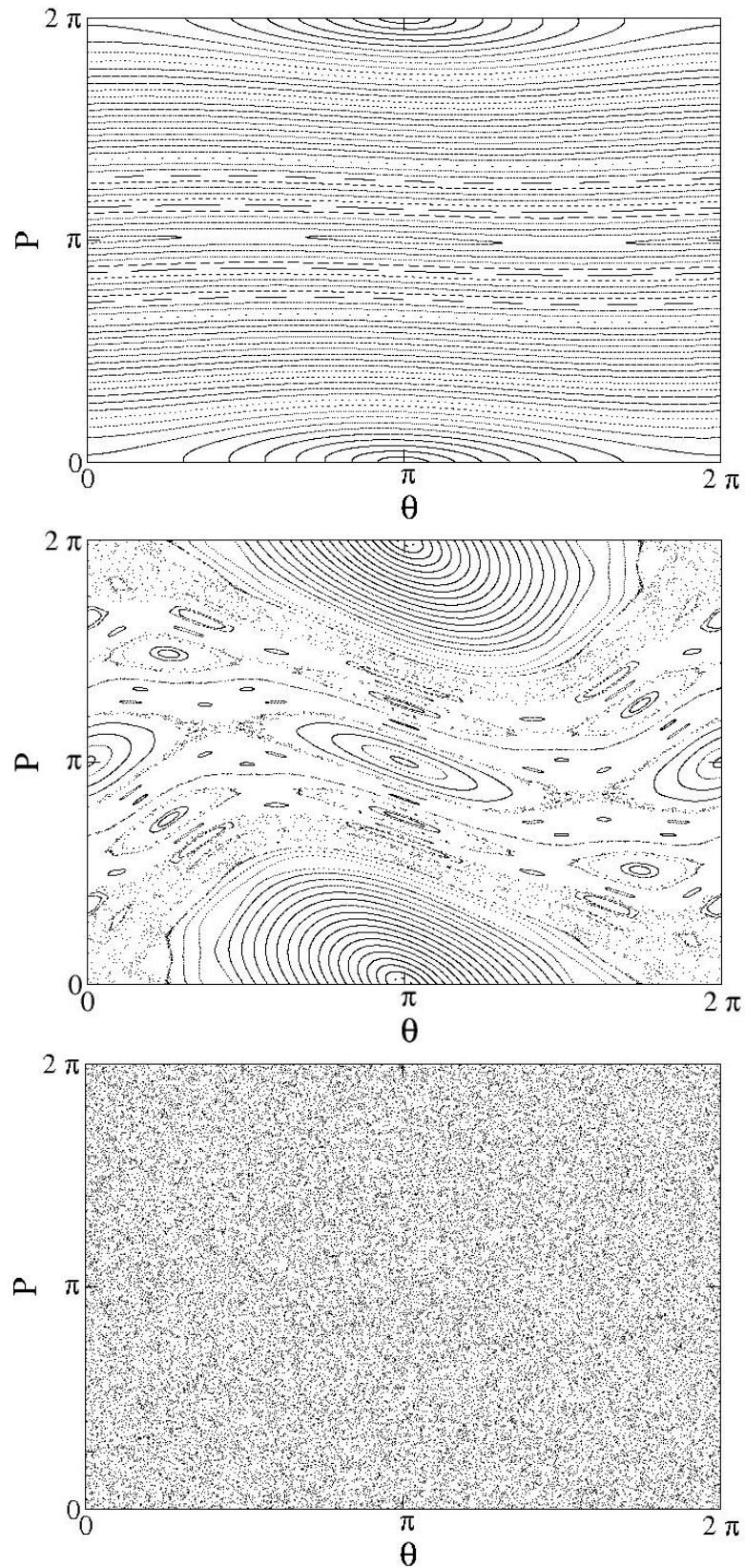


Figure 2.1: Illustration for regular ($K = 0.1$), mixed ($K = 1$), and chaotic ($K = 10$) behaviour of the Standard Map. We use 80 equidistant starting points along $\theta = \pi$ and iterate 500 times, resulting in 40000 points per picture.



Figure 2.2: Illustration of the difference in motion between the kicked rotor in theory and experiment.

we have to remember *Bloch's theorem*, which asserts that any wave function can be written as a Bloch wave, a product of a plane wave $e^{i\beta x}$ and a periodic wave function $\psi_\beta(x)$, assuming that the system is invariant under discrete translations:

$$\psi(x) = e^{i\beta x} \psi_\beta(x), \quad \psi_\beta(\pi) = \psi_\beta(-\pi). \quad (2.12)$$

Taking into account the spacing of the optical lattice a (for which the Hamiltonian of our system is periodic), we find β constricted to the Brillouin zone $[-\frac{\pi}{a}, \frac{\pi}{a}]$. By using an appropriate scaling to dimensionless units, we can ascertain that β lies between 0 and 1 and thus constitutes the fractional part of the momentum. It is a constant of motion (see above) and is also called *quasimomentum*. The total momentum then reads

$$P' = n + \beta, \quad n \in \mathbb{N}, \quad \beta \in [0, 1]. \quad (2.13)$$

A pair of wave functions $\psi_\beta(x)$ with identical β , but different kicking strength k' will be called β -rotor in the following.

In general, the wave packet of a particle will consist of a superposition of Bloch waves:

$$\psi(x) = \int_0^1 d\beta e^{i\beta x} \psi_\beta(x). \quad (2.14)$$

Here, the crucial importance of the quasimomentum is clearly visible. Taking all kinds of β , only very few will show resonant motion (see “quantum resonances” below) and the behaviour of the wave packet will be largely determined by the bulk of nonresonant rotors. Our motion is thus very much influenced by the fact that atoms in experiments move on a line and not on a circle. This difference is also illustrated by the new evolution operator. Inserting Eq. (2.13) into the Floquet operator and defining an angular momentum operator $\hat{N} = -i \frac{d}{d\theta}$ (as the conservation of β suggests), we obtain:

$$\hat{U}_\beta = e^{-ik' \cos \hat{\theta}} e^{-i \frac{\tau'}{2} (\hat{N} + \beta)^2} = e^{-ik' \cos \hat{\theta}} e^{-i \frac{\tau'}{2} (\hat{N}^2 + 2\hat{N}\beta + \beta^2)}. \quad (2.15)$$

The β^2 -part cancels out when calculating expectation values like the fidelity and can thus be neglected. The Floquet operator of Eq. (2.15) therefore differs from the original Floquet operator (2.10) for the kicked rotor by a phase $2\hat{N}\beta$.

Since all the relevant general rescalings have been performed by now, we shall return to the use of variables without dashes in order not to complicate the notation. Of course,

the variables will still refer to the rescaled quantities.

Quantum resonances

There are two relevant frequencies for kicked atoms: The characteristic frequency of the system, namely the atomic recoil frequency ($\frac{E_r}{\hbar}$), which is determined by the parameters of the standing wave, and the repetition rate of the pulses ($\frac{1}{\tau}$). If these happen to coincide, there is no phase shift in between different kicks and we find a regime of enhanced energy transport [17] which is otherwise suppressed by dynamical localisation [48, 49]. A number of subsequent kicks consequently have the same result as one kick with the added kicking strengths of all the kicks. We find quadratic energy growth (see Fig. 2.3 and Eq. (2.16)). This phenomenon has since been confirmed experimentally [50].

Assuming quantum resonance conditions, which will be derived in the next paragraph, results in a match of both the aforementioned frequencies. The mean energy can be calculated easily by taking the expectation value. We take a plane wave $\psi_0(\theta) = \frac{1}{\sqrt{2\pi}} e^{in_0\theta}$ with initial integer momentum n_0 as initial state (setting the quasimomentum to zero). We denote the discrete time, i.e. the number of kicks, as t . One obtains for the average energy:

$$\begin{aligned} E_{\text{av}}(t) &= \langle \psi(t, \theta) | -\frac{1}{2} \partial_\theta^2 | \psi(t, \theta) \rangle \\ &= -\frac{1}{2} \langle \psi_0^*(\theta) | \hat{U}^{-t} \partial_\theta^2 \hat{U}^t | \psi_0(\theta) \rangle \\ &= -\frac{1}{8\pi^2} \int_0^{2\pi} d\theta e^{-in_0\theta} e^{ikt \cos(\theta)} \partial_\theta^2 [e^{-ikt \cos \theta} e^{in_0\theta}] \\ &= \frac{k^2 t^2}{4} + \frac{n_0^2}{2}. \end{aligned} \quad (2.16)$$

Independently of the value of initial momentum, we find quadratic energy growth. If we used a Gaussian wave packet instead of a plane wave, there would be additional factors and the behaviour of energy growth would be obscured (since not only resonant rotors would take part).

What does this mean in terms of our notation, what are the conditions for ballistic spread occurring? The atomic recoil frequency is fixed. What we are able to change, though, is the time between subsequent kicks. As it was shown, the free motion part of the Floquet operator can be written in terms of integer (n) and fractional (β) part of momentum. Since any phase factors would have to originate in the motion between kicks, we set:

$$e^{-i\frac{\tau}{2}(n^2+2n\beta)} = 1. \quad (2.17)$$

Since we know $e^{-i\pi n^2}$ to be 1, it makes sense to take τ as a multiple of 2π . The first part with n^2 then gives the identity and only the second part (determined by β) matters. We shall calculate the result for the first two fundamental quantum resonances:

- $\tau = 2\pi$: $\beta = \frac{1}{2}$
- $\tau = 4\pi$: $\beta = \frac{1}{2}$ or the special case of the rotor on a circle, $\beta = 0$

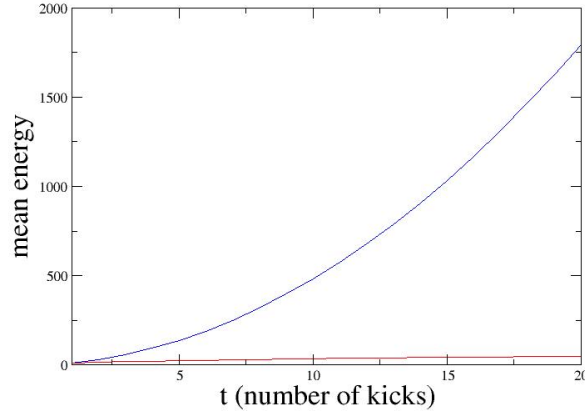


Figure 2.3: Energy growth in and out of quantum resonance. The blue curve displays unbounded ballistic energy growth for $\tau = 4\pi$, a fundamental quantum resonance, the red curve describes limited growth for $\tau = 1$.

In general, the following conditions define our quasimomentum if we want to explore quantum resonances:

Quantum resonance conditions:

$$\tau = 2\pi l \ (l \in \mathbb{N}), \beta = \frac{1}{2} + \frac{j}{l} \pmod{1}, \ j = 0, 1, \dots, l-1$$

For the rotor wave packet to spread ballistically, that is, for quadratic energy growth to occur, both conditions have to be fulfilled. If the condition in β is fulfilled, we speak of “resonant β -rotors”.

There exist also higher order resonances for periods consisting of fractions of π . The most general definition of quantum resonance conditions [17, 51] reads

$$\tau = 4\pi \frac{s}{q} \ (s, q \in \mathbb{N}), \beta = \frac{m}{2s}, \ 0 \leq m < s, \ s \in \mathbb{N}. \quad (2.18)$$

q here is called the *order* of the resonance. We can therefore identify our two examples as quantum resonances of second and first order respectively.

The quantum resonances of higher order are an interesting mathematical phenomenon [52], but they can almost always be neglected in practice, since they are difficult to resolve in experiments. However, as recent as 2006, experimental proof of the predicted higher-order resonances [18, 53, 54] was found [55, 56]. In the following chapters, though, we will only concentrate on fundamental quantum resonances.

Experimental realisation

The handling of cold ($T \approx 10\mu K$) and ultracold ($T \approx 100nK$) atoms has reached an unprecedented control in the last few years, allowing model Hamiltonians like the δ -kicked rotor to be realized almost to a point, without having to worry about impurities and decoherence [57]. Early experiments with cold atoms were realized at Oxford by

Summy et al. [58] and at NIST by Phillips et al. (who shared the Nobel Prize in 1997). In the last few years, the trend went towards ultracold atoms [59, 60], which permit a restriction of quasimomentum to a fraction of their range (up to 1%), allowing almost exact modelling of small intervals of β -rotors.

The idea of an experimental setup to realize the δ -kicked rotor system is conceivably simple. A cloud of atoms is exposed to a standing laser wave (see Fig. 2.4). Pulsing the laser in regularly spaced intervals creates the external driving force, with the free motion in between. Every time the laser is turned on, each atom experiences a force $\vec{F} = \vec{\nabla}V$, depending on the space coordinate. Sitting in one of the minima or maxima of the potential V , the force is zero, whereas it gets maximal in the points of inflexion. The final position distribution is easily obtained, as is the timing information, making it possible to calculate and evaluate momentum distributions, mean energy, and other observables of interest. For a detailed overview of experimental methods in atomic optics, see [19] and [61]. For their applications, it is worth it to look at [62, 63, 64] and [65].

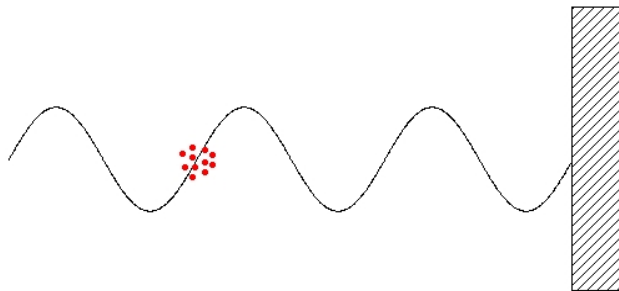


Figure 2.4: Experimental scheme for the realisation of the δ -kicked rotor model (here shown during a kick). A pulsed laser is reflected by a mirror, thus building a stroboscopic standing wave that gives the atoms a kick each time it is turned on.

2.2 Fidelity – a measure of stability in quantum dynamical systems

Definition, interpretation and significance

Fidelity is defined as the overlap of two initially identical wavefunctions which are subject to a slightly different time evolution operator. Rather than evaluating the exponential divergence of trajectories as it is done in classical systems, where the initial state is crucial to the evolution, we need to consider changes in the Hamiltonian for quantum systems. Due to unitarity, the distance $\langle\psi'|\psi\rangle$ between initial quantum states will not change by exposing them to the same evolution. This is why a different time evolution is chosen to define fidelity as a measure of stability in quantum dynamical systems:

$$F(t, \delta) = |\langle\psi|\psi_\delta\rangle(t)|^2 = \left| \langle\psi_0|U_0^\dagger U_\delta|\psi_0\rangle \right|^2 \quad (2.19)$$

where the propagator is given by the time-ordered exponential

$$U_\delta(t) = \widehat{T}e^{-\frac{i}{\hbar} \int_0^t dt' H_\delta(t')}, \quad H_\delta(t) = H_0(t) + \delta V(t), \quad (2.20)$$

where both H_0 and V are symmetric in time. δ is a small perturbation parameter ($\delta \ll 1$) in the evolution.

There are two different interpretations for the fidelity:

- The so-called “Loschmidt echo”: An initial state ψ_0 is evolved by an evolution operator with an undisturbed Hamiltonian H_0 to a time $\frac{t}{2}$, then it is evolved for another time $\frac{t}{2}$ using the slightly perturbed Hamiltonian H_δ . The overlap of the evolved state after time t with the original state ψ_0 is then interpreted as an echo.
- If two initially identical states are evolved with different Hamiltonians H_0 and H_δ , the overlap after a time t can be regarded as a measure of stability of the system.

Connection to the correlation function

There is a direct connection between fidelity decay and temporal correlation decay. We will derive it in detail here to underline that fidelity is nothing but a correlation function itself. The definitions and calculations in this paragraph closely follow [11]. By using the interpretation of fidelity as an echo, we define the echo-operator as the propagator in the interaction picture:

$$M_\delta(t) = U_0(-t)U_\delta(t). \quad (2.21)$$

This enables us to write the fidelity as the modulus square of the expectation value of $M_\delta(t)$:

$$F_\delta(t) = |\langle \psi_0 | U_0(-t)U_\delta(t) | \psi_0 \rangle|^2 = |\langle M_\delta(t) \rangle|^2. \quad (2.22)$$

We also transfer the perturbation operator into the interaction picture:

$$\tilde{V}(t) = U_0(-t)V(t)U_0(t) \rightarrow M_\delta(t) = \widehat{T}e^{-\frac{i}{\hbar} \delta \int_0^t dt' \tilde{V}(t')}. \quad (2.23)$$

$M_\delta(t)$ conveniently obeys the evolution equation with the effective Hamiltonian $\delta \tilde{V}(t)$,

$$\frac{d}{dt} M_\delta(t) = -\frac{i}{\hbar} \delta \tilde{V}(t) M_\delta(t). \quad (2.24)$$

For small ϵ , it is allowed to use a perturbative treatment. We therefore expand $M_\delta(t)$ in a Born series

$$M_\delta(t) = 1 + \sum_{m=1}^{\infty} \frac{(-i\delta)^m}{\hbar^m m!} \int_0^t dt_1 dt_2 \dots dt_m \widehat{T} \tilde{V}(t_1) \tilde{V}(t_2) \dots \tilde{V}(t_m), \quad (2.25)$$

and take the expectation value:

$$\langle M_\delta(t) \rangle = 1 - \frac{i\delta}{\hbar} \int_0^t dt' \langle \tilde{V}(t') \rangle - \frac{\delta^2}{\hbar^2} \int_0^t dt' \int_0^{t'} dt'' \langle \tilde{V}(t') \tilde{V}(t'') \rangle + O(\delta^3). \quad (2.26)$$

This leads to an approximation of the fidelity for small perturbations:

$$F_\delta(t) = 1 - \frac{\delta^2}{\hbar^2} \int_0^{t'} dt' \int_0^t dt'' C(t', t'') + O(\delta^4) \quad (2.27)$$

with the 2-point-correlation function of the perturbation

$$C(t', t'') = \langle \tilde{V}(t') \tilde{V}(t'') \rangle - \langle \tilde{V}(t') \rangle \langle \tilde{V}(t'') \rangle. \quad (2.28)$$

This approximation is valid for a regime where δ is appropriately small for the higher order terms not to interfere. It is known as the *linear response* expression for the fidelity. The only condition that has to be fulfilled is that $1 - F_\delta(t)$ has to be small, i.e., we have to have high fidelity. The expression is not necessarily restricted to small times. With this simple derivation of fidelity for small δ , the connection between fidelity and temporal correlation becomes clear: The faster the decay of $C(t', t'')$ augments as a function of $|t' - t''|$, the slower the fidelity decays and vice versa. This is one of the most important physical properties of quantum echo-dynamics.

For very short times (before the correlation function starts decaying), we only consider $C(0, 0)$, which causes the second part of the correlation function to drop out, and therefore always find quadratic decay (similar for time-independent H):

$$F(t) = 1 - \frac{\delta^2}{\hbar^2} \langle V^2 \rangle t^2 \quad (2.29)$$

This is an important result, since although there appear to be all kinds of fidelity decay for different systems, each decay starts out quadratically in the very beginning.

2.3 Kicked atoms in quantum resonance - a review

Fidelity for the kicked rotor at exact quantum resonance conditions has caused some commotion, since, unlike a lot of research on fidelity in different systems, fidelity for an ensemble of β -rotors averaged over quasimomenta shows an interesting effect on large timescales: It saturates. This was first discovered in [36] and has since been confirmed experimentally [35]. This behaviour is one of the few which can be calculated exactly, without any kind of semiclassical approximation.

In this section, we shall review these calculations, which are the basis for the research done in the vicinity of quantum resonances. However, we have to pay attention to the fact that the perturbation δ in this case is the difference in kicking strengths $\Delta k = k_2 - k_1$. We shall start with calculating fidelity for single β -rotors, for $\Delta k > 0$ and for the fundamental quantum resonances $2\pi l$. As initial state of a particle we will assume a plane wave with momentum $p_0 = n_0 + \beta$:

$$\psi_\beta(\theta) = \frac{1}{\sqrt{2\pi}} \delta(\beta - \beta_0) e^{in_0\theta}. \quad (2.30)$$

The form of the plane wave, composed of a δ -function and the translation to the integer momentum n_0 , originates in the form of the corresponding Fourier Transforms combined with Eq. (2.14). The time evolved wave function can then be calculated by applying the evolution operator (2.15):

$$\psi_\beta(t, \theta) = (\hat{U}_\beta)^t \psi_\beta(\theta), \quad (2.31)$$

with

$$\widehat{U}_\beta = e^{-ik \cos(\theta)} e^{-i\pi(2\beta+1)l\widehat{N}}. \quad (2.32)$$

Here, we have already used the identity $e^{-i\pi n^2 l} = e^{-i\pi n l}$ for the eigenvalues n of the angular momentum operator \widehat{N} . The second part is nothing but a translation in θ -space (see standard text books for quantum mechanics, e.g. [66]):

$$e^{-i\pi(2\beta+1)l\widehat{N}}\psi_\beta(\theta) = \psi_\beta(\theta - \pi l(2\beta + 1)). \quad (2.33)$$

By iterating the application of the t translations and the following kicks, we find

$$\psi_\beta(t, \theta) = (\widehat{U}_\beta)^t \psi_\beta(\theta) \quad (2.34)$$

$$= \exp \left\{ -ik \sum_{j=0}^{t-1} \cos(\theta - j\pi l(2\beta + 1)) \right\} \psi_\beta(\theta - \pi l(2\beta + 1)). \quad (2.35)$$

Denoting $\pi l(2\beta + 1) := z$, we can write the sum as

$$\sum_{j=0}^{t-1} \cos(\theta - jz) = |W_t| \cos(\theta + \arg(W_t)) \quad (2.36)$$

with $W_t = \sum_{j=0}^{t-1} e^{-ijz}$. This becomes clear when writing the cosine as sum of complex exponentials, factor out the $|W_t|$ and write the remaining complex exponentials once more as a cosine.

In order to calculate fidelity for one β -rotor, we sum two wavefunctions with different kicking strengths over all possible integer momenta:

$$F_\beta(t, k_1, k_2) = \left| \sum_{n=-\infty}^{\infty} \psi_\beta^*(t, n, k_1) \psi_\beta(t, n, k_2) \right|^2. \quad (2.37)$$

To calculate this explicitly, it is useful to write $\psi_\beta(\theta)$ in momentum representation:

$$\langle n | \widehat{U}_\beta^t \psi_\beta \rangle = \frac{1}{\sqrt{2\pi}} \int_0^{2\pi} d\theta e^{-in\theta - ik|W_t| \cos(\theta + \arg(W_t))} \psi_\beta(\theta - tz). \quad (2.38)$$

Shifting θ to $\theta + \arg(W_t)$, one obtains the simplified expression:

$$\langle n | \widehat{U}_\beta^t \psi_\beta \rangle = \frac{1}{\sqrt{2\pi}} e^{in \arg(W_t)} \int_0^{2\pi} d\theta e^{-in\theta - ik|W_t| \cos(\theta)} \psi_\beta(\theta - tz - \arg(W_t)). \quad (2.39)$$

Now we insert this into the fidelity and use the Fourier transform of the δ -function to calculate the fidelity as follows:

$$\begin{aligned} F_\beta(t, k_1, k_2) &= \left| \sum_{n=-\infty}^{\infty} \frac{1}{(2\pi)^2} \int_0^{2\pi} d\theta \int_0^{2\pi} d\theta' e^{-in(\theta - \theta') - i|W_t|(k_1 \cos(\theta) - k_2 \cos(\theta'))} \right|^2 \\ &= \left| \frac{1}{2\pi} \int_0^{2\pi} e^{-i|W_t|(k_1 - k_2) \cos(\theta)} \right|^2. \end{aligned} \quad (2.40)$$

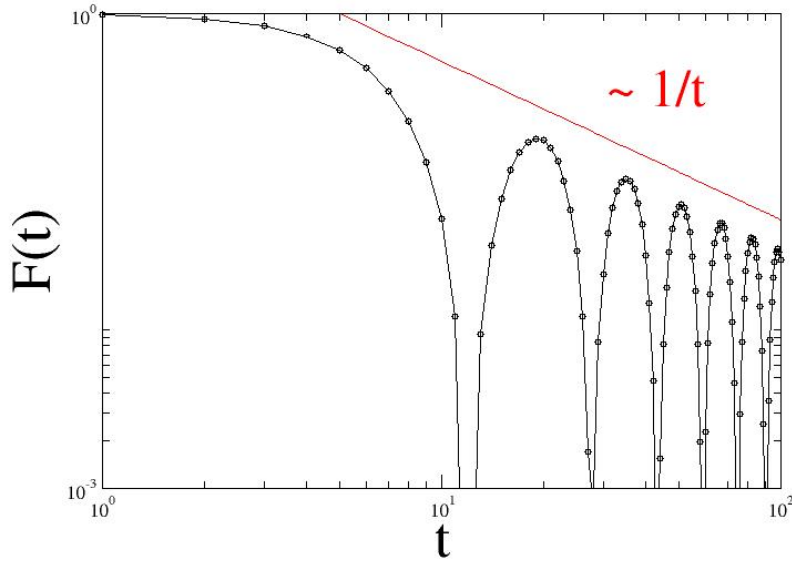


Figure 2.5: t^{-1} -decay of fidelity for the δ -kicked rotor, numerically calculated with $k_1 = 4.0$ and $k_2 = 4.1$.

Making use of (A.1), we obtain the final result for the single β -rotor

$$F_\beta(t) = J_0^2(|W_t|(k_2 - k_1)), \quad (2.41)$$

which nicely agrees with the numerical simulations (Fig. 2.5).

If both kicking strengths k_1 and k_2 are equal, fidelity does not decay, but stays constant at $F_\beta = 1$. If the quasimomentum fulfills quantum resonance conditions (that is $\beta = \frac{1}{2} + \frac{j}{l} \pmod{1}$, $j = 0, 1, \dots, l-1$), then $|W_t| = t$. We can now use the asymptotic approximation (A.2) to calculate the fidelity for resonant rotors for large times:

$$F_\beta(t) \simeq \frac{2}{\pi t \Delta k} \cos^2\left(t\Delta k - \frac{\pi}{4}\right). \quad (2.42)$$

The overlap decays like a power-law $\sim t^{-1}$ while oscillating, as can be seen in Fig. 2.5. The long-time approximation already takes hold after only few kicks, yielding a very good approximation of the numeric data.

We are now able to calculate the fidelity for the full ensemble of β -rotors. Full ensemble fidelity for a uniform distribution of quasimomenta is defined and computed as

$$\begin{aligned} F(t, k_1, k_2) &= \left| \sum_{n=-\infty}^{\infty} \int d\beta \psi_\beta^*(t, n, k_1) \psi_\beta(t, n, k_2) \right|^2 \\ &= \left| \int_0^1 d\beta J_0(|W_t|(k_2 - k_1)) \right|^2, \end{aligned} \quad (2.43)$$

thus averaging over an incoherent ensemble of β -rotors. It is very important to mark that the modulus square here is taken only after the averaging has been performed,

which is in accordance with the density operator definition of fidelity as it is used in statistical mechanics. Several years before, the analytical results for full fidelity that we will review in this chapter were supposed to be measured in an experimental setup in Oxford by d'Arcy et al. [67], but unfortunately, they summed incoherently over the quasimomenta – resulting in data with no assessable analytical equivalent. Without the modulus square only being taken in the end, one could not derive the following results.

Averaging over an incoherent ensemble of atoms yields:

$$F(t, k_1, k_2) = \left| \int_0^1 d\beta J_0(|W_t|\Delta k) \right|^2 \quad (2.44)$$

$$= \left| \int_{-\pi}^{\pi} \frac{dx}{2\pi} J_0(\Delta k \sin(tx) \csc(x)) \right|^2 \quad (2.45)$$

$$= \left| \int_{-\pi}^{\pi} \frac{dx}{4\pi^2} \sum_{j=0}^{t-1} \frac{2\pi}{t} J_0(\Delta k \sin(x) \csc(xt^{-1} + 2\pi jt^{-1})) \right|^2. \quad (2.46)$$

This describes the behaviour of fidelity for β -averaged ensembles accurately at all times. It is also possible in this case to find a long time approximation, because for $t \rightarrow \infty$ and $\frac{2\pi j}{t} \rightarrow \alpha$, the sum over j approximates the integral over α , resulting in

$$F(t \rightarrow \infty) \rightarrow \left| \frac{1}{(2\pi)^2} \int_{-\pi}^{\pi} dx \int_0^{2\pi} J_0(\Delta k \sin(x) \csc(\alpha)) \right|^2 \quad (2.47)$$

$$= \frac{1}{(2\pi)^2} J_0^2\left(\frac{\Delta k \csc(\alpha)}{2}\right), \quad (2.48)$$

where (A.3) was used to derive the latter expression. The asymptotic value for the fidelity therefore only depends on Δk , which is clearly visible in Fig. 2.6.

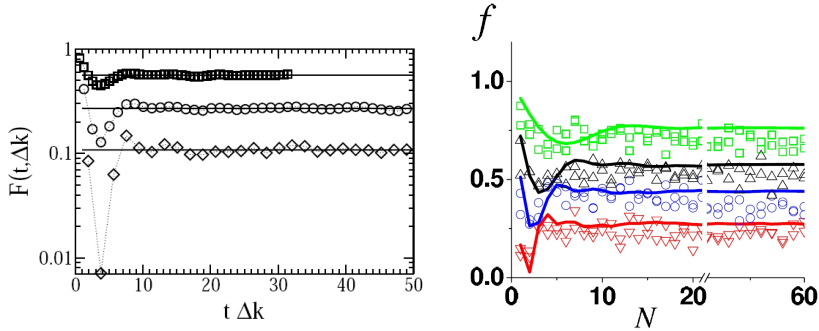


Figure 2.6: Saturation of fidelity at quantum resonance, on the left as calculated numerically in [33] and on the right as measured in the experiment at Harvard by Prentiss et al. [35]. In the first picture, the fidelity is plotted against the product Δkt for different values of Δk , so the dip is always at the same x-coordinate. In the second picture, fidelity is denoted as f and plotted against the discretized time, namely the number of kicks N , which leads to the dips of the different Δk -curves being dislocated.

After a small dip, saturation sets in and gives different, but constant values for different Δk . The initial decay is determined by the resonant β -rotors. However, those soon

surrender to the bulk of nonresonant rotors leading to saturation. There have been predictions of fidelity plateaus in other systems in the past, but those were mostly derived by semiclassical methods and unstable for larger times. The saturation of fidelity found for the kicked rotor is the first stable fidelity plateau that is accounted for so far.

As we have seen, fidelity in quantum resonance can nicely be calculated quantum-mechanically, but what about small detunings ϵ from $2\pi l$? This has also been investigated numerically in a rudimentary way in [36]. What was found is that for small perturbations ϵ in the kicking period τ , the saturation previously seen is destroyed and the fidelity globally starts decaying (see Fig. 2.7):

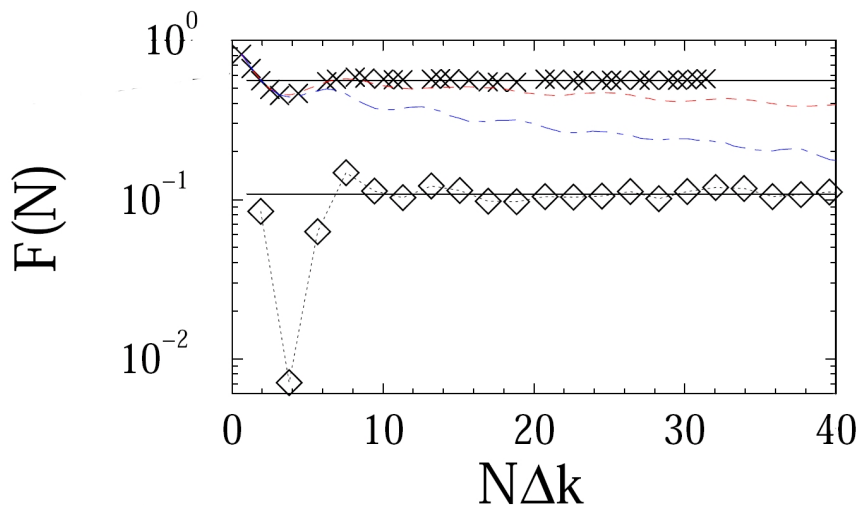


Figure 2.7: Decay of the fidelity for the kicked rotor at $\tau = 2\pi + \epsilon$, $k_1 = 0.6\pi$ and $k_2 = 0.8\pi$, taken from [36]. These values of the kicking strengths will be used frequently in this thesis, since they correspond to the original kicking strengths used in the Oxford experiment [24].

Unfortunately, it is impossible to fit the decay to some exponential or power-law decay, rendering further explorations difficult. It is at this point that we will start our numerical investigations in the next chapter.

The fascinating thing about the fidelity for full ensembles which we have calculated above is the fact that it is directly accessible in experiments. We will give an overview of the experiment proposed in [36], which is also close to the experimental setup at Harvard that first measured the predicted fidelity saturation. The experimental setup is given in Fig. 2.8. It was inspired by a proposal for an experimental realisation of the δ -kicked harmonic oscillator using an ion trap [68, 69].

The idea of the experiment is to use atoms with a forked substructure, such as the hyperfine structure for cesium atoms, where the $6^2S_{1/2}$ ground state is split into ($F = 3, m_F = 0$) and ($F = 4, m_F = 0$). A $\frac{\pi}{2}$ Ramsey pulse with a frequency suited to the energy level difference $E_2 - E_1$ produces an equal population of the two levels, operating on the initial state where all atoms are in the $F = 3$ state. After letting the particles evolve for a time t according to the δ -kicked rotor Hamiltonian, a second $\frac{\pi}{2}$ Ramsey pulse with a phase shift ϕ in reference to the first one returns the evolved states to their measurable ground states.

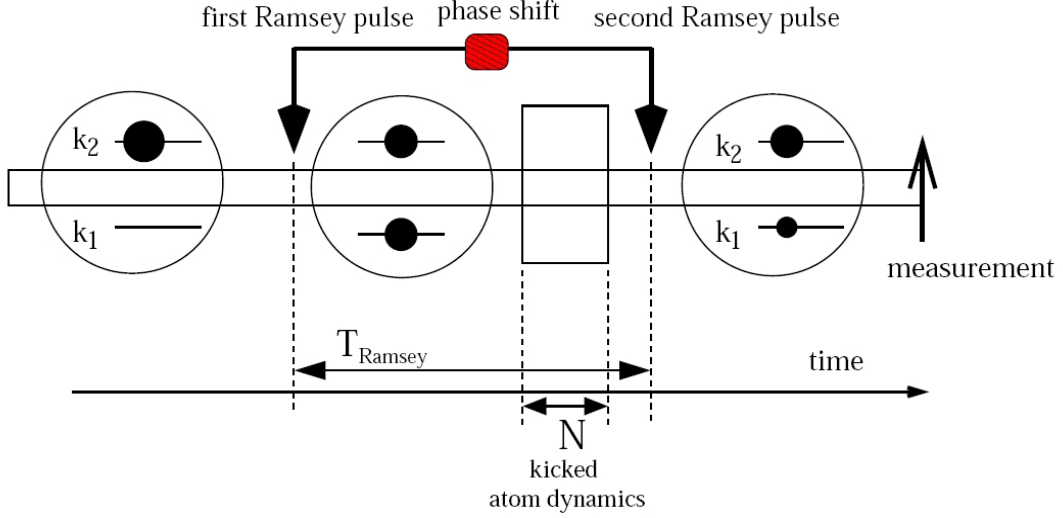


Figure 2.8: Experimental setup as proposed for the measuring of ensemble fidelity for the δ -kicked rotor, taken from [36]. The atomic hyperfine structure was used to prepare the atom in two equally populated sublevels by means of a Ramsey pulse. Since the two levels couple differently to the external driving, their evolution during time t differs and this difference is measurable after reprojected onto the two levels by a second Ramsey pulse.

One can express a Ramsey pulse with phase ϕ as:

$$\widehat{R}_\phi \begin{bmatrix} \psi_1 \\ \psi_2 \end{bmatrix} = \frac{1}{\sqrt{2}} \begin{bmatrix} 1 & e^{i\phi} \\ e^{-i\phi} & 1 \end{bmatrix} \begin{bmatrix} \psi_1 \\ \psi_2 \end{bmatrix}. \quad (2.49)$$

The Ramsey pulses are assumed to happen instantaneously at the beginning and the end of the kicked particle dynamics section (see Fig. 2.8). The phase between the two Ramsey pulses being ϕ , we can then describe the full evolution (including the kicked particle dynamics and the two Ramsey pulses) by the evolution operator

$$\widehat{U}_{t,\phi} = \widehat{R}_\phi \widehat{W}_t \widehat{R}_0, \quad (2.50)$$

which gives for the evolved states (assuming the initial states as $\psi_1 = 0$ and $\psi_2 = \psi$):

$$\psi_{1,\phi} = \frac{1}{2} e^{-iE_1 t} (\widehat{U}_{1,t} + e^{-i((E_2-E_1)t-\phi)} \widehat{U}_{2,t}) \psi, \quad (2.51)$$

$$\psi_{2,\phi} = \frac{1}{2} e^{-iE_2 t} (-\widehat{U}_{1,t} e^{-i((E_2-E_1)t-\phi)} + \widehat{U}_{2,t}) \psi. \quad (2.52)$$

What is measured in the experiment is the momentum distribution, in general for the lower state, which can be easily calculated:

$$P(p, t, \phi) = \frac{1}{4} |\langle p | \widehat{U}_{1,t} \psi \rangle|^2 + \frac{1}{4} |\langle p | \widehat{U}_{2,t} \psi \rangle|^2 + \frac{1}{2} \Re(e^{-i((E_2-E_1)t-\phi)} \langle \widehat{U}_{1,t} \psi | p \rangle \langle p | \widehat{U}_{2,t} \psi \rangle). \quad (2.53)$$

To obtain the total probability, it is necessary to integrate over p , which yields the probability for the particles to be in the lower level:

$$P(t, \phi) = \frac{1}{2} \left[1 + \Re \left(e^{-i((E_2-E_1)t-\phi)} \langle \widehat{U}_{1,t} \psi | \widehat{U}_{2,t} \psi \rangle \right) \right]. \quad (2.54)$$

This is already averaged over all the atoms of the experiment, i.e., over all quasimomenta, allowing us to derive the overlap of two evolved states with kicking strengths k_1 and k_2 from the result. In analogy to the statistical density operator definition of fidelity [33], it is possible to define the real part of $P(t, \phi)$ by the square root of the fidelity multiplied with a factor:

$$\Re \left[e^{-i((E_2 - E_1)t - \phi)} \langle \widehat{U}_{1,t} | \widehat{U}_{2,t} \psi \rangle \right] = \sqrt{F(t) \cos(\phi')}, \quad (2.55)$$

where ϕ' and ϕ differ by a constant shift. We have thus found the fidelity as a function of the total momentum probability. Using different values for ϕ , one can extract the fidelity as a function of time, which allows the analytical expressions above to be verified.

2.4 Underlying ϵ -classical phase space

Earlier in this chapter, the phenomenon of quantum resonance conditions has been described in detail and fidelity in the fundamental quantum resonance has been calculated explicitly. For the research done in the next two chapters, where we slightly deflect from resonance, we need to use a new description of the underlying phase space. In the original parameter regimes, we are deep in the chaotic regime ($k\tau \gtrsim 5$), but our effective Planck's constant τ is too big to resolve details. Therefore, we have to use a trick that has already been useful in the context of quantum accelerator modes for the δ -kicked rotor [27]. These calculations can also be found in [33, 28, 70] where ϵ -classical phase space was first derived by making use of the special combination $k|\epsilon|$ in the quantum kicked rotor.

We start out with the fundamental quantum resonances $\tau = 2\pi l$ ($l \in \mathbb{N}$) and take a look at their vicinity $\tau = 2\pi l + \epsilon$, with a small detuning ϵ . The idea is to map the quantum resonances to the classical nonlinear resonances of a similar model, thus producing a direct correspondence between quantum evolution and classical mapping. This classical mapping can further be retraced to the well-known Standard Map, as we shall see. The only difference to the quantum mapping and the Standard Map of the beginning of this chapter will be the effective Planck's constant: We will use ϵ instead of τ here in order to derive the iteration, which means that the "classical" limit here is not related to $\hbar \rightarrow 0$, but instead to $\epsilon \rightarrow 0$ (that is, approaching the resonance). This new effective Planck's constant also has the additional advantage of the resolution being improved vastly. The derived "classical" dynamics are baptized ϵ -classical in the following.

We start the semiclassical approximation by defining $I = |\epsilon|N = -i|\epsilon| \frac{d}{d\theta}$ and $k \rightarrow k|\epsilon|$, so that we can rewrite the free evolution part of the Floquet operator as

$$\begin{aligned} e^{-i\frac{\tau}{2}(n+\beta)^2} &= e^{-i\pi l n^2} e^{-i\frac{\epsilon}{2}n^2} e^{-i\tau n\beta} e^{-i\frac{\tau}{2}\beta^2} \\ &= e^{-i\pi l \frac{I}{|\epsilon|}} e^{-i\text{sign}(\epsilon) \frac{I^2}{2|\epsilon|}} e^{-i\tau\beta \frac{I}{|\epsilon|}} e^{-i\frac{\tau}{2}\beta^2}. \end{aligned} \quad (2.56)$$

We may once more drop the β^2 -part. As implied above, we now use ϵ as Planck's constant:

$$U_\beta(t) = e^{-\frac{i}{|\epsilon|} (\tilde{k} \cos(\theta) + \frac{1}{2} \text{sign}(\epsilon) I^2 + I(\pi l + \tau\beta))}. \quad (2.57)$$

Compared to Eq. (2.10), we find Eq. (2.57) to be the formal quantisation of the map:

$$\begin{aligned}\theta_{t+1} &= \theta_t \pm I_t + \pi l + \tau\beta \quad \text{mod } (2\pi), \\ I_{t+1} &= I_t + \tilde{k} \sin \theta_{t+1}.\end{aligned}\tag{2.58}$$

By a change of variables,

$$(J = \pm I + \pi l + \tau\beta, \vartheta = \theta + \pi(1 - \text{sign}(\epsilon)/2),$$

we get the well known Standard Map, which we will refer to as ϵ -classical Standard Map:

$$\begin{aligned}J_{t+1} &= J_t + \tilde{k} \sin \vartheta_{t+1}, \\ \vartheta_{t+1} &= \vartheta_t + J_t.\end{aligned}\tag{2.59}$$

In this notation, varying β from 0 to 1 is the same as scanning the phase space cell from π to 3π , so different β 's depict different sections of the ϵ -classical phase space. Depending on whether this makes for starting conditions on the resonance island in the Standard Map or not, we find librational or rotational (sometimes even with higher order resonances) motion. $\beta = \frac{1}{2}$ results in $J_0 = 2\pi$, which again gives the primary resonance island. For these resonant rotors ($\beta = \frac{1}{2}$), the trajectories are launched on the island itself, resulting in quadratic energy growth, as expected for the quantum resonances. The other values for β are symmetric around $\beta = \frac{1}{2}$, which is why only smaller values below 0.5 are plotted in Fig. 2.9. Therefore, the ϵ -classical approximation accounts for the quantum resonances in terms of the classical resonances of the Standard Map. The addition $\epsilon\beta$ to the starting conditions dislocates the center of the island by a small amount, but in most applications of ϵ -classics this is negligible.

For $\epsilon = 0$, this pseudoclassic approximation is trivially exact for all times. It is further valid only for very small values of ϵ ($\epsilon \ll 1$) and if the time scales are not exceptionally large (although this is also an automatic requirement imposed by the experiment). The ϵ -classic description has proven to be very accurate if these conditions are fulfilled. It is only spoiled by quantum effects such as tunneling on large time scales.

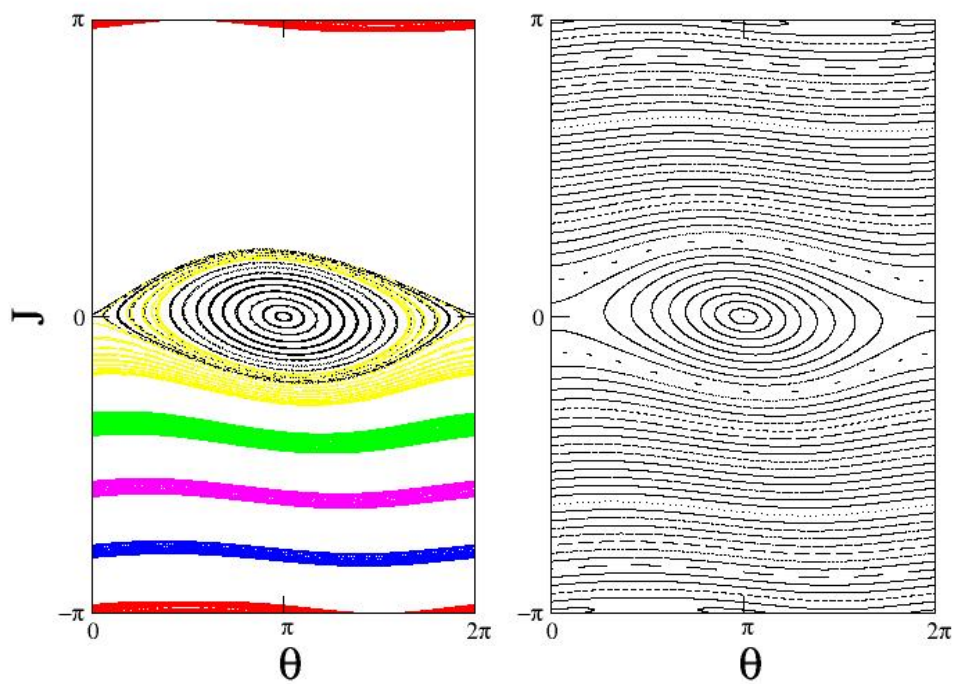


Figure 2.9: Phase space portraits for the map (2.59) with $k = 0.8\pi$ and $\epsilon = 0.05$. On the right is the ordinary Standard Map, on the left side single values of β partly reproduce it (red for $\beta = 0$, blue for 0.1, magenta for 0.2, green for 0.3, yellow for 0.4, black for 0.5).

Chapter 3

Numerical investigation of fidelity close to quantum resonance

In the last chapter, we have reviewed numerical and analytical observations of the behaviour of single β -rotors and ensembles at exact quantum resonance. This is only possible if the wave function is known analytically, which is very rarely the case. As soon as we leave the resonance even by a small deviation ϵ , it is not possible anymore to find an analytic expression for the wave function as time evolves. In this chapter, we will therefore focus on presenting numerical simulations showing the behaviour of kicked atoms in the immediate vicinity of quantum resonance. Without loss of generality, we concentrate our efforts on the fundamental quantum resonance (with dimensionless kicking period $\tau = 2\pi$), which means that our resonant rotors have quasimomentum $\beta = \frac{1}{2}$ (see also section 2.1).

At the beginning of this chapter, numerical results from quantum simulations showing a selection of interesting phenomena for the investigated parameter range are presented. We discuss in detail the dominant behaviour of the resonant rotors in the ensemble calculations. The resonant rotors turn out to be the most interesting rotors for further investigations since they even determine the behaviour of fidelity for full ensembles. We shall first calculate their behaviour numerically and later model them in an analytic expression (see chapter 4). Finally, we investigate the quantum-classical correspondence of fidelity for our modelling system. In order to do this, we define a classical fidelity which basically consists of counting the trajectories of the pseudoclassical ϵ -Standard Map (2.59) which return to some defined starting area. Comparing quantum to classical fidelity will then help to identify where the observed phenomena originate from.

3.1 Quantum calculations of fidelity close to resonance

3.1.1 Behaviour of fidelity for the full ensemble in β

As we observed in Fig. 2.7, fidelity for an averaged ensemble of β -rotors (with β uniformly distributed between 0 and 1) starts decaying as soon as we depart from exact quantum resonance. Taking a closer look, however, there is more to their behaviour than just decay: We observe characteristic fluctuations (see Fig. 3.1). The Fourier

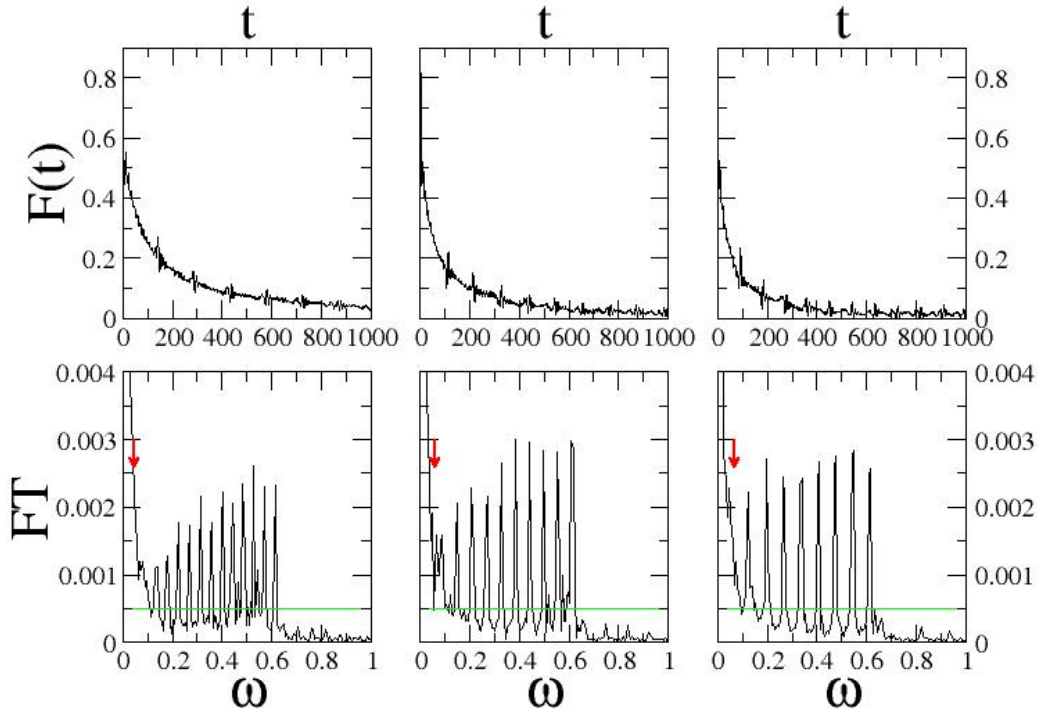


Figure 3.1: *Upper panels:* Fidelity close to resonance for an ensemble of 1000 β -rotors with kicking strengths $k_1 = 0.8\pi$ and $k_2 = 0.6\pi$ and $\epsilon = 0.04$ (*left*), $\epsilon = 0.07$ (*middle*), and $\epsilon = 0.1$ (*right*). β is uniformly distributed between 0 and 1. For full ensembles, we discover fluctuations with a characteristic frequency (marked by red arrows) and its higher harmonics, as can be seen by looking at the Fourier transform (*lower panels*). The spacing of the oscillations does obviously depend on ϵ . An estimate of the mean noise threshold is plotted as a green line.

Transform of the fidelity shows a spectrum with regularly spaced peaks. In order to decide which features of the Fourier Spectrum are of interest to us, we have to estimate the noise threshold – otherwise, some of the most interesting features of Fourier Spectra might turn out to be nothing but noise. To estimate the average noise, we look at the Fourier Transform of fidelity after subtracting the characteristic oscillations. The average of the remaining points of the Fourier Spectrum are displayed as the mean noise threshold in Fig. 3.1.

For large times, the spacing between the largest oscillations in the fidelity represents a period T , which corresponds to the smallest peak in the Fourier Transform. This peak is unfortunately not resolved due to its small size compared to the offset of the Fourier Transform (which is an inherent feature of the numeric realisation). We did analogue computations for a wide range of parameters ($0.01 < \epsilon < 0.2$ and $0.8 < k_1, k_2 < 5.0$), obtaining similar oscillations dependent on the values of ϵ , k_1 , and k_2 . We can deduce from these observations that what we have found is essentially one characteristic frequency and its higher harmonics. But what kind of characteristic frequency could we possibly be observing?

In order to find an answer to that question, we will have to simplify our system. The Hamiltonian for a kicked particle is too complicated to analytically derive any characteristic frequencies. Using different arguments, we will first approximate the kicked atom by a pendulum, and then the pendulum by the harmonic oscillator. This will lead us to discover the time scales which are characteristic for our system.

In the following parts of this chapter, we heuristically use arguments based on such approximations, whereas in chapter 4 we heavily rely on them to derive analytical predictions for close to resonant rotors (in our case $\tau = 2\pi + \epsilon$, $\beta \approx 0.5$).

Keeping in mind that we can map the evolution near the quantum resonance to the ϵ -classical phase space of chapter 2, we find that the regular oscillations must come from rotors situated on the island. The island section, however, is similar to the phase space of the pendulum (see Fig. 4.2). This approximation will be illustrated in detail in chapter 4 (see Fig. 4.2). Here, it will have to suffice that the Hamiltonian for the kicked atoms, namely

$$H_1 = \frac{\dot{\theta}^2}{2} + k\epsilon \cos(\theta) \sum_{j=-\infty}^{\infty} \delta(t - j\tau), \quad (3.1)$$

can be approximated by a pendulum Hamiltonian. Their phase space is very similar close to the fixed point, allowing a satisfying approximation. The main difference consists in the change from discrete time to the continuum. This is done by Fourier analysing the Hamiltonian in terms of the kick perturbation:

$$k\epsilon \cos(\theta) \sum_{j=-\infty}^{\infty} \delta(t - j\tau) = k\epsilon \sum_{j=-\infty}^{\infty} \cos(\theta - 2\pi j\tau t), \quad (3.2)$$

where $k\epsilon$ is small. Using a time averaging in order to eliminate the discrete time steps, the higher frequencies can be neglected and only the term for $j = 0$ is significant (since only this term is exactly on the resonance island and generates ballistic energy growth, see Fig. 2.3). This approximation results in the pendulum Hamiltonian:

$$H_{2a} = \frac{\dot{\theta}^2}{2} + k\epsilon \cos(\theta). \quad (3.3)$$

Displacing θ by π , we obtain a slightly modified pendulum Hamiltonian,

$$H_{2b} = \frac{\dot{\theta}^2}{2} - k\epsilon \cos(\theta), \quad (3.4)$$

from which we are now able to derive the harmonic oscillator by making use of a small angle approximation. We expand the cosine of θ around zero (which corresponds to the fixed point) and thus find as an approximation of second order in θ the harmonic oscillator with Hamiltonian

$$H_3 = \frac{\dot{\theta}^2}{2} + k\epsilon \frac{\theta^2}{2}, \quad (3.5)$$

where we have neglected the constant $k\epsilon$ (from the zeroth order of the expansion), since it has no significance when it comes to deriving equations of motion or expectation values like the fidelity. As already mentioned, this approximation is only valid for small angles θ , i.e., close to the fixed point.

ϵ	$T = 2\pi/\omega_{2b}$	$T_{measured}$
0.1	93.5	94 (± 2)
0.05	132.3	133 (± 2)
0.01	295.8	295 (± 2)

Table 3.1: Comparison of the periods of the calculated period T and the measured period from data like Fig. 3.1 for kicking strengths $k_1 = 0.8\pi$ and $k_2 = 0.6\pi$, and various ϵ . The agreement between both is excellent; the characteristic frequency is thus the beating frequency.

The harmonic oscillator, however, is a very simple system and has been investigated quite thoroughly in most textbooks on classical and quantum mechanics. Using the Hamilton-Jacobi equations, we can derive the equation of motion of a harmonic oscillator with frequency ω :

$$\frac{d^2\theta}{dt^2} = -\omega^2\theta. \quad (3.6)$$

This equation is solved by a plane wave with frequency ω . Comparing (3.6) with the equation of motion derived from (3.5), it follows that the harmonic oscillator approximation of ϵ -classics should yield a frequency $\omega = \sqrt{\epsilon k}$. As a consequence, a system consisting of two harmonic oscillators with kicking strength k_1 , respectively k_2 , is determined by two characteristic frequencies, namely the beating frequency ($\omega_1 - \omega_2$) and the sum of the characteristic frequencies of both systems ($\omega_1 + \omega_2$), where $\omega_i = \sqrt{\epsilon k_i}$. Keeping this in mind, the frequencies of the fluctuations which we observed can be identified with the beating frequency (baptized ω_{bf}):

$$\omega_{bf} = \omega_1 - \omega_2 = \sqrt{|\epsilon|}(\sqrt{k_1} - \sqrt{k_2}). \quad (3.7)$$

The frequency ($\omega_1 + \omega_2$) is too large for us to observe in our numerical calculations. The beating frequency can also be derived quantum mechanically. In order to do this, we write the initial state $\psi_0 = e^{in_0\theta}$ as a linear combination of the orthonormal set of stationary states $\{|\psi_n(\theta, t = 0)\rangle\} = \{|n\rangle\}$ of the quantum harmonic oscillator:

$$\psi_0 = \sum_n c_n \psi_n, \quad (3.8)$$

with coefficients $c_n = \int d\theta e^{-in_0\theta} \psi_n(\theta)$. For the evolution operator, we use the evolution of the harmonic oscillator, and thus obtain for $\psi(t)$:

$$\psi(t) = \sum_n c_n e^{-iE_n t} \psi_n(\theta). \quad (3.9)$$

Looking at the overlap of two such harmonic oscillators, we can use the fact that for small differences in the frequencies (respectively the energies), the stationary states stay the same in a first order approximation. Since our two frequencies, $\omega_1 = \sqrt{\epsilon k_1}$ and $\omega_2 = \sqrt{\epsilon k_2}$, are very close, we can assume that $|n\rangle \approx |n'\rangle$. After this diagonal approximation (due to the orthonormal stationary states, which produce a δ -function), the overlap reads:

$$\langle \psi(t) | \psi'(t) \rangle \approx \sum_n |c_n|^2 e^{in(\omega_1 - \omega_2)t}. \quad (3.10)$$

As expected, we find the beating frequency and its higher harmonics. Even taking the modulus square according to the definition of the fidelity (see Eq. (2.19)) does not

change that. The summed frequency $\omega_1 + \omega_2$ is lost in this first order approximation, but it can be recovered when considering higher terms of the Taylor expansion of the stationary states.

We have shown the origin of the beating frequency in the classical and the quantum harmonic oscillator. In Table 3.1, we now compare measured values for different ϵ to the ones calculated using Eq. (3.7). The agreement is more than convincing – we have discovered where the characteristic frequency that we have observed comes from.

The most characteristic behaviour of the fidelity for the full β -ensemble thus originates in the few resonant rotors. We shall illustrate their dominance in the next two sections of this chapter by reducing the intervals of the β -rotor ensembles around $\beta = \frac{1}{2}$. We expect to see an improvement in the resolution, since the bulk of non-resonant rotors becomes smaller and does no longer obscure the few resonant rotors.

3.1.2 Behaviour of fidelity for ensembles of near resonant rotors

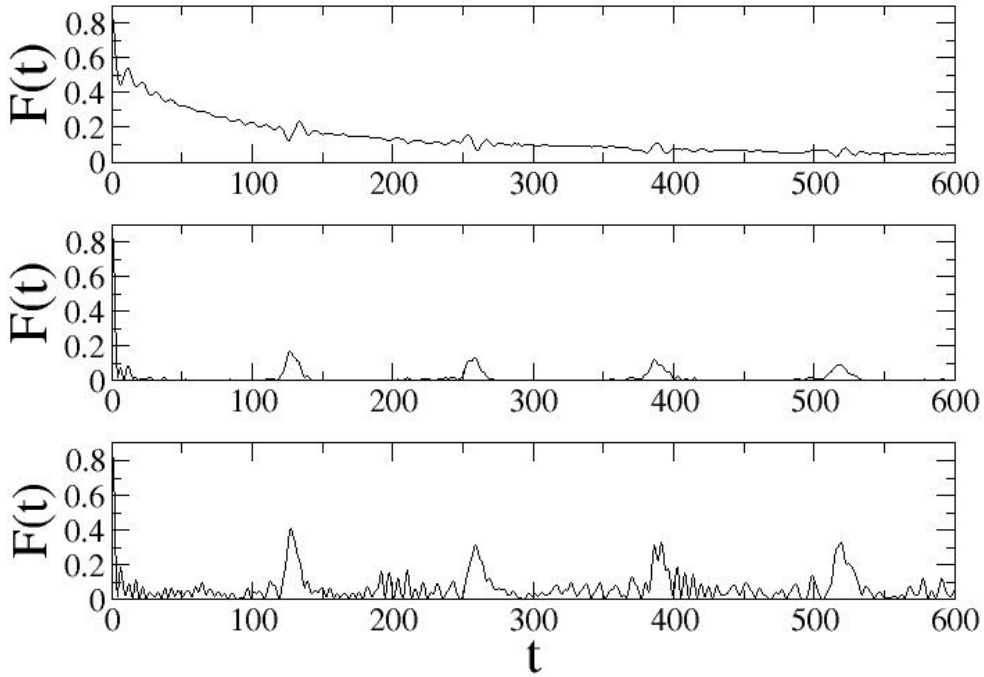


Figure 3.2: Fidelity close to resonance for ensembles of β -rotors with $\epsilon = 0.05$, $k_1 = 0.8\pi$ and $k_2 = 0.6\pi$, restricted in β . *Upper panel:* Fidelity for an ensemble that is uniformly distributed in β . *Central panel:* Fidelity for an ensemble where β is restricted to $[0.4;0.6]$. *Lower panel:* Fidelity for an ensemble where β is even further restricted to $[0.49;0.51]$. The origin of the oscillations obviously lies in the resonant rotors ($\beta = \frac{1}{2}$).

That the oscillations truly have their origin in the few resonant rotors of the ensemble can be shown by continuously reducing the intervals of the β -rotor ensembles. The

oscillations become well resolved revival peaks and those peaks grow higher and higher, the more we restrict the interval around $\beta = 0.5$. In Fig. 3.2, we first restrict the interval in β to 20%, then to 2% of its initial width in the upper panel. The revivals become visibly more pronounced with each restriction.

The observed revivals are also highly interesting from an experimentalist's point of view: They appear well within the measurable range ($t < 200$) [56] and recover more than one third of the signal at $t = 0$ in Fig. 3.2. With ultracold atoms, β can be limited to intervals of a size up to 0.01 [71, 72], making high resolution of the revival peaks possible. We shall look more closely at the resonant rotors that seem to be the origin for the characteristic fidelity peaks in the next section.

3.1.3 Behaviour of fidelity for resonant rotors

Before we return to the investigations of the revivals, which can also be found for single resonant rotors, we will look at the short-time behaviour of resonant rotors close to quantum resonance, which drastically changes compared to their behaviour at exact resonance.

Observations on small time scales – Breakdown of algebraic decay for the resonant rotor

We remember that the fidelity decays like t^{-1} in an oscillatory fashion at exact resonance, see Eq. (2.41). During the first few kicks, the deviation ϵ from resonance should not induce big changes. After a certain amount of kicks, however, the rotors have completely lost any phase relation towards the kicking, and we expect the fidelity to decay faster. Indeed, by once more taking momentum zero as the initial condition, we observe a breakdown of the t^{-1} -decay in Fig. 3.3. The onset of the breaktime depends on the variation of our parameters, which we discuss below.

It is hard to decide on an objective time where a difference between the two graphs of Fig. 3.3 is first visible – the t^{-1} -decay of the upper envelope is quite distinctive, but the influence of the perturbation on the lower envelope starts much earlier. We will restrict our measurements to the upper envelope, though, since it seems to be better resolved in our data.

The time of onset of the decay is measured manually as shown in Fig. 3.3. We are thus able to estimate a dependence on the parameters (kicking strengths k_1 and k_2 , and deviation ϵ from the characteristic kicking period of 2π , the primary quantum resonance) by scanning through single parameters while keeping the other parameters fixed. In Fig. 3.4, all results concerning the dependence of the time of onset on the perturbation and the kicking strengths are displayed. On the whole, we heuristically find the following formula for the onset of the breakdown of the original algebraic decay:

$$t_{\text{onset}}(k_1, k_2, \epsilon) \propto \frac{\sqrt{k_1} - \sqrt{k_2}}{\sqrt{\epsilon\sqrt{k_1 k_2}}}. \quad (3.11)$$

This is an important result because t_{onset} determines the time scale on which the perturbation in the kicking period first takes effect. This is both of interest to theoretical applications (since it determines the point where ϵ -classics are applicable) and to experimental realisations (where tiny defects of the setup might have long time effects according to Eq. (3.11)).

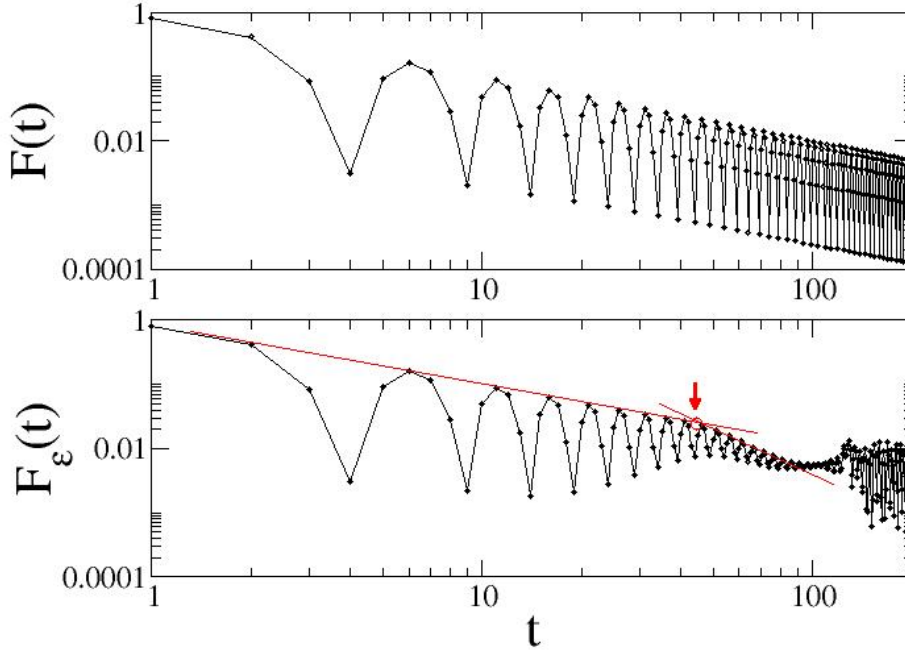


Figure 3.3: *Upper panel:* The expected algebraic decay of fidelity at exact quantum resonance is shown for a single resonant rotor with kicking strengths $k_1 = 0.8\pi$ and $k_2 = 0.6\pi$. *Lower panel:* Introducing a perturbation $\epsilon = 0.001$ in the kicking period to the system leads to a breakdown of the algebraic decay. The measured time t_{onset} is marked by a red arrow.

Observations on larger time scales

Now, we return to larger time scales. At the beginning of this chapter, we have found that the oscillations observed for the full β -ensemble become peaks when the interval around the resonant value for β ($\beta = \frac{1}{2}$) is restricted. We can therefore make an educated guess that the origin of the revivals is to be found with the resonant rotors. And indeed, we observe revivals for single resonant rotors in Fig. 3.5 – but more frequently than we had expected.

The frequency of the revivals is two times the beating frequency ω_{bf} , which we know to be the difference between the two resonance frequencies of the elliptic fixed point:

$$\omega_{res} = 2\omega_{bf} = 2\sqrt{|\epsilon|}(\sqrt{k_1} - \sqrt{k_2}). \quad (3.12)$$

Interestingly, for small deviations from the resonant value, such as $\beta = 0.49$, we find once more the beating frequency itself. This is an unexpected result – why should the frequency for $\beta = \frac{1}{2}$ differ so drastically from the beating frequency of the harmonic oscillator? The answer is surprisingly simple and actually has a classical origin, despite our system being purely quantum mechanical. For this reason, we will discuss this seemingly contradictory observation later in this chapter, when we look at the classical analogue of fidelity for the kicked rotor.

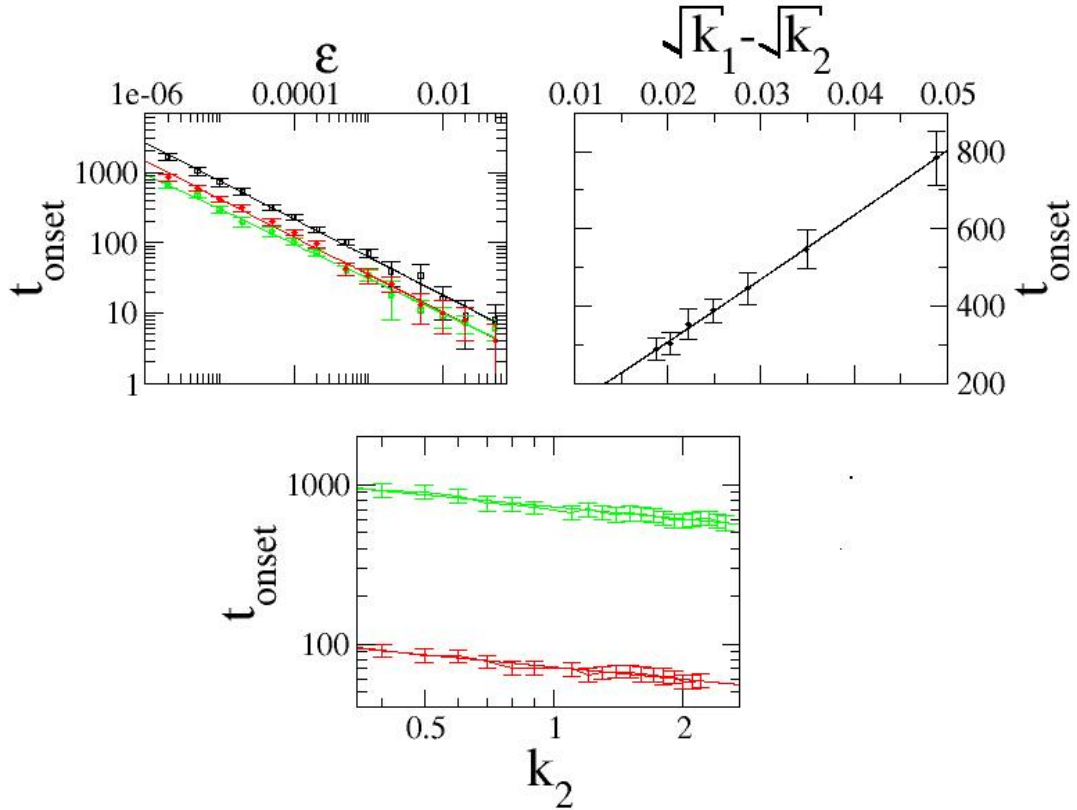


Figure 3.4: Measurements of t_{onset} against various parameters. We find $t_{\text{onset}} \propto \epsilon^{-0.5}$ (for $k_1 = 5.1$ and $k_2 = 5.0$ (black), $k_1 = 3.1$ and $k_2 = 3.0$ (red), and for $k_1 = 1.1$ and $k_2 = 1.0$ (green)), $t_{\text{onset}} \propto (k_1 k_2)^{-0.25}$ (for $\epsilon = 0.001$ (green) and $\epsilon = 0.00001$ (red)), and finally $t_{\text{onset}} \propto \sqrt{k_1} - \sqrt{k_2}$ (here, $\epsilon = 0.00001$). This altogether results in formula (3.11).

3.1.4 Behaviour of fidelity for nonresonant rotors

So far, we have only been looking at resonant rotors or at the effects caused by resonant rotors in ensembles. There is, however, a reason why we do not observe any characteristic effects from the nonresonant rotors in the full ensemble. While the rotors in the vicinity of the resonant value show essentially the same behaviour as the resonant rotors (namely revivals, even if not at the same frequency), the behaviour for nonresonant rotors far from $\beta = \frac{1}{2}$ (more precisely those for whom all corresponding classical trajectories lie outside the principal resonance island centered at $\beta = \frac{1}{2}$) changes drastically for small changes in β . It is therefore difficult to find a uniform description. Their behaviour differs so strongly because they essentially scan different regions in ϵ -classical phase space (see derivation in section 2.4). They follow rotational orbits outside the island. In Fig. 3.6, a selection of curves displaying the fidelity of nonresonant rotors as a function of time is shown.

One can see periodic oscillations for each nonresonant rotor, which makes sense in relation to the corresponding orbits in ϵ -classical phase space. We can, however, not set their different periods into context, since no description or explanation for the behaviour of the fidelity for nonresonant rotors has been found yet.

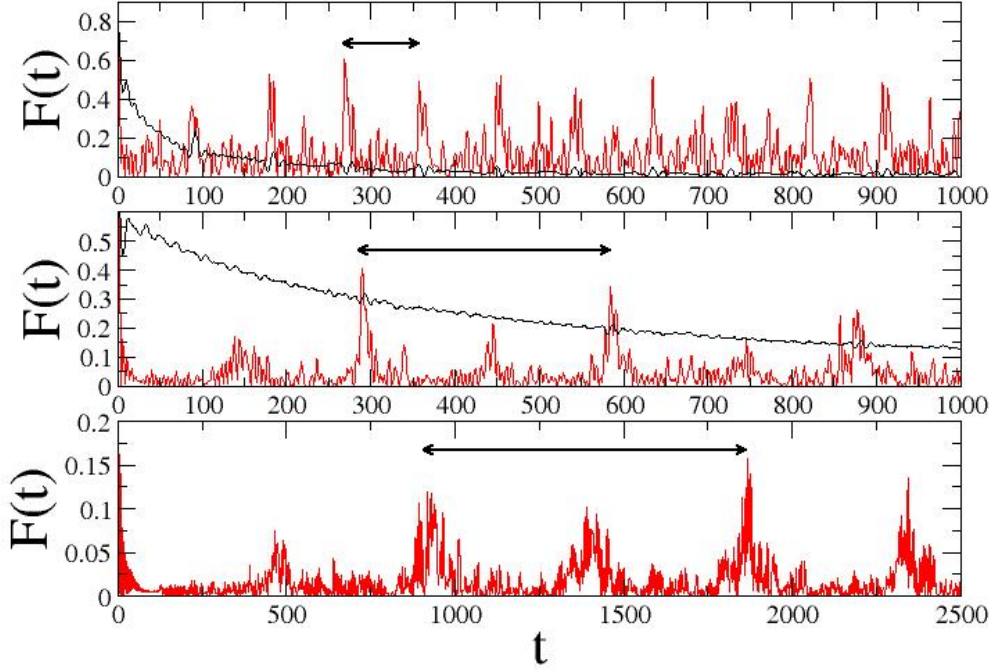


Figure 3.5: The revivals for a single resonant rotor with kicking strengths $k_1 = 0.8\pi$ and $k_2 = 0.6\pi$ are displayed in red for $\epsilon = 0.1$ (*upper panel*), $\epsilon = 0.01$ (*central panel*), and for $\epsilon = 0.001$ (*lower panel*). They have half the period of the beating, $T = \frac{\pi}{\omega_{bf}}$, which we observed for the full ensemble (*black curves in the two upper panels*). The period of the beating is also indicated by the arrows. The revivals are more and more obscured by quantum fluctuations with larger frequencies for growing ϵ up to $\epsilon = 0.1$, above which it is hard to make out the revivals.

A special case which we want to point out, though, is the so-called antiresonant rotor with $\beta = 1$ [73, 74]. The characteristic feature of this rotor is that without perturbation ($\epsilon = 0$), the free motion part of the unitary time evolution operator (2.10) changes sign after every period, so we always return to the full overlap of the wavefunctions with every second kick (see also the upper left panel of Fig. 3.7).

The amplitude of this hopping from full overlap to some smaller value depends on the difference in kicking strengths. The stronger the kicking strengths differ, the more distinct the corresponding wavefunctions.

If we now introduce a small perturbation, this does not hinder the beating back and forth, but adds an overlaying decay, which strongly depends on ϵ (see Fig. 3.7). For small but finite ϵ we also observe the building of an overlaying, unsteady but replicable structure with a longer oscillation period

$$T \propto \frac{1}{\epsilon}. \quad (3.13)$$

The antiresonant rotor is interesting in itself, but it does not make a noteworthy contri-

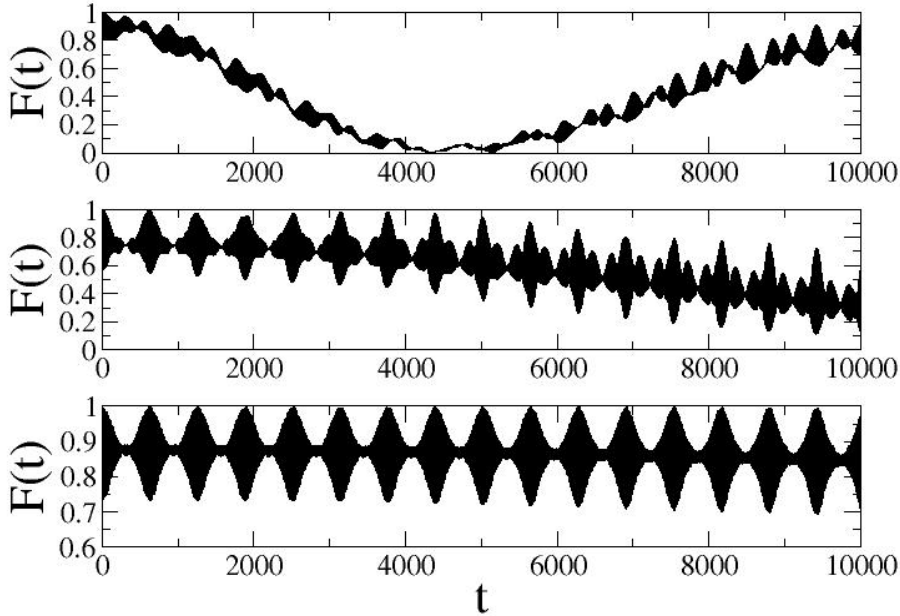


Figure 3.6: Irregular oscillations occurring in the fidelity of nonresonant rotors with kicking strengths $k_1 = 0.8\pi$ and $k_2 = 0.6\pi$, and a deviation $\epsilon = 0.01$ from the resonant kicking period. The oscillating periods widely differ for $\beta = 0$ (*upper panel*), $\beta = 0.3$ (*central panel*) and $\beta = 0.8$ (*lower panel*).

bution to the ensemble (because the antiresonant rotor has only few tori in ϵ -classical phase space, unlike the resonant rotor that occupies the full island) and will therefore not be considered here any further. We will instead focus on the resonant rotors that have such a huge impact on the ensemble. It is also the importance of the rotors with resonant value in β that we will discuss in the following section on quantum-classical correspondence.

3.2 Quantum-classical correspondence

So far, all the numerical data and observations have been provided by quantum simulations. However, we have also stressed the importance of the underlying pseudoclassical phase space to our dynamics. Consequently, it makes sense to take a look at a classical analog of the quantum fidelity, making use of the pseudoclassical phase space of Eq. (2.59). Considering that in the last few years, both investigating classical systems [75, 31] and comparing a classical phase space “fidelity” with its quantum counterpart [76] has yielded interesting new insights and results, this is a very promising ansatz. We will see which parts of the behaviour of quantum fidelity are really quantum mechanical effects and what the parallels between quantum and classical fidelity consist of.

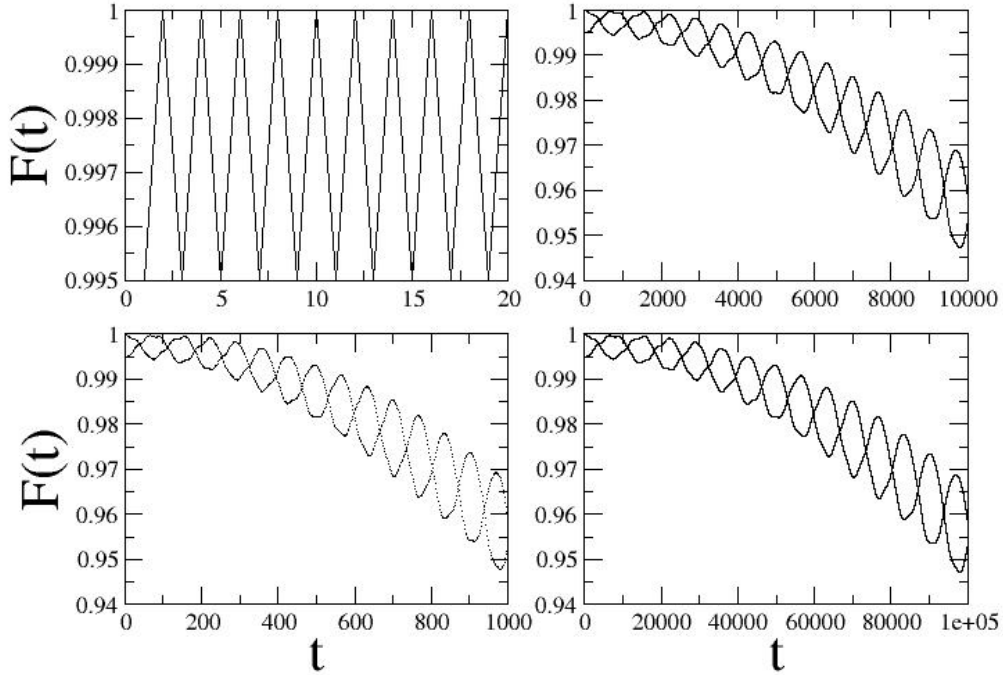


Figure 3.7: Behaviour of the fidelity for the antiresonant rotor with $k_1 = 1.1$ and $k_2 = 1.0$. *Upper left panel:* The saw-like structure in the fidelity of the antiresonant rotor at exact quantum resonance goes on infinitely. Introducing a perturbation to the kicking period, we find an overlaying decay to the beating. Here, we display $\epsilon = 0.1$ (*lower left*), $\epsilon = 0.01$ (*upper right*) and $\epsilon = 0.001$ (*lower right*).

3.2.1 Methods

The classical analog of the quantum fidelity that we will be using is defined as [31]:

$$F(t) = \int dqdp \varrho_{2t}(q, p) \varrho_0(q, p) \tag{3.14}$$

Keep in mind that the definition of fidelity in the classical case is very distinct from the definition in the quantum mechanical case. Here, we will be looking at trajectories and the probability for them to come back to an area close to the starting point, whereas for the quantum fidelity, we have computed probability amplitudes of wave functions. In the classical picture, a full ensemble means just averaging over all trajectories – in the quantum picture, we will have distinctive effects due to interference, as we shall see later. What is important here is to note that, even though we talk of classical fidelity, the classical definition does not correspond perfectly to the quantum definition.

For numerical calculations, we use a number of starting points with $I = 0$ and θ randomly chosen between 0 and 2π which correspond to the initial quantum wave function with momentum zero. After evolving these points for a time t according to

number of starting points	noise ratio
100	3.38
1000	2.96
5000	2.89
10000	2.82
20000	2.77
50000	2.79
100000	2.69

Table 3.2: Table of noise ratios for differently seized ensembles. For ensembles consisting of more than 20000 rotors, the noise ratio differs only very slightly – the curves are as smooth as possible. Using larger numbers does not show any visible effects.

the ϵ - classical standard map with kicking strength k_1 ,

$$\begin{aligned}\theta_n &= \theta_{n-1} + I_{n-1} + \pi + (2\pi + \epsilon)\beta, \\ I_n &= I_{n-1} + k_1\epsilon \sin(\theta_n),\end{aligned}\tag{3.15}$$

we use the inverted map

$$\begin{aligned}I_n &= I_{n-1} - k_2\epsilon \sin(\theta_{n-1}), \\ \theta_n &= \theta_{n-1} - I_n - \pi - (2\pi + \epsilon)\beta,\end{aligned}\tag{3.16}$$

with a different kicking strength k_2 to retrace trajectories, also counting t kicks. For $k_1 = k_2$, the trajectories resume their starting positions after a time $2t$. For slightly different kicking strengths, however, the end points differ from the starting points. This difference offers a way to obtain fidelity simply by counting the number of returned points in an interval of the size 2ϵ around the starting line. We have been using ensembles with about 20000 equidistantly distributed starting points, which gives us sufficient statistics. Using larger ensembles only contributes to a slight smoothing of the curves, as can be seen in Table 3.2. In the table, the noise ratio is defined as the biggest value (peak) of the fidelity divided by the time-averaged fidelity.

3.2.2 Results

As can be seen in Fig. 3.8, the qualitative behaviour of quantum fidelity is very nicely reproduced by our classical fidelity (3.14) based on the ϵ -classical map. For a single resonant rotor, two times the beating frequency is characteristic for both approaches. Interestingly, by averaging over the full ensemble in the classical approximation, any sign of the beating frequency completely disappears. This can be understood by the bulk of nonresonant rotors which participate in the average. In the quantum case, the visible survival of the oscillations must be attributed to phase factors which are not much influenced by the averaging. In the classical case, the revivals are only visible if the percentage of resonant rotors in the full ensemble is high enough: For example, in the case of 5000 nonresonant and 5000 resonant rotors, revivals with the beating frequency will still be visible, of course (see Fig. 3.9). For our calculation, though, the contingent of nonresonant rotors was much larger, since we used a practically equidistant distribution along the coordinate axis. This is why we do not see the oscillations anymore.

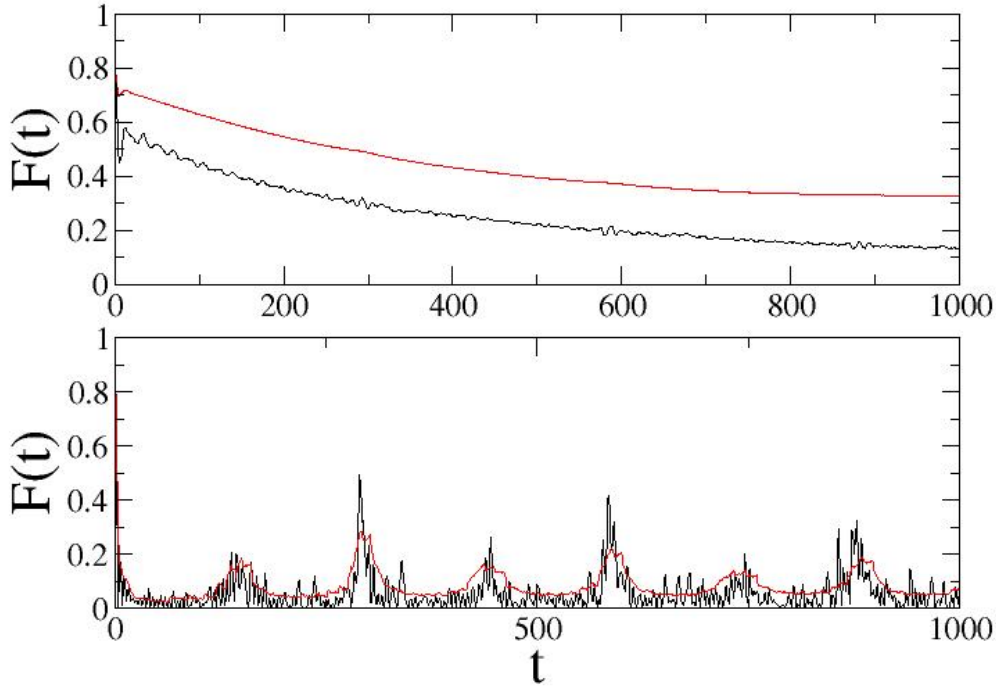


Figure 3.8: Comparison of classical (*red*) and quantum fidelity (*black*) for an ensemble of β -rotors with $0 \leq \beta \leq 1$ in the *upper panel* (the classical curve is shifted upwards by 0.2 for better visibility) and for a single resonant rotor in the *lower panel*. The kicking strengths are $k_1 = 0.8\pi$ and $k_2 = 0.6\pi$, the deviation from quantum resonance $\epsilon = 0.01$. For the single resonant rotor, the revivals are nicely reproduced by the classical fidelity, whereas they are completely averaged out for the full ensemble. For the quantum fidelity, the revivals remain visible in the latter case due to interference effects.

What is also very interesting about the classical analog of the fidelity is the fact that it is able to reproduce the doubling of the beating frequency for exactly resonant values of β . In Fig. 3.10, we observe the doubled beating frequency for $\beta = 0.5$, whereas for $\beta = 0.49$ only the beating frequency itself remains.

This can be explained very easily in its classical context by considering the symmetry of the starting area of the trajectories. The starting points are defined on a slip of width ϵ around $I = 0$ for $\beta = 0.5$ on the left side of Fig. 3.11, which displays the resonance island of the ϵ -classical Standard Map. Owing to the symmetry of this position, they return to this defined starting and counting area both after half a circle and after a full circle of angular difference in the evolutions. For example, a resonant rotor with kicking strength $k_1 = 0.8\pi$ and $\epsilon = 0.01$ has trajectories all along the island, which, according to the harmonic oscillator approximation, have a period of $T = \frac{2\pi}{\sqrt{k\epsilon}}$. However, since we perform the backward evolution with a slightly different period (due to different kicking strength), the trajectories do not return to the measuring area for a much longer time. Only when the angular distance between forward and backward evolution is equal to

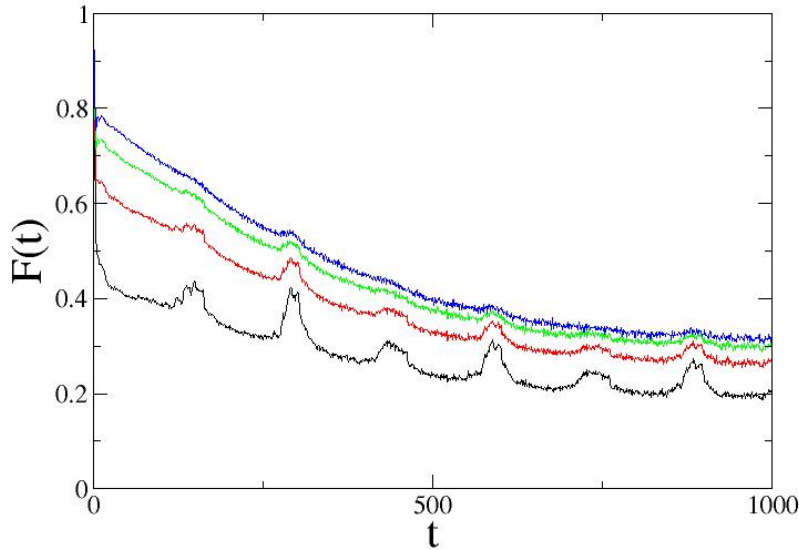


Figure 3.9: Classical fidelity with 10000 β -rotors. If half of them is resonant (*black curve*), the revivals are clearly visible and their frequency is twice the beating frequency. For 2500 (*red curve*) and 1250 (*green curve*) resonant rotors the amplitude visibly declines. For only 625 resonant rotors out of 10000 β -rotors, the revivals are barely visible anymore.

multiples of the full circle do the trajectories return to their original starting points, causing the revivals in the classical fidelity. However, this is also true for multiples of half a circle, since the initial distribution and its mirror image (reflected along the y -axis) cannot be distinguished. This causes the doubling of the beating frequency which we observe. For β slightly smaller or larger than the resonant value (see Fig. 3.11 on the right), we are still on the island, but the defined starting and counting area is no longer symmetric in its position on the island (see also the right panel of Fig. 3.12). This is why we now observe only the beating frequency. The suppression of every second revival is thus not due to coherence as one might be tempted to think, but instead due to the influence of the classical trajectories. This is also the case for the semiclassical and quantum observations, as we shall see in the next chapter.

The fact that the intermediate revivals occurring for the resonant rotor are slightly less pronounced is due to the elliptic form of the resonance island, which is additionally rotated in phase space by 45° with respect to the symmetric pendulum island (see, for instance, the island in Fig. 4.2).

We have always assumed the harmonic oscillator approximation to be valid without further assessment. But how good is this approximation truly? According to our results, it is appropriate, since we found excellent agreement with the exact numerical calculations. Taking a look at the ϵ -classical phase space, we soon find out why. In Fig. 3.12, we display the trajectories of a single resonant rotor for the first 10 kicks. As we can see, the different trajectories have different frequencies. For about the inner half of the resonance island, however, we find approximately the same frequency. This

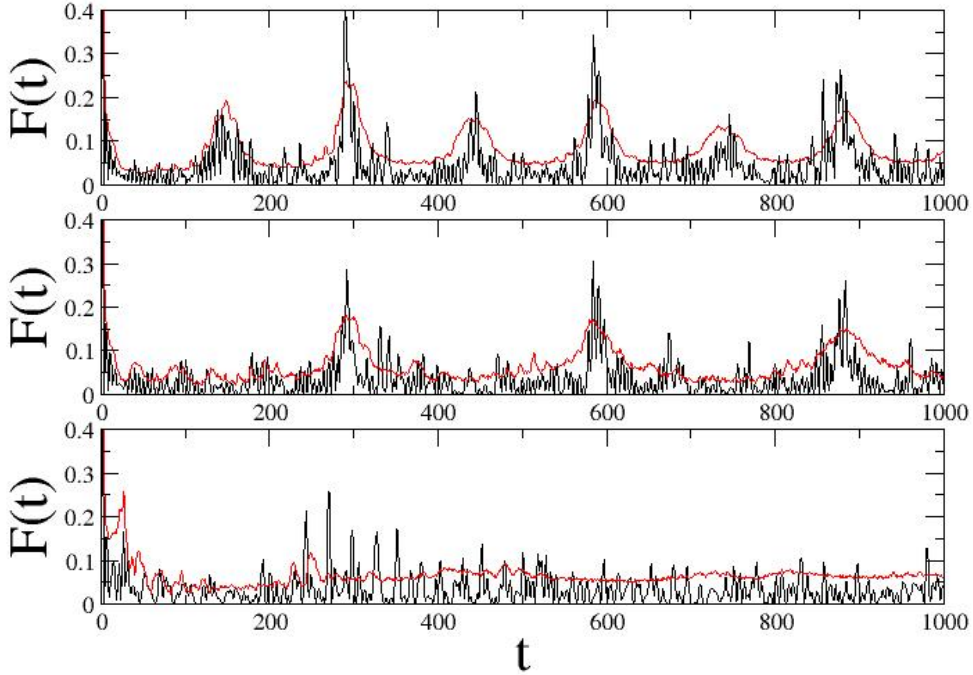


Figure 3.10: Comparison of classical (*red*) and quantum fidelity (*black*) for β -rotors with $\beta = 0.5$ in the *upper panel*, $\beta = 0.49$ in the *central panel* and $\beta = 0.47$ in the *lower panel*. The kicking strengths are as before $k_1 = 0.8\pi$ and $k_2 = 0.6\pi$, the deviation from quantum resonance $\epsilon = 0.01$. If we decrease β and thus depart from resonance, we first see a doubling of the frequency before the revivals completely disappear with growing distance of β from 0.5.

is the part which is well approximated by the harmonic oscillator. The trajectories close to the border of the island do not contribute to the revivals because their periods differ too much.

As we have seen, a purely classical understanding of the behaviour of the fidelity for the kicked rotor in quantum resonance is possible. The classical fidelity for a single resonant rotor recovers the characteristic feature, i.e. the revivals with the doubled beating frequency, and allows us to explain them from a classical point of view. For the full ensemble, it is only possible to recover the overall decay from the classical fidelity, quite unlike the quantum fidelity which still retains some of the structure from the resonant rotors after averaging. This is due to interference: For the quantum fidelity (2.43), we add the products of the wavefunctions for different β over all values of momentum before taking the modulus square.

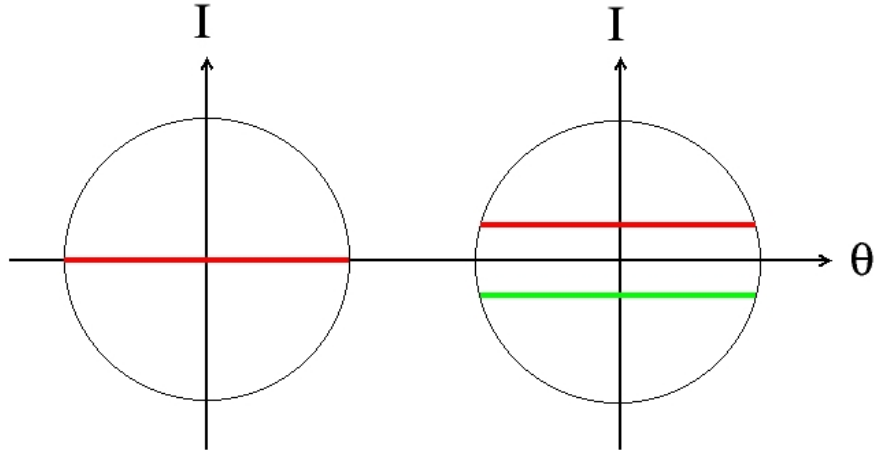


Figure 3.11: Schematic illustration of the starting and counting area on the resonance island in ϵ -classical phase space. For $\beta = \frac{1}{2}$, the starting points lay on the red strip along the x -axis inside the resonance island, to which they return after multiples of half the period. If β slightly differs from the resonant value (see red strip of starting values on the right), the symmetry is broken and revivals only occur after multiples of the full period. After half the period, they are in the green strip and, according to the definition of the classical fidelity (3.14), do not contribute to the fidelity.

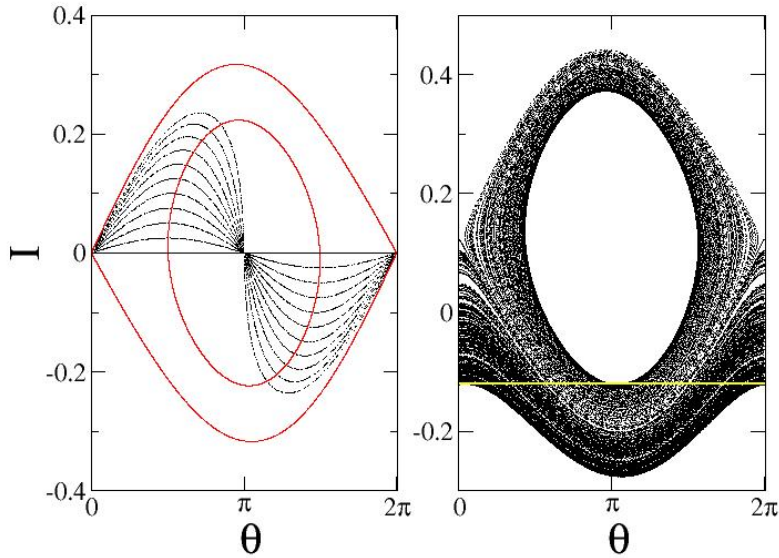


Figure 3.12: Phase space illustration with spatial coordinate θ and momentum I . We used kicking strength 0.8π and $\epsilon = 0.01$. *Left panel:* The black trajectories display the trajectories of an ensemble of 500 rotors started along the coordinate axis for the first 10 kicks (the red curves are trajectories for single rotors for 10000 kicks). It is clearly visible that only about the inner half of the circle has approximately the same period, which is assumed in the harmonic oscillator approximation. *Right panel:* Already for small deviations from the resonant $\beta = 0.5$ (here $\beta = 0.48$), the yellow starting points do not cover the whole resonance island and thus, the center of the island does not play a part in the calculation of fidelity anymore.

Chapter 4

Analytical theory for the behaviour of fidelity for resonantly kicked atoms

As we have seen in the last chapter, the behaviour of an ensemble of kicked atoms is dominated by the few resonant rotors of the ensemble. Our aim is therefore to find an analytic description of the fidelity for these most important rotors in the close vicinity to quantum resonance, where the motion can be described by the quasi-regular dynamics of ϵ -classical phase space (as reviewed in section 2.4). To reach this goal, however, we first have to understand the numerically observed t^{-1} -decay (see Fig. 2.5) at exact quantum resonance from the point of view of ϵ -classics in the case $\epsilon \rightarrow 0$. We shall start out by performing the complete quantum calculation of path integrals for multiply connected spaces (which in this context just means that we calculate the propagators for each separate kick and concatenate them to get the complete evolution, for a discussion of the basic concepts, see [77]) and then examine further simplifications of the dynamics, until only the most characteristic features remain. This is done by utilizing the pendulum dynamics, which will be shown to be a good fit for the resonant island, in a semiclassical approximation. After having shown that this still yields the expected t^{-1} -decay, we shall be looking at a further simplification: Once more we use a semiclassical approach, this time by approximating the pendulum by the harmonic oscillator. We once more derive the characteristic decay for this most basic of all dynamics.

In the end, after having illustrated that our simplifications do not change the characteristic decay, we can deflect from quantum resonance by a small perturbation ϵ and thus successfully derive the main result of this thesis, an analytical expression for the fidelity of resonant rotors close to quantum resonance. It is important to note that we consider only the vicinity of resonance for the harmonic oscillator. Otherwise, we would have to solve elliptic integrals even for the comparatively simple case of the classical pendulum, rendering our original problem nearly impossible to solve analytically.

4.1 Understanding the t^{-1} -decay from the ϵ -classical point of view

4.1.1 Quantum calculation with path integrals for multiply connected spaces

By means of path integration, it is possible to derive the well-known result Eq. (2.41), a Bessel function of zeroth order, which has been shown to describe the resonant rotor in quantum resonance. To this end, we make use of the substitutional variable $\hat{J} = \hat{I} + \tau\beta + \pi$, where \hat{I} is the operator $-i\epsilon \frac{d}{d\theta}$, acting on the Hilbert space of wave functions with periodic boundary conditions in θ (recall section 2.4). The eigenfunctions are therefore plane waves, which we also choose as initial wave functions, and we obtain the eigenvalues $\lambda = \tau\beta + \pi + n\epsilon$ for \hat{J} . Using the ϵ -classical picture [53], we take ϵ as \hbar , $k' = k\epsilon$ and \hat{J} as our momentum in the well-known Floquet operator:

$$\begin{aligned} \hat{U}_{\delta-kick} &= e^{-\frac{i}{\epsilon} \int_0^t dt H} \\ &= e^{-i\frac{k'}{\epsilon} \cos(\hat{\theta})} e^{-\frac{i}{\epsilon} \frac{\hat{J}^2}{2}} \\ &= e^{-ik \cos(\hat{\theta})} e^{-\frac{i}{\epsilon} \frac{\hat{J}^2}{2}}. \end{aligned} \quad (4.1)$$

The propagator amplitude G describes the propagation from θ to θ' :

$$\begin{aligned} G(\theta, \theta', k) &= \langle \theta | \hat{U}_{\delta-kick} | \theta' \rangle \\ &= \frac{1}{\sqrt{2\pi}} e^{-ik \cos \theta'} \sum_{n=-\infty}^{\infty} e^{in(\theta-\theta')} e^{-i\frac{(\tau\beta+\pi+n\epsilon)^2}{2\epsilon}} \\ &= \frac{1}{\sqrt{2\pi}} e^{-ik \cos \theta'} \sum_{n=-\infty}^{\infty} e^{in(\theta-\theta')} e^{-\frac{i}{2\epsilon} \tau^2 \beta^2} e^{-i\tau\beta n - i\frac{\epsilon}{2} n^2 - i\pi n - \frac{i}{\epsilon} \pi \tau \beta - i\frac{\pi^2}{2\epsilon}}. \end{aligned} \quad (4.2)$$

In the following, we will make use of a special trick [77] that can be performed using the Jacobi theta function. The Jacobi theta function is defined as

$$\Theta_3(z, s) \equiv \sum_{n=-\infty}^{\infty} e^{i\pi n^2 s + 2inz}, \quad (4.3)$$

and has a special property that follows from Poisson's summation formula:

$$\Theta_3(z, s) = \frac{1}{\sqrt{-is}} e^{\frac{z^2}{is\pi}} \Theta_3\left(\frac{z}{s}, -\frac{1}{s}\right). \quad (4.4)$$

In our propagator G , $z = \frac{1}{2}(\theta - \theta' - \tau\beta - \pi)$ and $s = -\frac{\epsilon}{2\pi}$. It can then be written as

$$\begin{aligned} G(\theta, \theta', k) &= \frac{1}{\sqrt{2\pi}} e^{-ik \cos \theta'} e^{-i\frac{\tau^2 \beta^2}{2\epsilon}} e^{-i\frac{\pi^2}{2\epsilon}} e^{-\frac{i}{2} \pi \tau \beta} \Theta_3\left(\frac{\theta - \theta' - \tau\beta - \pi}{2}, -\frac{\epsilon}{2\pi}\right) \\ &= \frac{1}{\sqrt{i\epsilon}} e^{-ik \cos \theta' - i\frac{\tau^2 \beta^2}{2\epsilon} - i\frac{\pi^2}{2\epsilon} - \frac{i}{2} \pi \tau \beta + i\frac{(\theta - \theta' - \tau\beta - \pi)^2}{2\epsilon}} \\ &\quad \cdot \sum_{n=-\infty}^{\infty} e^{\frac{i}{\epsilon} 2\pi^2 n^2 - i\frac{2n\pi}{\epsilon} (\theta - \theta' - \tau\beta - \pi)} \\ &= \frac{1}{\sqrt{i\epsilon}} e^{-ik \cos \theta' - i\frac{\tau^2 \beta^2}{2\epsilon} - i\frac{\pi^2}{2\epsilon} - \frac{i}{2} \pi \tau \beta} \sum_{n=-\infty}^{\infty} e^{\frac{i}{\epsilon} 2\pi^2 n^2 + \frac{i}{2\epsilon} (\theta - \theta' - \tau\beta - \pi - 2\pi n)^2}. \end{aligned} \quad (4.5)$$

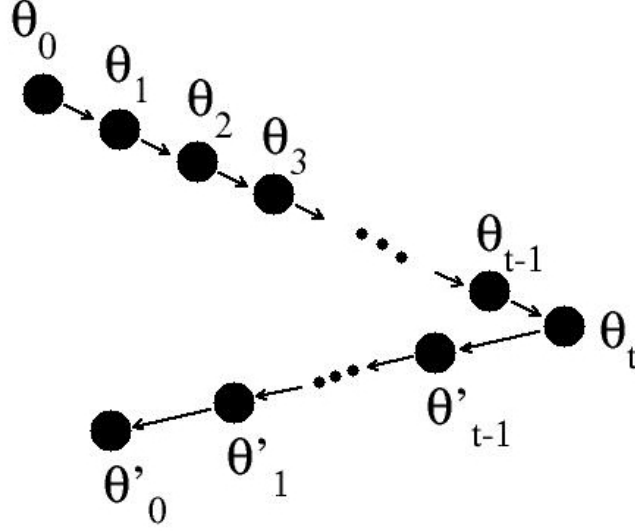


Figure 4.1: Illustration of the stepwise propagation needed while calculating the fidelity exactly by use of multiply connected spaces. This picture is based on the interpretation of fidelity as an echo measure.

We can now calculate the fidelity according to Fig. 4.1. As initial wave functions, we take $\psi(\theta_0)$ and $\psi(\theta'_0)$. The step from θ to θ' described by the propagator G is just one iteration in the discretized time t . To reach a point t in time, we therefore have to take this step t times to go from θ_0 , the starting point, to θ_t , our end point. Since the fidelity describes the motion with kicking strength k_1 up to a point t compared to its backward evolution with kicking strength k_2 , we also have to consider the way back from $\theta_t = \theta'_t$ to θ'_0 (see Fig. 4.1). The wave functions are all normalised by $\frac{1}{\sqrt{2\pi}}$, resulting in a factor $(\frac{1}{2\pi})^t$. This yields the following expression for the fidelity:

$$\begin{aligned}
 F &= \left| \int d\theta_0 G(\theta_0, \theta_1, k_1) \dots \int d\theta_t \int d\theta'_{t-1} G^*(\theta'_{t-1}, \theta'_t, k_2) \dots \right. \\
 &\quad \left. \int d\theta'_0 G^*(\theta'_0, \theta'_1, k_2) \Psi^*(\theta_0) \Psi(\theta'_0) \right|^2 \\
 &= \left| \frac{1}{2\pi} \left(\frac{1}{i\epsilon} \right)^t \int d\theta_0 \dots \int d\theta_t \int d\theta'_{t-1} \dots \int d\theta'_0 \right. \\
 &\quad \cdot \sum_{n, n'} e^{\frac{i}{2\epsilon} \sum_{k=1}^t (\theta_k - \theta_{k-1} - \tau\beta - \pi - 2\pi n)^2} \\
 &\quad \cdot e^{-\frac{i}{2\epsilon} \sum_{l=1}^t (\theta'_l - \theta'_{l-1} - \tau\beta - \pi - 2\pi n')^2} \\
 &\quad \left. \cdot e^{-ik_1 \sum_{k=1}^t \cos \theta_k} e^{ik_2 \sum_{l=1}^t \cos \theta'_l} \right|^2.
 \end{aligned} \tag{4.6}$$

The upper and lower bounds are not explicitly written down in Eq. (4.6). In this thesis, undefined integrals like that are to be understood as covering a phase space cell, i.e., going from 0 to 2π . Since the motion is restricted to this phase space cell anyway, we are able to expand the boundaries and obtain an integral going from $-\infty$ to ∞ . This will be very useful later on, when we are able to use standard formulae for these infinite integrals.

As wave functions at time $t = 0$, we use normalized plane waves $\frac{1}{\sqrt{2\pi}}e^{in_0\theta_0}$ with momentum $n_0 = 0$. In order to perform a stationary phase approximation [78], we forget about the kicking part of the propagator and only take into account the quadratic part of the action (called S in the following):

$$S = \frac{1}{2} \sum_{k=1}^t (\theta_k - \theta_{k-1} - \tau\beta - \pi - 2\pi n)^2 - \frac{1}{2} \sum_{k=1}^t (\theta'_k - \theta'_{k-1} - \tau\beta - \pi - 2\pi n')^2 \quad (4.7)$$

This is allowed because it means that we will only average over the oscillating phase of $e^{\frac{i}{\epsilon}S}$, leaving the exponential of the summed-up kicks alone. This averaging is done by means of a stationary phase approximation, which will be explained briefly.

The idea of the stationary phase approximation [79, 80], an asymptotic analysis of oscillatory integrals, is the following: For exponents consisting of a large prefactor (in our case $\frac{1}{\epsilon}$) and an analytic function with a global minimum, we may expand the function around this minimum, neglecting smaller function values as phases which will more or less cancel. Since λ is assumed as being small, an expansion up to second order is sufficient here. Thus, an integral of the form

$$I = \int_{-\infty}^{\infty} dx e^{-\lambda f(x)} \quad (4.8)$$

with large λ and analytic, oscillating $f(x)$ with Taylor expansion

$$f(x) = f(x_0) + f'(x_0)(x - x_0) + \frac{1}{2}f''(x_0)(x - x_0)^2 + \dots \quad (4.9)$$

around a global minimum x_0 (meaning $f'(x_0) = 0$) can be approximated by

$$\begin{aligned} I &= e^{-i\lambda f(x_0)} \int_{-\infty}^{\infty} dx e^{-\frac{\lambda}{2}f''(x_0)(x-x_0)^2} \\ &= \sqrt{\frac{2\pi}{\lambda f''(x_0)}} e^{-\lambda f(x_0)}. \end{aligned} \quad (4.10)$$

Now, we shall this to our case, which is slightly more complicated. We choose a fixed variable from among the θ_k and call it θ_p . For the first derivative $\frac{\partial S}{\partial \theta_p}$, we have to consider both the terms for $k = p$ and $k = p + 1$, resulting in

$$\frac{\partial S}{\partial \theta_p} = 2\theta_p - \theta_{p-1} - \theta_{p+1} \stackrel{!}{=} 0. \quad (4.11)$$

However, for the end point $k = t$ and the starting point $k = 0$, things are a bit different:

$$\begin{aligned} \frac{\partial S}{\partial \theta_t} &= \theta'_{t-1} - \theta_{t-1} + 2\pi(n' - n), \\ \frac{\partial S}{\partial \theta_0} &= \theta_0 - \theta_1 + \tau\beta + 2\pi n + \pi \\ &\implies \theta_k = \theta_0 + k(\tau\beta + \pi) \pmod{2\pi}. \end{aligned} \quad (4.12)$$

θ_p can thus be described in terms of θ_0 , as can all the other θ_k . We can therefore lose all the variables θ_k by performing stationary phase approximations, leading to the simplified expression for the fidelity,

$$F = \left| \frac{1}{2\pi} \det(A^{-\frac{1}{2}}) \int d\theta_0 e^{i(k_2 - k_1) \sum_{k=1}^t \cos(\theta_0 + k(\tau\beta + \pi))} \right|^2, \quad (4.13)$$

with the determinant of the matrix $A_{i,j} = \left(\frac{\partial^2 S}{\partial \theta_i \partial \theta_j} \right)^{-1/2}$ equal to 1 (for this notation, see [81]). We have thus performed two times t independent stationary phase approximation or 2 multidimensional ones, resulting in the well-known expression for the fidelity, Eq. (4.13). Analogous to the derivation for the single resonant rotor in section 2.3, Eq. (4.13) can be written as:

$$F(k_1, k_2, t) = J_0^2(t |k_1 - k_2|). \quad (4.14)$$

We have just successfully retrieved the same expression for the fidelity decay of the resonant rotor as derived by the purely quantum-mechanical calculation. Unfortunately, it is impossible to deduce the characteristics of the resonant rotor that is slightly out of resonance from this comprehensive path integration. The stationary phase approximation singles out just one orbit, so we would have to find some way to stop half-way through the stationary phase approximation, which is something for which (at least to our knowledge) the proper mathematical tools are missing. But as we will see, it is not necessary to use the exact quantum computation – much simpler approximations turn out to be sufficient for our purpose.

4.1.2 Semiclassical approximation with the propagators for the pendulum

In the literature describing ϵ -classical phase space [28, 82], the dynamics of resonant rotors are usually approximated by substituting the area near the resonance island of the Standard Map of ϵ -classics corresponding to quantum resonance by the appropriate pendulum phase space. This means that while we had a stroboscopic picture of phase space before, we now switch to continuous time (i.e., the pendulum is exposed to $k\epsilon \cos(\theta)$ at all times). While the trajectories of the pendulum take the form of a circle close to the center and become more and more eye-shaped when approaching the separatrix, the invariant curves of resonant motion in ϵ -classical phase space take a more elliptic form and are rotated by about 45° in clockwise direction (see Fig. 4.2). The congruency between both trajectories and therefore the quality of the pendulum approximation obviously improves the closer one gets to the stable elliptic fixed point. We will see, by deriving the t^{-1} -decay from this approximation, that the substitution of the true phase space by the pendulum one is sufficient in our case.

The pendulum Hamiltonian (corresponding to its ϵ -classical analogon) is

$$H = \frac{I^2}{2} - k\epsilon \cos(\theta) \quad (4.15)$$

and the equation of motion

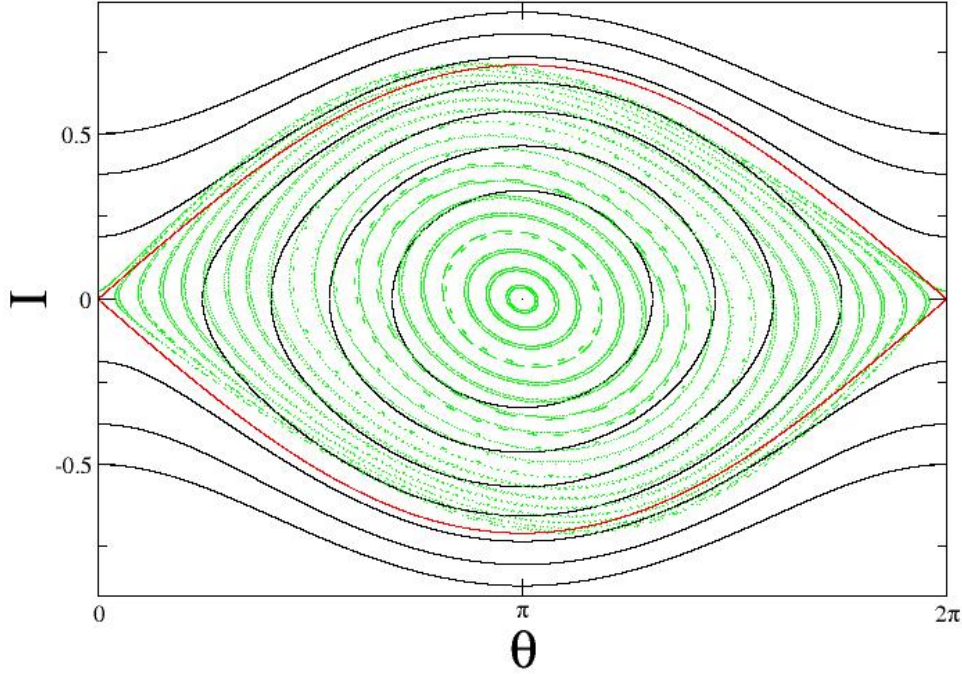


Figure 4.2: Comparison of the phase space portraits of the pendulum (*black*) with separatrix (*red*) and the ϵ -classical Standard Map (*green*) of Eq. (2.59). Both curves were plotted for kicking strength $k = 0.8\pi$ and perturbation $\epsilon = 0.05$. The differences between their trajectories are clearly visible, yet our approximation is good enough to yield reasonable analytical results.

$$\ddot{\theta}(t) = -k\epsilon \sin(\theta(t)). \quad (4.16)$$

Phase space portraits for the pendulum display trajectories of the form

$$I = \pm \sqrt{2(E + k\epsilon \cos(\theta(t)))}, \quad (4.17)$$

with the total energy of the system E . For $E < -k\epsilon$, we obtain no curves (since $\dot{\theta}$ is imaginary). If $-k\epsilon < E < k\epsilon$, the curves are closed curves, corresponding to the pendulum swinging forth and back (oscillatory motion). Oscillations near the center are almost circular, which is why the approximation for small angles by the first terms of the Taylor expansion is good. $E = k\epsilon$ results in the separatrix which divides librational and rotational motion. For $E > k\epsilon$, the curve is open, corresponding to the pendulum swinging through complete circles (rotational motion).

Now we make use of the pendulum approximation. For $\tau = 2\pi + \epsilon$ and $\beta = \frac{1}{2}$, we start on the resonance island centered at zero in ϵ -phase space. First, we rescale our spatial coordinate, which will simplify our later considerations significantly:

$$\tilde{\theta}(t) = \theta(t\sqrt{k\epsilon}), \quad (4.18)$$

leading to the equation of motion

$$\ddot{\tilde{\theta}}(t) = k \epsilon \ddot{\theta}(t\sqrt{k\epsilon}) = -k \epsilon \sin(\tilde{\theta}(t)). \quad (4.19)$$

Using this, we can write for the action

$$\begin{aligned} S(\theta, \theta', t, k\epsilon) &= \int_0^t dt' \left[\frac{1}{2} \frac{d\tilde{\theta}(t')^2}{dt'} - k\epsilon \cos(\tilde{\theta}) \right] \\ &= k\epsilon \int_0^t dt' \left[\frac{1}{2} \dot{\tilde{\theta}}^2(t'\sqrt{k\epsilon}) - \cos(\theta(t'\sqrt{k\epsilon})) \right] \\ &= \sqrt{k\epsilon} \int_0^{t\sqrt{k\epsilon}} dt' \left[\frac{1}{2} \dot{\theta}^2 - \cos(\theta) \right] \\ &= \sqrt{k\epsilon} S(\theta, \theta', t\sqrt{k\epsilon}, 1) \\ &\simeq \frac{(\theta(t\sqrt{k\epsilon}) - \theta_0)^2}{2t} - tk\epsilon \cos(\theta_0), \end{aligned} \quad (4.20)$$

where we used a linear approximation for small times in the last line.

The semiclassical propagator for the motion defined by Eq. (4.19) is given by

$$G(\theta, \theta', t) = \frac{1}{\sqrt{2\pi i \epsilon}} \sqrt{|V(\theta, \theta', t)|} e^{\frac{i}{\epsilon} S(\theta, \theta', t) + i\phi} \quad (4.21)$$

with the so-called *Van Vleck determinant* (for more background on semiclassical methods and definition of path integration, see [81])

$$V(\theta, \theta', t) = \det \left(\frac{\partial^2 S(\theta, \theta')}{\partial \theta \partial \theta'} \right). \quad (4.22)$$

ϕ is the *Maslov index* (and therefore dependent on the topology of the phase space), and will not be of further interest or significance to us here since it just adds a phase that drops out when calculating the fidelity.

The definition of fidelity via the propagator amplitudes reads:

$$\begin{aligned} F(t, \epsilon, k_1, k_2) &= |\langle \Psi(k_1, t) | \Psi(k_2, t) \rangle|^2 \\ &= \left| \int d\theta \int d\theta' \int d\theta'' G_1^*(\theta, \theta', t) G_2(\theta'', \theta', t) \Psi_0(\theta'') \Psi_0^*(\theta) \right|^2, \end{aligned} \quad (4.23)$$

with $\Psi_0(\theta'')$ and $\Psi_0^*(\theta)$ once more plane waves with momentum zero and normalisation factor $\frac{1}{\sqrt{2\pi}}$.

Now we insert the propagator (4.21) for the pendulum into the fidelity:

$$\begin{aligned} F &= \left| \frac{1}{2\pi} \int d\theta_0 \int d\theta_1 \int d\theta_2 \sqrt{|V_1| |V_2|} \frac{1}{2\pi i \epsilon} e^{i \frac{(\theta_1 - \theta_0)^2}{2t\epsilon} - itk_1 \cos \theta_0} \right. \\ &\quad \left. e^{-i \frac{(\theta_1 - \theta_2)^2}{2t\epsilon} + itk_2 \cos \theta_1} \right|^2. \end{aligned} \quad (4.24)$$

Here, both Van Vleck determinants yield t^{-1} (one is in fact negative, but this is of no importance for the fidelity itself because of the modulus square in its definition). A

first stationary phase approximation with respect to θ_0 ($\lambda = \frac{1}{\epsilon}$) yields $\theta_0 = \theta_1$, since we average over the phase S_1 (which is a part of the action S times a factor i),

$$\begin{aligned} S_1 &= \frac{i}{2t} (\theta_1 - \theta_0)^2, \\ \frac{\partial S_1}{\partial \theta_0} &= -\frac{i}{t} (\theta_1 - \theta_0), \\ \frac{\partial^2 S_1}{\partial \theta_0^2} &= \frac{i}{t}. \end{aligned} \quad (4.25)$$

We thus obtain for the fidelity according to Eq. (4.10):

$$F = \left| \frac{1}{4\pi^2 \epsilon} \int d\theta_1 \int d\theta_2 \sqrt{|V_1| |V_2|} \sqrt{2\pi \epsilon t} e^{it \cos \theta_1 (k_2 - k_1)} e^{-i \frac{(\theta_1 - \theta_2)^2}{2t\epsilon}} \right|^2. \quad (4.26)$$

A second stationary phase approximation in analogy to the one above, but this time with respect to θ_2 , leads to

$$F = \left| \frac{1}{2\pi} \int d\theta_1 e^{it \cos \theta_1 (k_2 - k_1)} \right|^2, \quad (4.27)$$

where t^{-1} has been inserted for each Van Vleck determinant. The last integral gives us the Bessel function of zeroth order and a factor of 2π (see (A.1.) in the appendix), which means that the fidelity of one resonant rotor at $\epsilon = 0$ is as expected

$$F(k_1, k_2, t) = J_0^2(t |k_2 - k_1|). \quad (4.28)$$

We have thus retrieved the result of section 2.3 by use of the pendulum approximation. However, as soon as we deflect from $\epsilon \rightarrow 0$ (the case that we have just calculated), elliptic integrals will appear and make the calculation very difficult, if not impossible. For this reason, we will have a look whether any further simplification is possible.

4.1.3 Semiclassical approximation with the propagators for the harmonic oscillator

We have succeeded in deriving the desired result $J_0^2(t |k_2 - k_1|)$ by use of the pendulum approximation. Now, we go one step further and approximate the pendulum by the harmonic oscillator. We do not explicitly calculate the propagator for the harmonic oscillator via the action here as we did in the last section, but instead help ourselves to the well-known propagator for the quantum-mechanical case (the derivation is performed in detail in Appendix B), exchanging \hbar with ϵ in accordance with ϵ -classics. We will then use stationary phase approximations to derive the characteristic algebraic decay once more.

Our initial wavefunctions are once more equal to $\frac{1}{\sqrt{2\pi}}$, since we use plane waves with momentum zero. We recall the definition of the fidelity in the propagator formalism:

$$F(t, \epsilon, k_1, k_2) = \left| \int d\theta \int d\theta' \int d\theta'' G_1^*(\theta, \theta', t) G_2(\theta'', \theta', t) \Psi(\theta'') \Psi^*(\theta) \right|^2 \quad (4.29)$$

We use the following formula for the harmonic oscillator propagator in ϵ -classics [70] (by taking ϵ as the new Planck's constant):

$$G(\theta, \theta', t) = \left(\frac{\omega}{2\pi i \epsilon \sin(\omega t)} \right)^{1/2} e^{\frac{i\omega}{2\epsilon \sin(\omega t)} \{(\theta^2 + \theta'^2) \cos(\omega t) - 2\theta\theta'\}}. \quad (4.30)$$

A proper derivation of this propagator is given in the appendix. For ω , we use the harmonic oscillator frequency $\sqrt{k\epsilon}$ of ϵ -classics (3.6), which we derived in the previous chapter. Now, we make the assumption that $\omega t \ll 1$, which is roughly the same as requesting the time to be smaller than one period of the beating. Then we can expand the sines and cosines in the above formula as follows:

$$\frac{\omega}{\sin(\omega t)} \approx \frac{1}{t} \frac{\omega t}{\omega t - \frac{(\omega t)^3}{6}} \approx \frac{1}{t} \left(1 + \frac{k\epsilon}{6} t^2 \right) = \left(\frac{1}{t} + \frac{k\epsilon}{6} t \right), \quad (4.31)$$

$$\cos(\omega t) \approx 1 - \frac{(\omega t)^2}{2} \approx 1 - \frac{k\epsilon}{2} t^2. \quad (4.32)$$

Inserting these perturbation series and the propagators into the definition of fidelity leads to

$$\begin{aligned} F(t, \epsilon, k_1, k_2) &= \left| \frac{1}{2\pi} \int d\theta \int d\theta' \int d\theta'' \frac{1}{2\pi i \epsilon} \left(\frac{1}{t} + \frac{k_1 \epsilon}{6} t \right)^{\frac{1}{2}} \left(-\frac{1}{t} - \frac{k_2 \epsilon}{6} t \right)^{\frac{1}{2}} \right. \\ &\quad \cdot e^{\frac{-i}{2\epsilon t} (1 + \frac{k_1}{6} t^2) \{(\theta'^2 + \theta^2)(1 - \frac{\epsilon k_1}{2} t^2) - 2\theta\theta'\}} \\ &\quad \left. \cdot e^{\frac{i}{2\epsilon t} (1 + \frac{k_2}{6} t^2) \{(\theta''^2 + \theta'^2)(1 - \frac{\epsilon k_2}{2} t^2) - 2\theta'\theta''\}} \right|^2 \\ &= \left| \frac{1}{4\pi^2 \epsilon t} \left(1 + \frac{(k_1 + k_2)\epsilon}{6} t^2 + \frac{k_1 k_2 \epsilon^2}{36} t^4 \right)^{\frac{1}{2}} \int d\theta \int d\theta' \int d\theta'' \right. \\ &\quad \cdot e^{\frac{i}{2\epsilon t} \{(\theta'' - \theta')^2 - (\theta' - \theta)^2\}} e^{\frac{itk_1}{6} \{\theta'^2 + \theta^2 + \theta'\theta\}} \\ &\quad \left. \cdot e^{\frac{-itk_2}{6} \{\theta'^2 + \theta''^2 + \theta'\theta''\}} \right|^2. \end{aligned} \quad (4.33)$$

Now, we perform a stationary phase approximation with respect to θ and obtain:

$$\begin{aligned} F &= \left| \frac{\sqrt{2\pi\epsilon t}}{4\pi^2 \epsilon t} \left(1 + \frac{(k_1 + k_2)\epsilon}{6} t^2 + \frac{k_1 k_2 \epsilon^2}{36} t^4 \right)^{\frac{1}{2}} \int d\theta' \int d\theta'' \right. \\ &\quad \left. \cdot e^{\frac{i}{2\epsilon t} (\theta' - \theta'')^2} e^{\frac{itk_1}{2} \theta'^2} e^{-\frac{itk_2}{6} (\theta'^2 + \theta''^2 + \theta'\theta'')} \right|^2 \end{aligned} \quad (4.34)$$

by using

$$S_1 = \frac{i}{2t} (\theta' - \theta'')^2, \quad \frac{\partial S_1}{\partial \theta} = -\frac{i}{t} (\theta' - \theta) \stackrel{!}{=} 0, \quad \frac{\partial^2 S_1}{\partial \theta^2} = \frac{i}{\epsilon t}. \quad (4.35)$$

A second stationary phase approximation, this time with respect to θ'' , is performed and leads to:

$$\begin{aligned}
F &= \left| \frac{1}{2\pi} \left(1 + \frac{(k_1 + k_2)\epsilon}{6} t^2 + \frac{k_1 k_2 \epsilon^2}{36} t^4 \right)^{\frac{1}{2}} \int d\theta' e^{\frac{it}{2} \theta'^2 (k_1 - k_2)} \right|^2 \\
&= \frac{1}{t(k_1 - k_2)} \left(1 + \frac{(k_1 + k_2)\epsilon}{6} t^2 + \frac{k_1 k_2 \epsilon^2}{36} t^4 \right) \\
&= \frac{1}{(k_1 - k_2)} \left(\frac{1}{t} + \frac{(k_1 + k_2)\epsilon}{6} t + \frac{k_1 k_2 \epsilon^2}{36} t^3 \right), \tag{4.36}
\end{aligned}$$

where Eq. (A.5.) has been used.

Although we cannot recover the Bessel functions by this relatively coarse approximation, the overall t^{-1} -decay for small time scales is nicely visible. The other terms can be neglected since we assume both ϵ and t to be small.

The harmonic oscillator approximation is the most simple way to retrieve the most important of the characteristics of the single resonant rotor: It allows us to derive the typical t^{-1} -decay. Plus: The harmonic oscillator naturally has a characteristic frequency, which corresponds to $\sqrt{\epsilon k}$ (compare section 3.1). It is therefore only to be expected that a pair of harmonic oscillators is characterized by the sum and the difference of its frequencies, $\sqrt{\epsilon}(\sqrt{k_1} + \sqrt{k_2})$ and $\sqrt{\epsilon}(\sqrt{k_1} - \sqrt{k_2})$ (a frequency which we have already observed in our numerical investigations). We may thus assume the approximation by the harmonic oscillator to be adequate. We shall now see whether this proves to be true.

4.2 Semiclassical approximation close to quantum resonance for resonant and near-resonant rotors

We have already proven the accuracy of approximating our resonant rotors by the harmonic oscillator for small times. Now, in order to illustrate the validity of the harmonic oscillator approximation which we will further use in this section, we take a closer look at what exactly happens on the principal resonance island in phase space. As already mentioned, this island has often been substituted very successfully by the corresponding pendulum in literature [28, 82]. To even further simplify our dynamics, we have then approximated the pendulum by the harmonic oscillator. But does this simplification really still preserve our necessary information? To show that it does indeed, we place a coherent state on the island representing the non-linear resonance of the ϵ -classical phase space. As expected, it does not decay [39], but instead oscillates regularly (see Fig. 4.3), with the observed frequency equal to the beating frequency of the harmonic oscillator. We also observe higher harmonics, which is only to be expected for a quantum system (just remember the harmonic oscillator itself, with its spectrum of equidistant frequencies).

Semiclassical approximation for resonant rotors

As we have just seen, the resonant δ -kicked rotors are very well described by the harmonic oscillator approximation. Therefore, we shall start our attempt to comprehend their behaviour by using the semiclassical propagator as derived from the ϵ -classical picture.

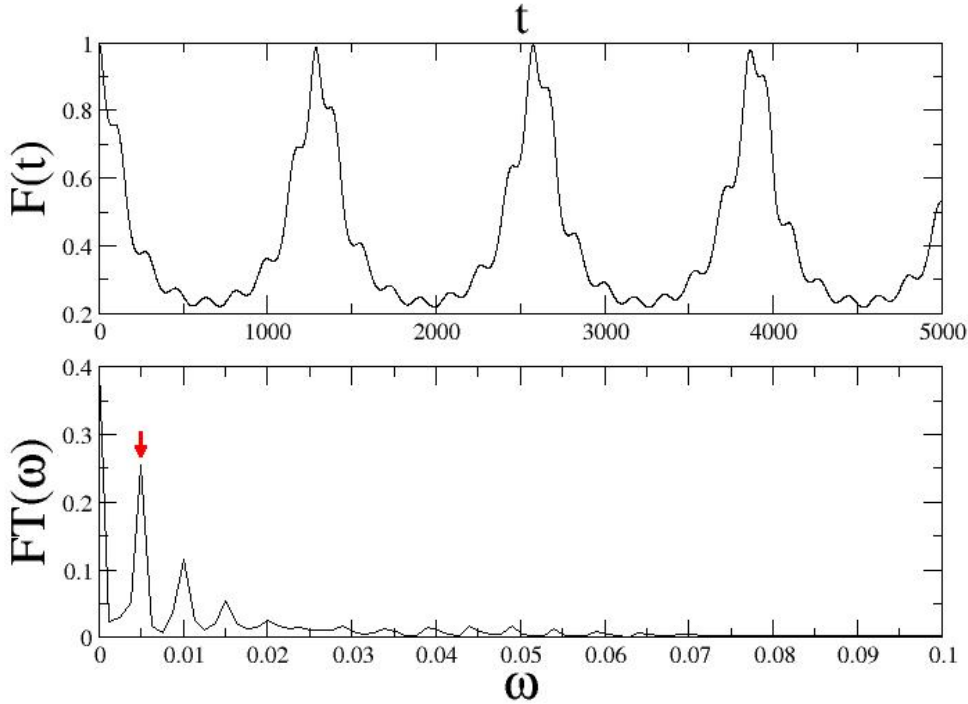


Figure 4.3: Fidelity (*upper panel*) and its Fourier Transform (*lower panel*) for a coherent initial state on the principal resonance island shown in Fig. 4.2, with parameter values $k_1 = 3.9$, $k_2 = 3.0$, $\beta = 0.5$, and $\epsilon = 0.0001$. We observe revivals after a time $T = \frac{2\pi}{\omega}$, where ω corresponds to two times the beating frequency $\omega = 2\sqrt{\epsilon}(\sqrt{k_1} - \sqrt{k_2}) = 0.005$ (see arrow in the lower panel) of the harmonic oscillator, thus illustrating the validity of the harmonic oscillator approximation.

We may again scale our action by $\eta = \sqrt{k\epsilon}$ as follows (see Eq. (4.20)):

$$S(\theta, \theta', t, k) = \eta S(\theta, \theta', t\eta, 1). \quad (4.37)$$

The rescaled harmonic oscillator is then described by the Lagrangian

$$L = \frac{1}{2}\dot{\theta}^2 - \frac{1}{2}\theta^2, \quad (4.38)$$

and the solution to its equation of motion is also well known:

$$\theta(t) = \theta_0 \cos(t) + I_0 \sin(t), \quad (4.39)$$

where $I_0 = \dot{\theta}$ denotes the initial momentum (using the ϵ -classical notation), which will later be set to zero (according to our initial condition).

The spatial coordinate θ is already restricted to one phase space cell, as expected from ϵ -classics. The periodicity in θ is also implied by the image of the pendulum and the harmonic oscillator themselves. We do not put any constraints on the momentum.

Our action is thus

$$S = \int_0^\eta ds \left[\frac{1}{2} \dot{\theta}^2(s) - \frac{1}{2} \theta^2(s) \right], \quad (4.40)$$

and we can make the following semiclassical ansatz for the fidelity:

$$F = \left| \frac{1}{4\pi^2 i \epsilon} \iiint d\theta_0 d\theta'_0 d\theta \sqrt{\frac{\partial^2 S(\theta_0, \theta, t\eta_1, 1)}{\partial \theta_0 \partial \theta}} \sqrt{\frac{\partial^2 S(\theta_0 \theta'_0, t\eta_2, 1)}{\partial \theta \partial \theta'_0}} \cdot e^{\frac{i}{\epsilon} \eta_1 S(\theta_0, \theta, t\eta_1, 1)} e^{-\frac{i}{\epsilon} \eta_2 S(\theta_0 \theta'_0, t\eta_2, 1)} \right|^2. \quad (4.41)$$

In order to use the stationary phase approximation to eliminate θ_0 , we need to determine the extremum for which

$$\frac{\partial S}{\partial \theta_0} = 0, \quad (4.42)$$

which is essentially the same as setting I_0 to zero. This results in the action

$$\begin{aligned} S &= \int_0^{\eta t} ds \left[\frac{1}{2} \dot{\theta}^2(s) - \frac{1}{2} \theta^2(s) \right] \\ &= \frac{1}{2} \int_0^{\eta t} ds \left[\theta_0^2 \sin^2(s) - \theta_0^2 \cos^2(s) \right] \\ &= -\frac{1}{2} \int_0^{\eta t} ds \theta_0^2 \cos(2s) \\ &= -\frac{1}{4} \theta_0^2 \sin(2\eta t) \\ &= -\frac{1}{2} \theta^2 \tan(\eta t). \end{aligned} \quad (4.43)$$

Using this and the fact that

$$\frac{\partial^2 S}{\partial \theta_0^2} = -\frac{\partial p_0}{\partial \theta_0} = -\eta \frac{\partial}{\partial \theta_0} \left(\frac{\theta - \theta_0 \cos(t)}{\sin(t)} \right) = +\eta \frac{1}{\tan(t)}, \quad (4.44)$$

$$\frac{\partial^2 S}{\partial \theta_0 \partial \theta} = -\frac{\partial p_0}{\partial \theta} = -\eta \frac{\partial}{\partial \theta} \left(\frac{\theta - \theta_0 \cos(t)}{\sin(t)} \right) = -\eta \frac{1}{\sin(t)} \quad (4.45)$$

(the factor of η comes from the scaled action, which we are considering here) in the stationary phase approximation over θ_0 and performing a second stationary phase approximation, this time with respect to θ'_0 , leads to

$$F = \left| \frac{1}{2\pi \sqrt{\cos(\eta_1 t) \cos(\eta_2 t)}} \int d\theta e^{\frac{i}{2\sqrt{\epsilon}} \theta^2 [\sqrt{k_1} \tan(\eta_1 t) - \sqrt{k_2} \tan(\eta_2 t)]} \right|^2. \quad (4.46)$$

Since we already know that this “imaginary Gaussian” is centred in our primary ϵ -classical phase space cell, we are able to resize the integral from minus to plus infinity without changing the result. Thus, we are able to use the formula

$$\int_{-\infty}^{\infty} dx e^{-ix^2} = \sqrt{\frac{\pi}{2}} (1 - i), \quad (4.47)$$

which can be found in [83, 84] and obtain (after a simple coordinate transformation $x^2 = \frac{1}{2\sqrt{\epsilon}}\theta^2 [\sqrt{k_2} \tan(\eta_2 t) - \sqrt{k_1} \tan(\eta_1 t)]$) as our final result

$$\begin{aligned}
 F &= \left| \frac{\sqrt{\epsilon}}{2\pi \cos(\eta_1 t) \cos(\eta_2 t)} \right| \left| \frac{1}{\sqrt{k_1} \tan(\eta_1 t) - \sqrt{k_2} \tan(\eta_2 t)} \right| \\
 &= \left| \frac{\sqrt{\epsilon}}{2\pi \sqrt{k_1} \sin(\eta_1 t) \cos(\eta_2 t) - \sqrt{k_2} \sin(\eta_2 t) \cos(\eta_1 t)} \right|. \tag{4.48}
 \end{aligned}$$

Comparing this formula with our numerical results from section 3.1.3, we find a surprisingly accurate agreement (see Fig. 4.4), considering that the approximation we used was rather rough.

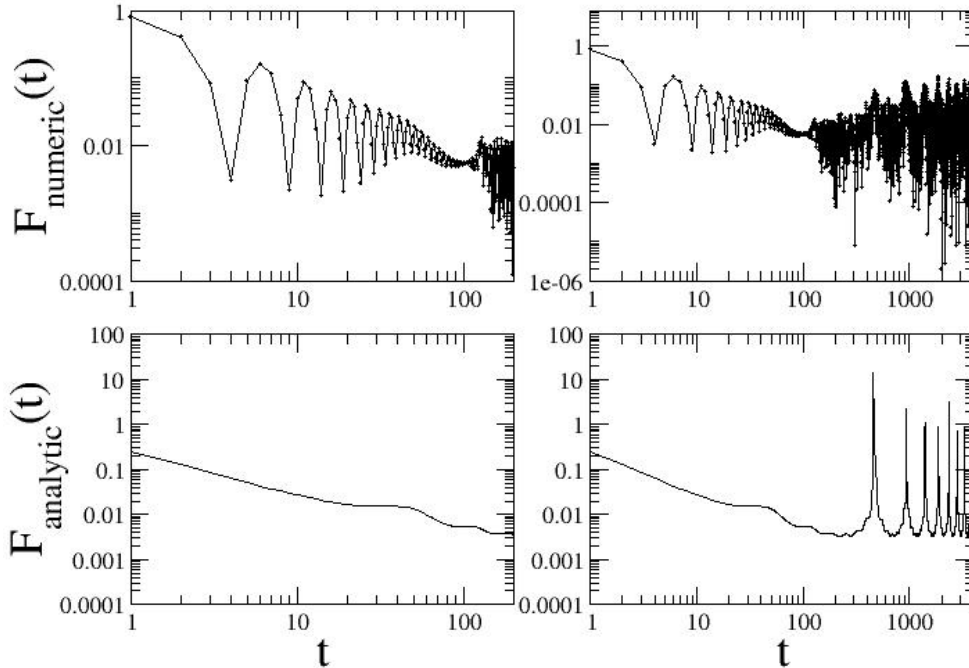


Figure 4.4: *Upper panels:* The numerical simulations exhibit characteristic features: A time of onset where the t^{-1} -decay of the resonant rotor breaks down (*left*), and revivals with two times the beating frequency of the harmonic oscillator ($\omega = 2\sqrt{\epsilon}(\sqrt{k_1} - \sqrt{k_2})$) (*right*). *Lower panels:* Those features are also observed in the plots of the analytical expression of Eq. (4.48). The figures were plotted for kicking strengths $k_1 = 0.8\pi$ and $k_2 = 0.6\pi$ and a deviation $\epsilon = 0.001$ from quantum resonance in the kicking period.

Please note that our analytical result is not the envelope of the numeric curve, but rather gives a qualitative description of the curve's global behaviour. For small times, we observe the expected t^{-1} -decay, whereas for long times revivals with the period of the beating frequency prevail.

Let us now take a look at the revivals, which are clearly visible in the plots for the analytical expression for the fidelity (Fig. 4.4, lower panels). Since the resolution is

restricted by the number of numerical values of the analytical expression for the fidelity, they only approximate the singularities of Eq. (4.48). Those singularities originate in the denominator, which we can further simplify by making use of the addition theorem for cosines:

$$\begin{aligned} & \sqrt{k_1} \sin(\eta_1 t) \cos(\eta_2 t) - \sqrt{k_2} \sin(\eta_2 t) \cos(\eta_1 t) \\ &= \frac{1}{2} \left[\left(\sqrt{k_1} + \sqrt{k_2} \right) \sin(\eta_1 t - \eta_2 t) + \left(\sqrt{k_1} - \sqrt{k_2} \right) \sin(\eta_1 t + \eta_2 t) \right]. \end{aligned} \quad (4.49)$$

We shall call the relevant part of the denominator A in the following:

$$A \equiv \left(\sqrt{k_1} + \sqrt{k_2} \right) \sin(\eta_1 t - \eta_2 t) + \left(\sqrt{k_1} - \sqrt{k_2} \right) \sin(\eta_1 t + \eta_2 t). \quad (4.50)$$

Plotting A versus t in Fig. 4.5 yields the singularities of Eq. (4.48): The zeros of A coincide with the singularities of the fidelity. We can therefore graphically solve the problem of finding the singularities for the analytical expression of fidelity. Using Fourier transformation, we find the frequencies with which A oscillates – and those are nothing but half the frequencies of the revivals, since the zeros of A equal the revivals here. Since Eq. (4.50) is comparatively simple, it is also possible to calculate the Fourier Transform by hand (or by using symbolic computation software like Mathematica), using the convention of a positive exponential and a prefactor of $\frac{1}{\sqrt{2\pi}}$ for the Fourier Transform. The result is:

$$\begin{aligned} FT(\omega) = & i \sqrt{\frac{\pi}{2\epsilon}} \left[\eta_+ \delta(-\eta_- + \omega) - \eta_+ \delta(\eta_- + \omega) \right. \\ & \left. + \eta_- \delta(-\eta_+ + \omega) - \eta_- \delta(\eta_+ + \omega) \right], \end{aligned} \quad (4.51)$$

with $\eta_- = \omega_{bf} = \eta_1 - \eta_2$ and $\eta_+ = \eta_1 + \eta_2$. As expected, we obtain δ -functions for the frequency dependence. In Fig. 4.5, we plot the power spectrum (created by squaring the Fourier Transform). We observe two frequencies: The doubled beating frequency $2\eta_- = 2\eta_1 - 2\eta_2$ and the doubled summed frequency $2\eta_+ = 2\eta_1 + 2\eta_2$. The beating frequency is clearly dominant, since its amplitude is much bigger.

Comparing the power spectra of the numerical simulation for the fidelity and the relevant part of the denominator of its analytic expression (Fig. 4.5), we can retrace both frequencies, although $2\eta_+$ is almost invisible due to higher harmonics of $2\eta_-$ (which is a special feature of the harmonic oscillator), whose amplitude hides away the smaller $2\eta_+$ -contribution. This also explains the higher frequency component that we have observed in the Husimi function (Fig. 4.3). It corresponds to $2\eta_+$ and is barely visible in the Fourier Transform due to its small amplitude.

However, the fact why we observe higher harmonics at all in the numerical quantum calculations is not yet explained. We will elaborate on this open question in the conclusion.

Let us have a look at t_{onset} now. In the last chapter, it was defined as the time where the breakdown of the characteristic t^{-1} -decay of the resonant rotor at exact quantum resonance is first visible. However, this definition turns out to be problematic for our analytical expression, since it only describes the behaviour of the upper envelope, whereas the stationary phase approximation entails an averaging over the oscillations – what we find is thus not a pure envelope. The definition of t_{onset} is also questionable

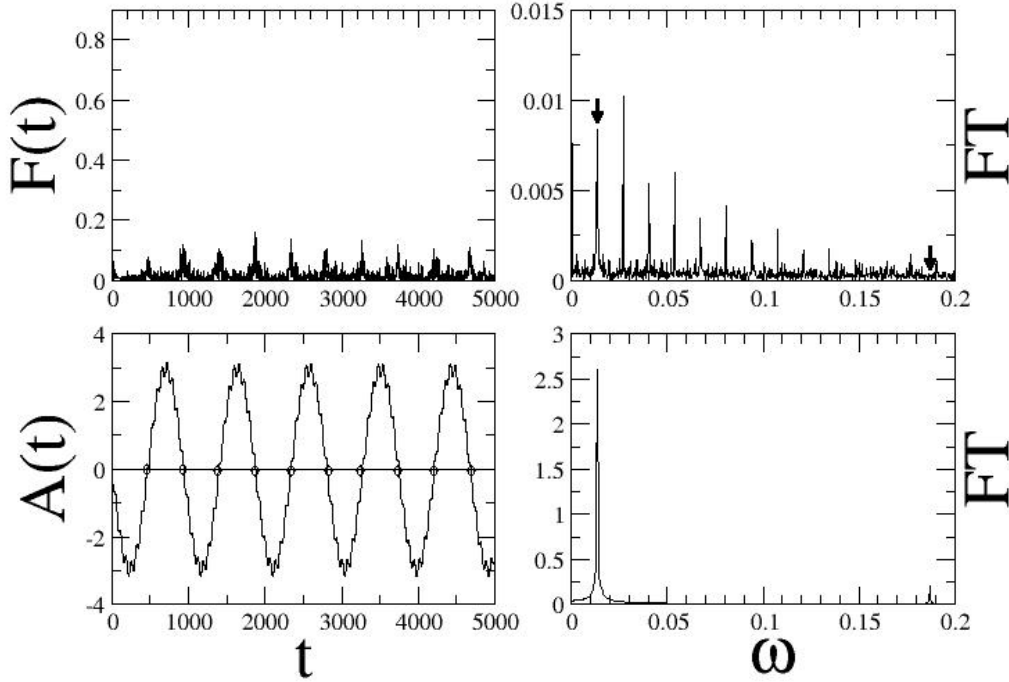


Figure 4.5: *Upper left panel:* Numerical observation of the fidelity revivals with a period $T = \frac{\pi}{\omega_b f}$ for a kicked rotor with $\epsilon = 0.001$, $k_1 = 0.8\pi$ and $k_2 = 0.6\pi$. *Upper right panel:* Fourier Transform of the numerical result. *Lower left panel:* The denominator A produces the revival frequency by the frequency of its zeroes (marked by small circles). *Lower right panel:* Only the two frequencies $2\eta_-$ and $2\eta_+$ occur in the power spectrum of A . They are indicated in the upper panel by arrows.

because the deviation from the results in exact resonance starts much earlier, at least for the lower envelope. If there was any hint towards something similar to t_{onset} in the analytical expression, it would have to be in the same interval as for the numerical calculation in Fig. 4.6 – but we cannot find any extrema or anything else that could possibly correspond to the onset of the breakdown.

We have to accept that our analytical expression, given by Eq. (4.48), is not able to retrieve t_{onset} . Otherwise, however, it is an adequate description of the behaviour of the fidelity of the resonant rotor in the vicinity to quantum resonance – it even reproduces the revivals at longer interaction times!

Our semiclassical ansatz was successful for the resonant rotor. But what about the nonresonant rotors, is there any way to perform similar calculations for them? The main problem here is that we could not find any expression for the form of the tori of the nonresonant rotors, which is crucial in their case. So unfortunately, the behaviour of the non-resonant rotors remains yet unsolved. It will take a more complicated theory to describe the behaviour of fidelity in the case of nonresonant values for β .

What we can do, however, is to expand our analytical expression to an ensemble of

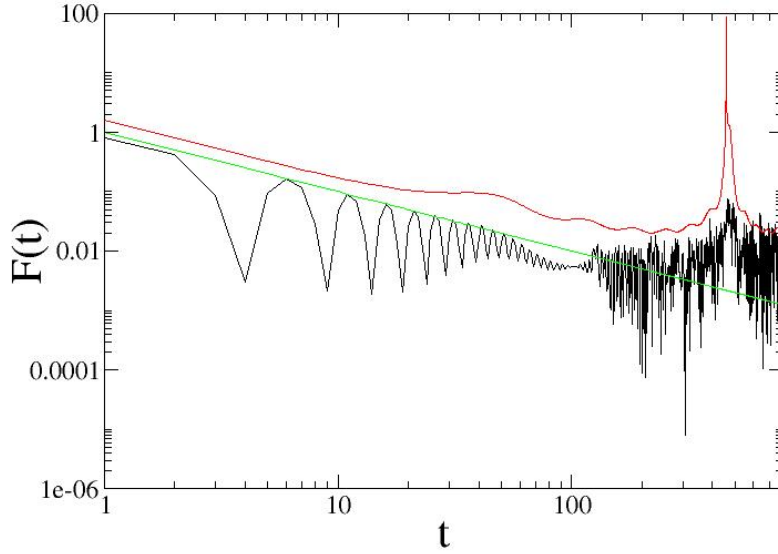


Figure 4.6: Fidelity decay with parameters $\epsilon = 0.001$, $k_1 = 0.8\pi$ and $k_2 = 0.6\pi$. In the numerical curve (*black*), the breakdown of the t^{-1} -decay (see *green* line) is visible. Unfortunately, the analytical expression Eq. (4.48) (*red*) does not reproduce this breakdown of the algebraic decay. In this plot, the red curve of the analytical expression was multiplied by a factor 10 for better visibility.

near-resonant rotors in the immediate vicinity of the resonant value of β . We shall calculate this in the next section.

Semiclassical approximation for near-resonant rotors

The harmonic oscillator approximation works well in and close to the quantum resonance with $\tau = 2\pi + \epsilon$ and $\beta = \frac{1}{2}$, i.e., for resonant values of quasimomentum. Since we have observed a doubling of the beating frequency for the exact resonant value, however, we now investigate small integrals around the resonant β , and hope to find where the transition to the single beating frequency comes from. For wide enough integrals, we expect to retrieve the beating frequency.

Again we start out from the ϵ -classical map (see section 2.4) and apply the harmonic oscillator approximation. This time, however, we explicitly keep the term depending on $\tau\beta$ to arrive at the Hamiltonian

$$H = \frac{1}{2}(I + \tilde{\beta})^2 + \frac{1}{2}\theta^2, \quad (4.52)$$

where $\tilde{\beta}$ is a small deviation from the fixed point (we assume that $p_0 = 0$, which is confirmed by the first stationary phase approximation). In the convention of ϵ -classics, $\tilde{\beta}$ is a small deflection from the center of the resonance island. This means that for resonance conditions with $\beta = 0.5$, $\tilde{\beta} = \tau(\beta - \frac{1}{2}) = (2\pi + \epsilon)(\beta - \frac{1}{2})$ is the deflection. For resonance conditions where $\beta = 0$, $\tilde{\beta} = \tau\beta = (2\pi + \epsilon)\beta$ applies.

The equations of motion read:

$$\dot{I} = -\theta, \quad \dot{\theta} = I + \tilde{\beta} \equiv \tilde{I}. \quad (4.53)$$

We now plug the Lagrangian,

$$L = I\dot{\theta} - H = \frac{1}{2}\dot{\theta}^2 - \frac{1}{2}\theta^2 - \tilde{\beta}\dot{\theta}, \quad (4.54)$$

into our action, resulting in

$$S(\theta, \theta', \eta t, 1) = \frac{1}{2} \int_0^{\eta t} \left[\dot{\theta}^2(s) - \theta^2(s) \right] ds - \tilde{\beta}(\theta - \theta_0), \quad (4.55)$$

with starting point $\theta_0 = \theta(0)$ and end point $\theta = \theta(\eta t)$. We have used once more the scaled action, see Eq. (4.20).

As before, we define $\eta = \sqrt{k\epsilon}$. Analogous to the case of the resonant rotors, we use the expression for the fidelity in the semiclassical ansatz and we perform a stationary phase approximation with respect to θ_0 :

$$\frac{\partial S}{\partial \theta_0} = 0 \rightarrow I_0 = 0 \rightarrow \tilde{I}_0 = \dot{\theta}_0 = \tilde{\beta}. \quad (4.56)$$

Now, the solution to the equations of motion differs slightly from Eq. (4.39):

$$\begin{aligned} \theta(t) &= \theta_0 \cos(t) + \tilde{\beta} \sin(t), \\ \dot{\theta}(t) &= -\theta_0 \sin(t) + \tilde{\beta} \cos(t). \end{aligned} \quad (4.57)$$

Plugging this into the action, Eq. (4.55), we obtain:

$$\begin{aligned} S(\theta, \theta_0, \eta t, 1) &= \frac{1}{4}(\tilde{\beta}^2 - \theta_0^2) \sin(2\eta t) - \tilde{\beta}\theta_0 \sin^2(\eta t) - \tilde{\beta}(\theta - \theta_0), \\ &= \tilde{\beta}\theta \left(\frac{1 - \cos(\eta t)}{\cos(\eta t)} \right) - \frac{1}{2}(\tilde{\beta}^2 + \theta^2) \tan(\eta t), \end{aligned} \quad (4.58)$$

since $\theta_0 = \frac{\theta - \tilde{\beta} \sin(\eta t)}{\cos(\eta t)}$. The Van Vleck determinants and the second derivatives are the same as for the case of the resonant rotor, see Eq. (4.44) and Eq. (4.45).

Another stationary phase approximation, this time with respect to θ_0' (completely analogous to the one we have performed with respect to θ_0), yields for the fidelity of a small ensemble of nearly resonant β -rotors (in the interval $[-\tilde{\beta}, \tilde{\beta}]$):

$$F_{\tilde{\beta}}(t) = \left| \frac{1}{2\pi \sqrt{\cos(\eta_1 t) \cos(\eta_2 t)}} \int_{-\tilde{\beta}}^{\tilde{\beta}} d\beta' e^{\frac{i}{\sqrt{\epsilon}} \left(a - \frac{b^2}{4a} \right) \beta'^2} \int_0^{2\pi} d\theta e^{\frac{i}{\sqrt{\epsilon}} \left(\sqrt{a}\theta + \frac{b}{2\sqrt{a}}\beta' \right)^2} \right|^2, \quad (4.59)$$

using the abbreviations

$$\begin{aligned} a &= a(t) \equiv \frac{1}{2}(\sqrt{k_2} \tan(\eta_2 t) - \sqrt{k_1} \tan(\eta_1 t)), \\ b &= b(t) \equiv \sqrt{k_1} \left(\frac{1 - \cos(\eta_1 t)}{\cos \eta_1 t} \right) - \sqrt{k_2} \left(\frac{1 - \cos(\eta_2 t)}{\cos \eta_2 t} \right). \end{aligned}$$

Assuming the Gaussian of the integral over θ to be centred in our primary ϵ -classical phase space cell, we may once more use Eq. (4.47) for the infinite integral. After a coordinate transformation with $x^2 = \frac{-1}{\sqrt{\epsilon}} \left[\sqrt{a}\theta + \frac{b}{2\sqrt{a}}\beta \right]^2$, we obtain our final result:

$$\begin{aligned} F_{\tilde{\beta}}(t) &= \left| \frac{\sqrt[4]{\epsilon}}{2\sqrt{\pi a \cos(\eta_1 t) \cos(\eta_2 t)}} \int_{-\tilde{\beta}}^{\tilde{\beta}} d\beta' e^{\frac{i}{\sqrt{\epsilon}} \left(a - \frac{b^2}{4a}\right) \beta'^2} \right|^2 \\ &= \left| \frac{\sqrt{\epsilon}}{2\pi \cos(\eta_1 t) \cos(\eta_2 t)} \cdot \frac{1}{(\sqrt{k_2} \tan(\eta_2 t) - \sqrt{k_1} \tan(\eta_1 t))} \right| \\ &\quad \cdot \left| \int_{-\tilde{\beta}}^{\tilde{\beta}} d\beta' e^{\frac{i}{\sqrt{\epsilon}} \left(a - \frac{b^2}{4a}\right) \beta'^2} \right|^2. \end{aligned} \quad (4.60)$$

For $\tilde{\beta}$ very close to zero, we get the expected expression for the fidelity of resonant rotors, Eq. (4.48), which we shall call $F_{resonant}$ from now on:

$$F_{resonant}(t) = \left| \frac{\sqrt{\epsilon}}{2\pi \cos(\eta_1 t) \cos(\eta_2 t)} \cdot \frac{1}{(\sqrt{k_2} \tan(\eta_2 t) - \sqrt{k_1} \tan(\eta_1 t))} \right|.$$

The interesting part is now the integral over the complex Gaussian. Let us denote

$$Z(\tilde{\beta}) \equiv \left| \int_{-\tilde{\beta}}^{\tilde{\beta}} d\beta' e^{\frac{i}{\sqrt{\epsilon}} \left(a - \frac{b^2}{4a}\right) \beta'^2} \right|^2. \quad (4.61)$$

Unfortunately, it is not possible to find a solution for finite boundaries. However, assuming that $Z(\tilde{\beta})$ has significant values only close enough around 0, we can expand the boundaries to $\pm\infty$. $Z(\tilde{\beta})$ converges towards $Z(\infty)$ for all times, as illustrated in Fig. 4.7 for $t = 100$.

Let us look at the result for the fidelity which we get for the case $Z(\infty)$ (again making use of Eq. (4.47)):

$$F_{fullbeta}(t) = \left| \frac{\epsilon}{2 \cos(\eta_1 t) \cos(\eta_2 t)} \cdot \frac{1}{(\sqrt{k_2} \tan(\eta_2 t) - \sqrt{k_1} \tan(\eta_1 t))} \right| \cdot \left| \frac{1}{a - \frac{b^2}{4a}} \right|. \quad (4.62)$$

Plotting both cases (see Fig. 4.8), we find that $F_{resonant}$ displays the doubled beating frequency. $F_{fullbeta}$ on the other hand, for which we expanded the boundaries to infinity, shows revivals with just the beating frequency. An additional interesting feature is the double peak at the beginning of the revivals in $F_{fullbeta}$.

Fig. 4.8 indicates that the transition from doubled to ordinary beating frequency is due to the finite boundaries of the complex Gaussian integral. We would expect the doubled frequency to disappear as soon as $\tilde{\beta}$ is larger than some critical value $\tilde{\beta}_{crit}$. We can calculate an estimate based on the prefactor $\frac{a-b^2/4a}{\sqrt{\epsilon}} = \frac{4a\epsilon^{-1/2}}{4a^2-b^2}$. Interpreting

$$\sigma \equiv \sqrt{\frac{\sqrt{\epsilon}}{2}} \sqrt{\frac{4a}{4a^2 - b^2}} \quad (4.63)$$

as the half width of the Gaussian integral of Eq. (4.61) in the complex plane gives a scaling for the critical value $\tilde{\beta}_{crit}$. Measuring the values of $\tilde{\beta}$ for which the transition

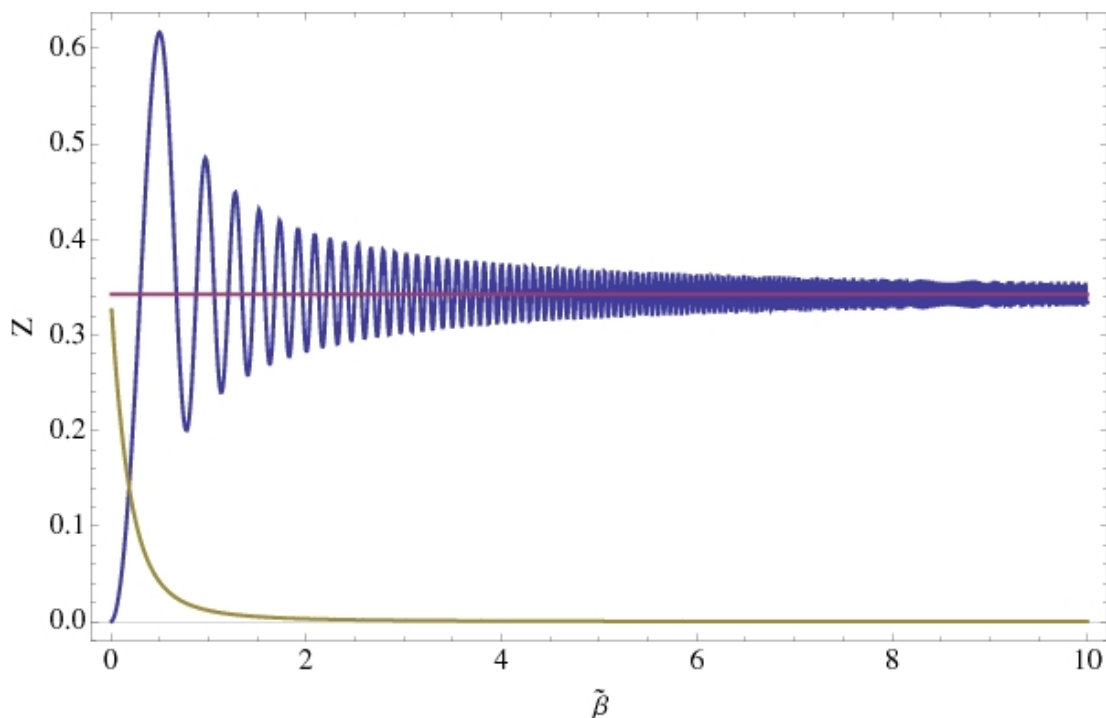


Figure 4.7: Plot of the modulus square of the integral (*in blue*) over the complex Gaussian for different boundaries $[-\tilde{\beta}, \tilde{\beta}]$ and of modulus square of the complement of this integral (*yellow*) for a fixed time t (here after 100 kicks). The time only has an effect on the absolute height of the curve. As $\tilde{\beta}$ increases, the blue curve oscillates more and more closely about the curve for the exact analytical expression for the integral with boundary conditions $[-\infty, \infty]$ (*in red*), while the complement oscillates around zero. We used kicking strengths $k_1 = 0.8\pi$ and $k_2 = 0.6\pi$, and a perturbation $\epsilon = 0.001$ in this plot.

occurs (see Table 4.1), we numerically confirm this $\tilde{\beta}$ (defined as its value where the intermediate peaks disappear in results as shown in Fig. 4.8):

$$\tilde{\beta}_{crit} \propto \sigma \propto \epsilon^{1/4}. \quad (4.64)$$

This is a bit of a handwaving argument, however, since both a and b are time-dependent. Even though the ϵ -dependence is nicely reproduced, the rest term has singularities reproducing the revivals.

Since the value of Z is determined by how large we choose $\tilde{\beta}$, this means that for our corresponding quantum calculations, we have to remember the scaling and thus consider $\beta = \frac{\tilde{\beta}}{\tau} + \frac{1}{2}$ in our case. The presence of τ in the scaling is particularly useful in experiments. For $\tau = 2\pi l + \epsilon$ ($l \in \mathbb{N}$), $l \rightarrow \infty$, the interval around the resonant value of quasimomentum (in our notation $\beta = \frac{1}{2}$) will become infinitely small which will aggravate observing the doubling of the beating frequency in experiments. On the other hand, for the case $\tau \rightarrow 0$, corresponding again to resonant driving [26], the interval around $\beta = \frac{1}{2}$ becomes arbitrarily large – heavenly conditions for experimentalists. Varying the kicking period τ thus might even make it possible to observe the phenomenon with cold atoms without needing to resort to ultracold atoms. This makes the effect of the frequency doubling near resonant values of quasimomentum even more attractive.

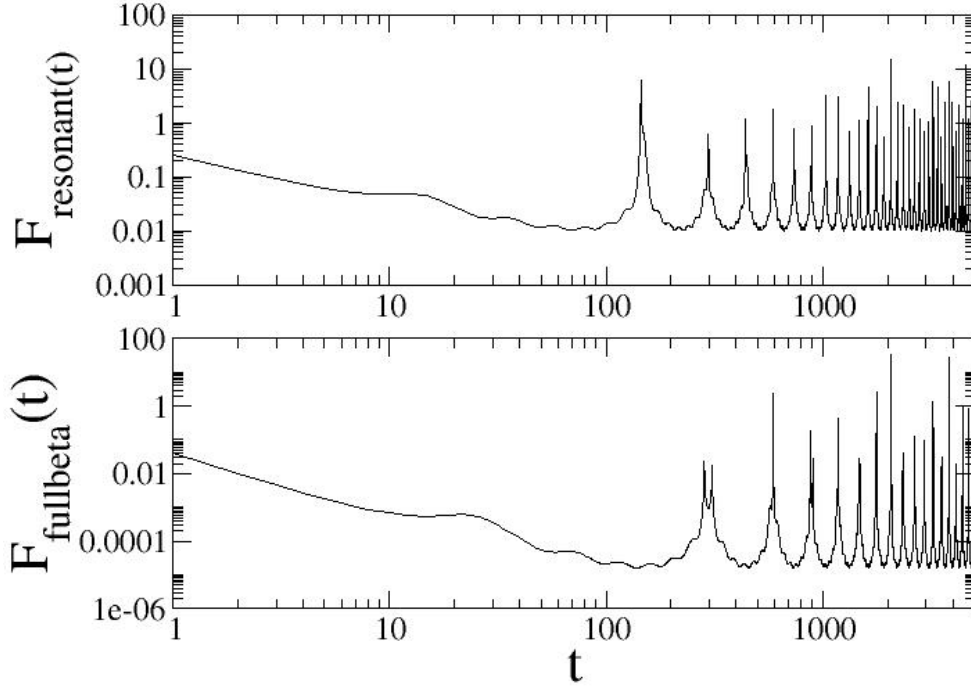


Figure 4.8: Comparison of the fidelity for a single resonant rotor (*upper panel*) and the fidelity for small ensembles around the resonant value of β (*lower panel*) with kicking strengths $k_1 = 0.8\pi$ and $k_2 = 0.6\pi$, and perturbation $\epsilon = 0.01$. Including the values near the resonant value of β , we find the beating frequency of the harmonic oscillator. The doubling of the beating frequency only occurs for exactly resonant β .

ϵ	transition value of $\tilde{\beta}$
0.00001	0.03
0.0001	0.05
0.001	0.1
0.01	0.2
0.1	0.3

Table 4.1: The $\tilde{\beta}$ for which one first sees a disappearing of the frequency doubling observed for resonant values of $\tilde{\beta}$ is measured for different values of ϵ . Fitting the values in a curve, we find that the best fit is found for the fourth root of ϵ , which agrees well with our estimate (4.64).

Chapter 5

Conclusion

5.1 Summary

Theoretical investigations into the fidelity of quantum systems like the δ -kicked rotor have always been enriched by fruitful collaborations with experimental realisations of the system. This is no different in our case, which is why one of the main foci of this summary will be on the inspirations for the experiment that our research might provide. To this end, we shall shortly review how the experiments to measure fidelity are implemented. As explained in the introduction, there are basically two types of realisations of the δ -kicked rotor model: cold and ultracold atoms. Cold atoms fill larger intervals of quasimomentum, whereas ultracold atoms (BEC) are able to reduce the width in quasimomentum to very small intervals of β [56]. With ultracold atoms (BEC), the width in quasimomentum can be restricted up to 1% of the Brillouin zone ($[0, 1)$ in our dimensionless units), i.e., it is possible to restrict β to intervals of a width of 0.01. This choice in experimental realisations also divides our results into two categories, as we will shortly see.

In this thesis, we investigate the behaviour of fidelity in the close vicinity of the fundamental quantum resonance of δ -kicked atoms. After comprehensive numerical studies on different parameter ranges in the kicking strengths k_1 and k_2 , deviations ϵ from quantum resonance, and quasimomentum β , we focus on several special points of interest. According to the most interesting numerical results, the near-resonant rotors around $\beta = \frac{1}{2}$ produce periodic revivals with the beating frequency of two harmonic oscillators, which survive even for the full ensemble in β . This is attractive for experiments because the revivals actually occur on relatively short time scales. Fidelity for the full ensemble can already be measured experimentally with cold atoms, since the quasimomentum may fill the whole Brillouin zone. Such measurements could, e.g., be performed with the current experimental setup of the Prentiss group at Harvard [35]. That the origin of the revivals lies in the resonant rotors can be illustrated by restricting the quasimomentum to small intervals around the resonant value of β . This, however, would experimentally necessitate the use of ultracold atoms. The β -intervals which have been obtained with cold atoms are simply too wide for this purpose.

In our numerical simulations, we find that the further we restrict the intervals around $\beta = \frac{1}{2}$, the higher and better resolved are the observed revivals. When looking at the fidelity of single resonant rotors themselves, however, we are in for a surprise: At

exactly resonant values of quasimomentum, we observe a doubling of the beating frequency. This unexpected and puzzling phenomenon has its origin in its pseudo-classical counterpart, namely the ϵ -classical phase space. We are able to explain the doubling in frequency by a symmetry breaking in the initial state. Apart from this, the calculations of classical fidelity performed on the basis of our pseudo-classical phase space yield results which agree very well with our quantum calculations. This demonstrates once more the applicability and usefulness of ϵ -classics.

The numerics form the first part of the research done in the framework of this thesis. The second part is an analytical description of the main numerical observations. We use a semiclassical ansatz to find an analytical expression for the fidelity of single resonant rotors. Conveniently, ϵ -classical phase space can be approximated by the pendulum phase space close to the fixed point. The following small angle approximation of the pendulum by the harmonic oscillator is also a wellknown technique to simplify the calculations. After our system has thus been simplified, the calculation of quantum fidelity for resonant and near-resonant values of quasimomentum within this approach is successful. Not only do we find the analytical expression of fidelity we were looking for, but we are also able to explain the doubling in frequency for the exactly resonant quasimomentum from the point of view of semiclassics. It is thus possible to draw parallels between the numerical and the analytical research chapters, combining both with excellent agreement.

Altogether, this work goes a long way towards a complete and comprehensive understanding of the near-resonant behaviour of the fidelity for the δ -kicked rotor. We now understand where the revivals in the fidelity of the full ensemble come from, and we can even derive the behaviour of the revivals analytically by our semiclassical expression for the resonant and near-resonant rotors. However, there is always something left to do. Therefore, we will shortly sum up open questions and possible starting points for further investigations in the following section.

5.2 Outlook – ideas and perspectives

One of the next logical steps to take is, as already mentioned, to find a similar analytical expression for the nonresonant rotors as we did for the resonant ones. This is difficult because we do not know the exact form of the tori outside the resonance island where the pendulum and harmonic oscillator approximation is applicable. However, the form of their tori is essential in order to calculate the propagators in a semiclassical ansatz. The harmonic oscillator approximation will obviously not work outside of the resonance island. However, it might be promising to find an appropriate expression by using the pendulum approximation.

An experiment with ultracold atoms as we proposed to measure the fidelity for ensembles of near-resonant rotors could also measure the fidelity of small β -intervals of nonresonant rotors. But even for the realisations with cold atoms that have been used so far [23, 35], finding an analytical expression for the nonresonant rotors would make it possible to derive an expression predicting the overall form of the fidelity decay (which cannot be fitted to some simple exponential or power-law function). The slope of the decay could then be directly compared to the results of the experiment (either with cold or ultracold atoms).

Another open question concerns the Fourier spectrum of the fidelity for the full ensemble (see Fig. 3.1). The beating times and its higher harmonics are very well visible in the Fourier spectrum, but there is an abrupt truncation after a number of higher harmonics. It would be of interest to find an explanation why the higher harmonics disappear so suddenly for frequencies larger than the truncation frequency. An idea here is to calculate the size of the island (one is sufficient, since the difference in kicking strengths k_1 and k_2 is typically small) and estimate how many quantized states of the size $\hbar = 2\pi\epsilon$ fit on the island. Doing this for various parameter ranges, we find that, while the order of magnitude is the same, there are notable differences in the accuracy of the match. For some values, our argument of quantized states sitting on the island fits very well, while for others, it is a rough fit at best.

While there are still a number of things to investigate numerically and analytically (as illustrated above) to fully understand the behaviour of quantum fidelity with the underlying phase space of ϵ -classics, the solutions and explanations we have found could already be stimulating for the experiments going on at Harvard [35] and other places, based on cold atoms which essentially populate all β -values uniformly [28].

As already mentioned, there is the possibility to explore new experimental realisations using the resources which ultracold atoms offer. This creates new options in implementing fidelity experiments that are able to retrace the revivals back to their origin, namely to the near-resonant rotors. Intervals around the resonant value of quasimomentum can be reduced step by step to illustrate the influence of the resonant rotors.

Another point of interest to the experiment is the scaling of $\tilde{\beta}$ investigated in section 4.2. The dependence of $\tilde{\beta}$ on the kicking period τ opens a load of experimental possibilities. Choosing the kicking period as an arbitrarily high multiple of 2π (to conserve resonance conditions), the boundaries inside which the effect of frequency doubling is visible are infinitely small – only the beating frequency will be detected. If the kicking period goes to zero on the other hand (which essentially introduces a dynamical evolution like at quantum resonance, see [26]), the boundaries go to infinity and the effect will become observable even for large β -ensembles. This allows to realise an experiment with cold instead of ultracold atoms to observe this interesting phenomenon.

We are looking forward to obtain experimental verification of the predictions made in this thesis during the next few years. Hopefully, our research will prove as fruitful and inspiring to the experiment as we hope and have portrayed in this outlook.

Appendix A

Formulae

The mathematical formulae and approximations used in this thesis were taken from [83] and [84]. They are listed in an overview below:

$$\frac{1}{2\pi} \int_{\alpha}^{\alpha+2\pi} d\theta e^{iz \cos(\theta)} e^{-in\theta} = i^n J_n(z) \quad (\text{A.1})$$

$$|z| \rightarrow \infty : J_0(z) \rightarrow \sqrt{\frac{2}{\pi z}} \cos\left(z - \frac{\pi}{4}\right) \quad (\text{A.2})$$

$$\int_{-\pi}^{\pi} dx J_{2n}(2z \sin(x)) = 2\pi J_n^2(z) \quad (\text{A.3})$$

$$\int_{-\infty}^{\infty} dx e^{ax^2+bx} = \sqrt{\frac{\pi}{-a}} e^{-b^2/4a} \quad (\text{A.4})$$

$$\int_{-\infty}^{\infty} dx e^{-iax^2} = \sqrt{\frac{\pi}{ia}} \quad (\text{A.5})$$

Appendix B

Derivation of the propagator for the harmonic oscillator

In order to derive the harmonic oscillator propagator from scratch, we use the definition of the Van Vleck propagator, a semiclassical expression for the propagator taken from [81]:

$$G(\theta, \theta', t) = \frac{1}{(2\pi i \hbar)^{d/2}} \sum_j |V_j(\theta, \theta', t)|^{1/2} e^{\frac{1}{2}S_j(\theta, \theta', t) - i\frac{\pi}{2}\nu_j(\theta, \theta', t)}. \quad (\text{B.1})$$

V_j are the Van Vleck determinants, d the dimension of our system (in our case, therefore, 1) and ν_j the Maslov index, which we already know can be neglected. The sum is over all trajectories (labelled by the index j).

For the harmonic oscillator, there is only a single trajectory in the sum. First, we calculate the action of the harmonic oscillator. The Lagrangian

$$L = \frac{1}{2}(\dot{\theta}^2 + \omega^2\theta^2) \quad (\text{B.2})$$

leads to the equation of motion

$$\ddot{\theta} + \omega^2\theta = 0, \quad (\text{B.3})$$

with the general solution

$$\theta(t) = A \sin(\omega t) + B \cos(\omega t). \quad (\text{B.4})$$

For the propagation, we want to move from point a to point b . We define the time at point a as t_a and the time when we reach point b as t_b . The difference is then $T \equiv t_b - t_a$. The ansatz

$$\theta_a(t) = A \sin(\omega t_a) + B \cos(\omega t_a), \quad \theta_b(t) = A \sin(\omega t_b) + B \cos(\omega t_b) \quad (\text{B.5})$$

allows us to calculate the prefactors A and B , resulting in

$$\begin{aligned} A &= \frac{\theta_b \cos(\omega t_a) - \theta_a \cos(\omega t_b)}{\sin(\omega T)}, \\ B &= \frac{\theta_a \sin(\omega t_b) - \theta_b \sin(\omega t_a)}{\sin(\omega T)}. \end{aligned} \quad (\text{B.6})$$

Now, we insert A and B into Eq. (B.4), and then the new expression for $\theta(t)$ into the Lagrangian. After some computations, we obtain

$$L = \frac{\omega^2}{2} [(A^2 - B^2) \cos(2\omega t) - 2AB \sin(2\omega t)]. \quad (\text{B.7})$$

Integrating L from t_a to t_b yields the action. After simple, but lengthy calculations we obtain

$$S = \frac{\omega}{2 \sin(\omega T)} [(\theta_a^2 + \theta_b^2) \cos(\omega T) - 2\theta_a \theta_b]. \quad (\text{B.8})$$

For the Van Vleck determinant, we calculate

$$V = \left| \frac{\partial^2 S}{\partial \theta \partial \theta'} \right| = \frac{\omega}{\sin(\omega T)}, \quad (\text{B.9})$$

and thus obtain the well known propagator for the harmonic oscillator:

$$G(\theta, \theta t) = \left(\frac{\omega}{2\pi i \hbar \sin(\omega T)} \right)^{1/2} \exp\left(\frac{i\omega}{2\hbar \sin(\omega T)} [(\theta_a^2 + \theta_b^2) \cos(\omega T) - 2\theta_a \theta_b] \right). \quad (\text{B.10})$$

Bibliography

- [1] A. Peres, *Stability of quantum motion in chaotic and regular systems*, Phys. Rev. A **30** (1984), 1610–1615.
- [2] A. Lichtenberg and M. Leibermann, *Regular and stochastic motion*, Applied Mathematical Sciences, vol. 38, Springer Verlag, New York, 1983.
- [3] T. Prosen and M. Žnidarič, *Stability of quantum motion and correlation decay*, J. Phys. A **35** (2002), 1455–1481.
- [4] N. R. Cerruti and S. Tomsović, *Sensitivity of wave field evolution and manifold stability in chaotic systems*, Phys. Rev. Lett. **88** (2002), 054103.
- [5] P. H. Jacquod, P. G. Silvestrov, and C. W. J. Beenakker, *Golden rule decay versus lyapunov decay of the quantum loschmidt echo*, Phys. Rev. E **64** (2001), 055203.
- [6] R. A. Jalabert and H. M. Pastawski, *Environment-independent decoherence rate in classically chaotic systems*, Phys. Rev. Lett. **86** (2001), 2490.
- [7] F. M. Cucchietti, C. H. Lewenkopf, E. R. Mucciolo, H. M. Pastawski, and R. O. Vallejos, *Measuring the Lyapunov exponent using quantum mechanics*, preprint (2001), arXiv:nlin/0112015v1.
- [8] A. Goussev, D. Waltner, K. Richter, and R. A. Jalabert, *Loschmidt echo for local perturbations: non-monotonic cross-over from the fermi-golden-rule to the escape-rate regime*, New Journal of Physics **10** (2008), 093010.
- [9] R. Schäfer, H.-J. Stöckmann, T. Gorin, and T. H. Seligman, *Experimental verification of fidelity decay: From perturbative to fermi golden rule regime*, Phys. Rev. Lett. **95** (2005), 184102.
- [10] R. Höhmann, U. Kuhl, and H.-J. Stöckmann, *Algebraic fidelity decay for local perturbations*, Phys. Rev. Lett. **100** (2008), 124101.
- [11] T. Gorin, T. Prosen, T. H. Seligman, and M. Žnidarič, *Dynamics of Loschmidt echoes and fidelity decay*, Phys. Rep. **435** (2006), 33 – 156.
- [12] P. Jacquod and C. Petitjean, *Dynamics of decoherence, entanglement and quantum irreversibility*, preprint (2008), arXiv:0806.0987v1.
- [13] J. C. Robinson, C. Bharucha, F. L. Moore, R. Jahnke, G. A. Georgakis, Q. Niu, M. G. Raizen, and B. Sundaram, *Study of quantum dynamics in the transition from classical stability to chaos*, Phys. Rev. Lett. **74** (1995), 3963–3966.

- [14] B.V.Chirikov, J.Ford, and F. Izrailev, *Stochastic behavior of a quantum pendulum under a periodic perturbation*, Stochastic Behavior in Classical and Quantum Hamiltonian Systems (G. Casati and J. Ford, eds.), Lecture Notes in Physics, vol. 93, Springer Verlag, Berlin, 1979, pp. 334 – 351.
- [15] R. Blümel and W. P. Reinhardt, *Chaos in atomic physics*, Cambridge University Press, Cambridge, 1997.
- [16] E. Ott, *Chaos in dynamical systems*, Cambridge University Press, Cambridge, 1993.
- [17] F. Izrailev and D. Shepelyansy, *Quantum resonance for the rotor in a non-linear periodic field*, Dok. Akad. Nauk SSSR **249** (1979), 1103.
- [18] I. Dana and D. L. Dorofeev, *General quantum resonances of the kicked particle*, Phys. Rev. E **73** (2006), 026206.
- [19] O. Morsch and M. Oberthaler, *Dynamics of bose-einstein condensates in optical lattices*, Reviews of Modern Physics **78** (2006).
- [20] S. Wimberger and M. Sadgrove, *The role of quasi-momentum in the resonant dynamics of the atom-optics kicked rotor*, J. Phys. A **38** (2005), 10549–10557.
- [21] W. M. Itano, J. C. Bergquist, J. J. Bollinger, J. M. Gilligan, D. J. Heinzen, F. L. Moore, M. G. Raizen, and D. J. Wineland, *Quantum projection noise: Population fluctuations in two-level systems*, Phys. Rev. A **47** (1993), 3554–3570.
- [22] W. M. Itano, J. C. Bergquist, J. J. Bollinger, J. M. Gilligan, D. J. Heinzen, F. L. Moore, M. G. Raizen, and D. J. Wineland, *Erratum: Quantum projection noise: Population fluctuations in two-level systems [phys. rev. a 47, 3554 (1993)]*, Phys. Rev. A **51** (1995), 1717.
- [23] M. B. d’Arcy, R. M. Godun, D. Cassettari, and G. S. Summy, *Accelerator-mode-based technique for studying quantum chaos*, Phys. Rev. A **67** (2003), 023605.
- [24] M. K. Oberthaler, R. M. Godun, M. B. d’Arcy, G. S. Summy, and K. Burnett, *Observation of quantum accelerator modes*, Phys. Rev. Lett. **83** (1999), 4447–4451.
- [25] S. Wimberger, M. Sadgrove, S. Parkins, and R. Leonhardt, *Experimental verification of a one-parameter scaling law for the quantum and “classical” resonances of the atom-optics kicked rotor*, Phys. Rev. A **71** (2005), 053404.
- [26] M. Sadgrove, S. Wimberger, S. Parkins, and R. Leonhardt, *Ballistic and localized transport for the atom optics kicked rotor in the limit of a vanishing kicking period*, Phys. Rev. Lett. **94** (2005), 174103.
- [27] S. Fishman, I. Guarneri, and L. Rebuzzini, *A theory for quantum accelerator modes in atom optics*, Journal of Statistical Physics **110** (2003), 911–943.
- [28] S. Wimberger, I. Guarneri, and S. Fishman, *Quantum resonances and decoherence for delta-kicked atoms*, Nonlinearity **16** (2003), 1381.

-
- [29] M. Sadgrove, S. Wimberger, S. Parkins, and R. Leonhardt, *Scaling law and stability for a noisy quantum system*, Phys. Rev. E **78** (2008), 025206.
- [30] R. Sankaranarayanan and A. Lakshminarayan, *Recurrence of fidelity in nearly integrable systems*, Phys. Rev. E **68** (2003), 036216.
- [31] G. Benenti, G. Casati, and G. Veble, *Decay of the classical Loschmidt echo in integrable systems*, Phys. Rev. E **68** (2003), 036212.
- [32] F. Haug, M. Bienert, W. P. Schleich, T. H. Seligman, and M. G. Raizen, *Motional stability of the quantum kicked rotor: A fidelity approach*, Phys. Rev. A **71** (2005), 043803.
- [33] S. Wimberger, *Chaos and localisation: quantum transport in periodically driven atomic systems*, Ph.D. thesis, LMU, Munich and Università degli Studi dell’Insubria, Como, 2003.
- [34] S. Schlunk, M. B. d’Arcy, S. A. Gardiner, D. Cassettari, R. M. Godun, and G. S. Summy, *Signatures of quantum stability in a classically chaotic system*, Phys. Rev. Lett. **90** (2003), 054101.
- [35] S. Wu, A. Tonyushkin, and M. G. Prentiss, *Observation of coherence revival and fidelity saturation in a delta-kicked rotor potential*, preprint (2008), arXiv:0801.0475v3.
- [36] S. Wimberger and A. Buchleitner, *Saturation of fidelity in the atom-optics kicked rotor*, J. Phys. B **39** (2006), L145–L151.
- [37] H.-J. Stöckmann, *Quantum chaos, an introduction*, Cambridge University Press, New York, 1999.
- [38] F. M. Izrailev, *Simple models of quantum chaos: Spectrum and eigenfunctions*, Phys. Rep. **196** (1990), 299 – 392.
- [39] A. Buchleitner, D. Delande, and J. Zakrzewski, *Non-dispersive wave packets in periodically driven quantum systems*, Phys. Rep. **368** (2002), 409 – 547.
- [40] G. Casati, B. V. Chirikov, D. L. Shepelyansky, and I. Guarneri, *Relevance of classical chaos in quantum mechanics: The hydrogen atom in a monochromatic field*, Phys. Rep. **154** (1987), 77 – 123.
- [41] P. M. Koch and K. A. H. van Leeuwen, *The importance of resonances in microwave “ionization” of excited hydrogen atoms*, Phys. Rep. **255** (1995), 289 – 403.
- [42] J. D. Meiss, *Visual explorations of dynamics: the standard map*, preprint (2008), arXiv.org:0801.0883.
- [43] A. Bäcker, R. Ketzmerick, S. Löck, M. Robnik, G. Vidmar, R. Höhmann, U. Kuhl, and H.-J. Stöckmann, *Dynamical tunneling in mushroom billiards*, Phys. Rev. Lett. **100** (2008), 174103.
- [44] A. Shudo and K. S. Ikeda, *Complex trajectory description for chaotic tunneling*, Progress of Theoretical Physics Supplement **139** (2000), 246–256.

- [45] A. Lyon and M. Colyvan, *The Explanatory Power of Phase Spaces*, *Philosophia Mathematica* **16** (2008), 227–243.
- [46] A. Tomadin, *Quantum chaos with ultracold atoms in optical lattices*, Diplomarbeit, Università di Pisa, 2006.
- [47] W. Press, S. Teukolsky, W. Vetterling, and B. Flannery, *Numerical recipes in FORTRAN*, 2nd ed., Cambridge University Press, Cambridge, UK, 1992.
- [48] F. Haake, *Quantum signatures of chaos*, Springer Series in Synergetics, vol. 54, Springer-Verlag, 1991.
- [49] G. Casati, I. Guarneri, F. Izrailev, and R. Scharf, *Scaling behavior of localization in quantum chaos*, *Phys. Rev. Lett.* **64** (1990), 5–8.
- [50] M. Sadgrove, M. Horikoshi, T. Sekimura, and K. Nakagawa, *Coherent control of ballistic energy growth for a kicked bose-einstein condensate*, *The European Physical Journal D* **45** (2007), 229–234.
- [51] F. Izrailev and D. Shepelyansy, *Quantum resonance for a rotator in a non-linear periodic field*, *Theor. Math. Phys.* **43** (1980), 353.
- [52] S. Wimberger, R. Mannella, O. Morsch, and E. Arimondo, *Resonant nonlinear quantum transport for a periodically kicked bose condensate*, *Phys. Rev. Lett.* **94** (2005), 130404.
- [53] I. Guarneri and L. Rebuzzini, *Quantum accelerator modes near higher-order resonances*, *Phys. Rev. Lett.* **100** (2008), 234103.
- [54] L. Rebuzzini, I. Guarneri, and R. Artuso, *Spinor dynamics of quantum accelerator modes near higher order resonances*, preprint (2008), arXiv:0811.1156v1.
- [55] J. F. Kanem, S. Maneshi, M. Partlow, M. Spanner, and A. M. Steinberg, *Observation of high-order quantum resonances in the kicked rotor*, *Phys. Rev. Lett.* **98** (2007), 083004.
- [56] C. Ryu, M. F. Andersen, A. Vaziri, M. B. d’Arcy, J. M. Grossman, K. Helmerson, and W. D. Phillips, *High-order quantum resonances observed in a periodically kicked bose-einstein condensate*, *Phys. Rev. Lett.* **96** (2006), 160403.
- [57] M. B. d’Arcy, R. M. Godun, G. S. Summy, I. Guarneri, S. Wimberger, S. Fishman, and A. Buchleitner, *Decoherence as a probe of coherent quantum dynamics*, *Phys. Rev. E* **69** (2004), 027201.
- [58] S. Schlunk, M. B. d’Arcy, S. A. Gardiner, and G. S. Summy, *Experimental observation of high-order quantum accelerator modes*, *Phys. Rev. Lett.* **90** (2003), 124102.
- [59] V. Ramareddy, G. Behinaein, I. Talukdar, P. Ahmadi, and G. S. Summy, *Resonances of the quantum δ -kicked accelerator*, preprint (2007), arXiv:0706.1587v1.
- [60] G. Behinaein, V. Ramareddy, P. Ahmadi, and G. S. Summy, *Exploring the phase space of the quantum delta kicked accelerator*, preprint (2006), arXiv:physics/0609203v2.

-
- [61] I. Bloch, J. Dalibard, and W. Zwerger, *Many-body physics with ultracold gases*, Reviews of Modern Physics **80** (2008), 885.
- [62] V. S. Malinovsky and P. R. Berman, *Momentum transfer using chirped standing-wave fields: Bragg scattering*, Phys. Rev. A **68** (2003), 023610.
- [63] T. Salger, G. Ritt, C. Geckeler, S. Kling, and M. Weitz, *Bloch oscillations of a bose-einstein condensate in a subwavelength optical lattice*, Phys. Rev. A **79** (2009), 011605.
- [64] I. de Vega, D. Porras, and J. I. Cirac, *Matter-wave emission in optical lattices: Single particle and collective effects*, Phys. Rev. Lett. **101** (2008), 260404.
- [65] S. Chu, *Nobel lecture: The manipulation of neutral particles*, Reviews of Modern Physics **70** (1998), 685.
- [66] J. J. Sakurai, *Modern quantum mechanics (2nd edition)*, Addison Wesley, 1994.
- [67] M. d'Arcy, *Quantum chaos in atom optics*, Ph.D. thesis, University of Oxford, Oxford, Hillary Term 2002.
- [68] S. A. Gardiner, J. I. Cirac, and P. Zoller, *Quantum chaos in an ion trap: The delta-kicked harmonic oscillator*, Phys. Rev. Lett. **79** (1997), 4790–4793.
- [69] S. A. Gardiner, J. I. Cirac, and P. Zoller, *Erratum: Quantum chaos in an ion trap: The delta-kicked harmonic oscillator [phys. rev. lett. 79, 4790 (1997)]*, Phys. Rev. Lett. **80** (1998), 2968.
- [70] S. Wimberger, I. Guarneri, and S. Fishman, *A classical scaling theory of quantum resonances*, Phys. Rev. Lett. **92** (2004), 084102.
- [71] E. W. Hagley, L. Deng, M. Kozuma, M. Trippenbach, Y. B. Band, M. Edwards, M. Doery, P. S. Julienne, K. Helmerson, S. L. Rolston, and W. D. Phillips, *Measurement of the coherence of a bose-einstein condensate*, Phys. Rev. Lett. **83** (1999), 3112–3115.
- [72] S. Peil, J. V. Porto, B. L. Tolra, J. M. Obrecht, B. E. King, M. Subbotin, S. L. Rolston, and W. D. Phillips, *Patterned loading of a bose-einstein condensate into an optical lattice*, Phys. Rev. A **67** (2003), 051603.
- [73] M. Bienert, F. Haug, W. P. Schleich, and M. G. Raizen, *Kicked rotor in wigner phase space*, Fortschritte der Physik **51** (2003), 474.
- [74] G. J. Duffy, S. Parkins, T. Müller, M. Sadgrove, R. Leonhardt, and A. C. Wilson, *Experimental investigation of early-time diffusion in the quantum kicked rotor using a bose-einstein condensate*, Phys. Rev. E **70** (2004), 056206.
- [75] G. Benenti, G. Casati, and G. Veble, *Stability of classical chaotic motion under a system's perturbations*, Phys. Rev. E **67** (2003), 055202.
- [76] G. Benenti and G. Casati, *Quantum-classical correspondence in perturbed chaotic systems*, Phys. Rev. E **65** (2002), 066205.

- [77] L. S. Schulman, *Techniques and applications of path integration*, Wiley, New York, 1981.
- [78] C. Bender and S. Orszag, *Advanced mathematical methods for scientists and engineers*, McGraw-Hill, 1978.
- [79] H. Kleinert, *Path integrals in quantum mechanics, statistics, polymer physics, and financial markets*, World Scientific, Singapore, 2006.
- [80] R. P. Feynman and A. R. Hibbs, *Quantum mechanics and path integrals*, McGraw-Hill, New York, 1965.
- [81] R. Artuso, *Semiclassics: Gutzwiller trace formula*, in *Proceedings of the International School of Physics Enrico Fermi, Course CXLIII*, no. New Directions in Quantum Chaos, 1991, pp. 397–412.
- [82] S. Wayper, M. Sadgrove, W. Simpson, and M. D. Hoogerland, *Atom optics kicked rotor: experimental evidence for a pendulum description of the quantum resonance*, preprint (2005), arXiv:quant-ph/0504219v1.
- [83] M. Abramowitz and I. A. Stegun, *Handbook of mathematical functions with formulas, graphs, and mathematical tables*, Dover Publications, New York, 1964.
- [84] I. Gradshteyn and I. Ryzhik, *Table of integrals, series, and products*, Academic Press, New York, 1980.

Acknowledgements

At the end of this thesis (and of my studies), there are a few people to whom I want to express my gratitude.

First of all, I want to thank my advisor Sandro Wimberger, who suggested this interesting topic and always had an open ear for any questions. Whether it was a technical question or paperwork, he was always quick to answer or offer advice, for which I am very grateful. I really learned lots during the last year!

He also made it possible for me to visit Como in order to collaborate with Prof. Italo Guarneri, who is the second person I owe gratitude to. Prof. Guarneri made me realize that it is possible to solve almost any problem – if you have got the right tools to do it (which he did).

I also want to say thank you to Laura and Lucia, with whom I shared the office at Università dell’Insubria: Our coffee breaks really made for a pleasant change from all the pages of analytical calculations!

Back to Heidelberg now: Thanks to Patrick Plötz, Alexander Merle and Tobias Paul, who proofread this thesis and eliminated the numerous small mistakes, it has finally become a readable text (at least I hope so). Also due to Patrick and Tobias, but also to the other people of our group, Ghazal, Sandro, Benedikt, Michael, Lev, and Anas, I always enjoyed coming up to the institute in the mornings – otherwise, the walk up might have taken much longer... So thank you all!

Special thanks also go to my two best friends: Rita, who always brightens up my days with her funny stories, and Renate, who both calmed me down when I was panicking about exams, or when I was getting too enthusiastic about them. I also want to thank Carina, Katja, Sabrina and Michael for all the fun we had during the last few years – without you, studying at Heidelberg would just not have been the same.

Last but not least, I want to express my gratitude to my parents. They have always been backing me all the way as well as supported me in any decisions I made. For this, and all their love, I will be eternally grateful.

I also want to thank my sister Sabine – without your wake-up calls last year I would have overslept more than once. ;-)

A big thank you and an even bigger kiss goes to my boyfriend Alex – thank you for all your support and love! I am so looking forward to our future! :)

Ich versichere, dass ich diese Arbeit selbstständig verfaßt und keine anderen als die angegebenen Quellen und Hilfsmittel benutzt habe.

Heidelberg, den 27. Februar 2009

